Revealing cyto-nuclear interactions through phenotypic variation: a study on cybrids of outdoor grown *Arabidopsis thaliana*

Aaron Lawson, M.Sc. Plant Sciences, minor thesis
Department of Genetics, Wageningen University and Research, Wageningen, The Netherlands
July 3rd, 2020

WAGENINGEN UNIVERSITY
WAGENINGEN UR

Revealing cyto-nuclear interactions through phenotypic variation: a study on cybrids of outdoor grown *Arabidopsis thaliana*

Aaron Lawson (ID# 890701505070)

M.Sc. Plant Sciences (Plant Pathology and Entomology) Minor Thesis (36 ECTS)

Supervisors: TPJM (Tom) Theeuwen M.Sc. and prof.dr. MGM (Mark) Aarts

Examiner: TPJM (Tom) Theeuwen M.Sc. and prof.dr. BJ (Bas) Zwaan

Contents

Summary

Anterograde and retrograde signalling between the nucleus and other organelles is highly complex and difficult to investigate. Moreover, the effects of the chloroplast and mitochondrial DNA (unitedly termed the plasmotype) need to be separated from nucleus-derived effects in order to further understand these interactions. The use of various plasmotype-nucleotype combinations (cybrids) in *Arabidopsis thaliana* has been successful for measuring the resultant phenotypic variation. The growth of an expanded panel of 217 *A. thaliana* cybrid lines intended to assess the level of plasmotypic variation and phenotypic performance for plasmotypes that were phylogenetically diverse. Additionally, growth in outdoor conditions was implemented to expose the plants to variable environmental conditions versus cybrids that were previously phenotyped under highly controlled conditions. This study further confirmed evidence that there is significant phenotypic variation among cybrids with different plasmotypes. Moreover, the Bur-0 plasmotype possesses elevated, additive photosynthetic capabilities when compared to other plasmotypes in the panel. The Kas-1 plasmotype was a novel and notable observation in its ability to produce significantly higher levels of surface area and relatively higher levels of biomass compared to all the other plasmotypes tested. The effects of the Kas-1 plasmotype, however, are largely epistatic as they are only driven by three of the four nucleotype backgrounds. The results encourage the continued exploration of the genetic basis of the high photosynthetic performance in the Bur-0 plasmotype and also that of other plasmotypic variation for a range of additional phenotypes.

Keywords: cybrid, natural variation, plasmotypic variation, phenotype, photosynthesis

Introduction

Plant cells possess functional genetic material in three separate organelles: mitochondria, chloroplasts and the nucleus. The nuclear genome, however, contains the largest quantity of a plant's genetic material and coding genes. For example, the nuclear genome of *Arabidopsis thaliana* is ~135 Mb in size on five chromosomes (The Arabidopsis Genome Initiative, 2000), while the genome sizes of the chloroplast and mitochondria are ~154 kb and ~367 kb, respectively (Sato *et al.*, 1999; Sloan *et al.*, 2018). The transcription of a plant's nuclear genes results in the synthesis of intra- and intercellular proteins for development and maintenance. Moreover, the nucleus is highly involved in anterograde and retrograde signalling with the genomes of the mitochondria and chloroplasts (Glaßer *et al*., 2014). However, the effects of these interactions on a plant's phenotype remains poorly understood and requires further analysis of plastid genomes, their phenotypic effects and evolutionary history.

The existence of genetic material in mitochondria has prompted several theories regarding their origins and functional roles in modern plants. The most widely accepted theory addressing eukaryogenesis and mitochondrial establishment is an endosymbiotic event that occurred between a α-Proteobacteria and a host cell, likely a relative of Asgard archaea (Spang *et al.*, 2019). Physical evidence for this hypothesis was first confirmed with the discovery of conserved genes in mitochondrial genomes that were clustered with α-Proteobacterial genes in phylogenetic trees (Schwartz and Dayhoff, 1978). Furthermore, nearly all known eukaryotic nuclear genomes contain mitochondrial genes, suggesting that mitochondrial endosymbiosis occurred prior to the branching of all modern eukaryotic lineages (Karnkowska *et al.*, 2016). Although the general hypothesis is widely accepted throughout the field of eukaryogenesis, many questions remain unanswered such as the timing of the event and the biological motivation behind this phenomenon. Nevertheless, current research efforts to further understand this critical stage in eukaryotic evolution are extensive and widespread. The most recent findings suggest that the archaeal host was a fermentative organoheterotroph that produced reduced compounds capable of being metabolized by the endosymbiont (Spang *et al.*, 2019). Conversely, the protomitochondria have evolved to provide the host cell with energy metabolism and oxygen respiration, key elements for the evolution of contemporary eukaryotes (López-García *et al.,* 2017). Moreover, some of the α-Proteobacterial genes are thought to have been transferred to

the host cell's nuclear genome via direct DNA transfer during the early stages of eukaryogenesis (Henze and Martin, 2001). In fact, an entire mitochondrial genome can be found on chromosome two of *A. thaliana* (Lin *et al.* 1999; Stupar *et al.* 2001). Conversely, in some cases many of these genes have been lost entirely or retained in the mitochondrial genome. Nevertheless, the addition of mitochondrial genes to the nuclear genome was essential for plant evolution and modern function as they are involved in several cellular processes such as DNA repair and cytoplasmic signalling (Lin *et al.*, 2007).

The evolution of chloroplasts and their genomes also offers valuable insights into how they may influence the phenotype of modern plants. Endosymbiotic theory suggests that ca. 1.2 billion years ago early eukaryotic cells engulfed a photosynthetic cyanobacterium (Parfrey *et al.*, 2011). The acquisition of cyanobacteria resulted in the host cell's inheritance of several attributes such as photosynthesis and genes encoding cell division proteins. Phylogenetic analysis has confirmed that the closest homologs of chloroplast sequences do indeed come from this phylum of bacteria (Douglas and Raven, 2003). Similar to mitochondria, the pre-plastids lost, retained and transferred genes to the nucleus over the course of evolution (Herrmann, 1997). Additionally, the symbiosis resulted in the invention of protein import machinery that facilitated the donation of plastid genes to the nucleus (Osteryoung and McAndrew, 2001). Genomic analysis shows that contemporary chloroplast genomes encode between 60-200 proteins, whereas the nucleus is the source of over 5,000 chloroplast targeted genes (Martin *et al.*, 2002). Furthermore, the loss of genes in the pre-plastid has been attributed to the high maintenance cost of redundant orthologous genes. The explanation for plastid derived gene transfer to the nucleus remains largely inconclusive but is thought to be a response to stress conditions (Cullis *et al.*, 2009). Regardless of evolutionary motivations, and processes for gene distribution among organelles, cyto-nuclear interactions may explain variation in plant development and phenotypic attributes.

The complex network of gene signalling between a plant's organelles may provide further insight into how the genomes of the chloroplasts and mitochondria (collectively termed the plasmotype) have an effect on phenotype. Retrograde signalling (organelle-to-nucleus) has a large role in nuclear gene expression and is generally divided into two classes: chloroplast and photosystem biogenesis (biogenic control) and those involved in chloroplast responses to environmental conditions (Kleine and Leister, 2016). Examples of these signals include

chloroplast metabolites such as heme (Woodson *et al.*, 2011), phosphonucleotide PAP (Estevillo *et al.*, 2011), oxidation products of β-carotene (Ramel *et al.*, 2012), precursors of carotenoids (Xiao *et al.*, 2012) and several transcription factors (Koussevitsky *et al.*, 2007). Moreover, signalling involving these molecules often includes cytoplasmic intermediaries, increasing the complexity and difficulty of understanding these pathways (Kleine and Leister, 2016). Anterograde (nucleus-to-organelle) signalling is also a key phenomenon for many cellular processes. Nucleus encoded molecules are critical for relaying information to the chloroplasts and therefore influencing gene expression in the organellular genome (Berry *et al.*, 2013). These nucleus-derived regulators include sigma proteins, plastid transcriptional factors and posttranscriptional regulatory factors (Berry *et al.*, 2013). Many of these regulators not only participate in chloroplast biogenesis but also influence the photosynthetic capacity under variable environmental conditions (Berry *et al.*, 2013). Lastly, transcriptional regulation and intermediary interactions between the mitochondria and chloroplasts has been observed and described as organellular cross-talk. For example, both the mitochondria and chloroplasts produce reactive oxygen species (ROS) that influence pathways for nuclear transcription signalling. Similarly, mitochondria produce nitric oxide and ascorbate as signalling molecules to the chloroplast (Raghavendra and Padmasree, 2003). Understanding the complexity of the aforementioned pathways and how they affect a plant's phenotype calls for novel approaches to analyze a plants plasmotypic variation.

One method of exploring cyto-nuclear interactions requires analyzing plasmotypic variation and its effect on a plant's phenotype. This approach requires separating the effects of the nuclear genome from the mitochondria and chloroplast genomes. Several methods such as reciprocal cross designs and back-cross designs have been previously utilized to observe various nucleotype-plasmotype combinations, however, they are inefficient and limited in accuracy (Joseph *et al.*, 2013; Tang *et al.*, 2014; Roux *et al.*, 2016). Alternatively, the use of the *A. thaliana* haploid inducer line *GFP-tailswap* has proven to much more successful (Flood and Theeuwen *et al.*, 2020). In this approach, the zygote of *GFP-tailswap* loses its nuclear genome when pollinated with a wild-type (WT) plant, resulting in haploid progeny with a paternally derived nuclear genome and maternally derived mitochondria and chloroplasts (Fig. 1.a) (Flood *et al.*, 2020). Genome duplication or restitutional meiosis subsequently results in stable, doubled haploid lines with the potential to contain various plasmotype-nucleotype combinations,

alternatively termed cybrids. This method was used by Flood and Theeuwen *et al.* (2020) to create a panel of cybrids that originated from six natural occurring *A. thaliana* accessions representing genetic and geographical diversity. A seventh naturally occurring accession was included as a control as it contains a large-effect mutation in the *PsbA* gene that causes reduced photosystem II (PSII) efficiency(Φ_{PSII}). The plasmotype-nucleotype combinations resulted in a test panel of 46 cybrids and seven WT progenitors. These plants were grown and analyzed for absolute and relative growth rate, biomass accumulation, epinastic leaf movement, Φ_{PSII}, non-photochemical quenching (NPQ), a reflectance-based estimate of chlorophyll, flowering time, germination, pollen abortion and primary metabolites. Several experiments were conducted in conditions such as climate chambers that simulated "natural" and variable conditions by subjecting the panel to germination under osmotic stress and fluctuating light. The experiment yielded 1,859 phenotypes from which 92 were selected to eliminate any non-informative phenotypes. The average contribution to broad sense heritability (H^2) from the nucleotype, plasmotype and nucleotype-plasmotype combination was 91.9, 2.9 and 5.2 percent, respectively. These values, however, do not include the Ely plasmotype due to its *PsbA* mutation that represented most of the plasmotype-derived additive variation. Moreover, a key observation was that not only did the Bur plasmotype exhibit increased Φ_{PSII} under normal conditions compared to the other plasmotypes (1.6 percent), but this parameter was even further increased under fluctuating light intensity (Fig. 1.b) (3.5 percent increase). Additionally, the fraction of H^2 from plasmotype increased under fluctuating light intensities (Fig. 1.c). Chloroplastic variation was postulated to be the source of this increase as mitochondrial respiration rates were normal and contained no large-effect mutations in the plasmotypes genome. Increased phenotypic variation due to plasmotypic variation under stressful conditions merits more extensive investigations that focus on the impact of these factors on a plant's phenotype.

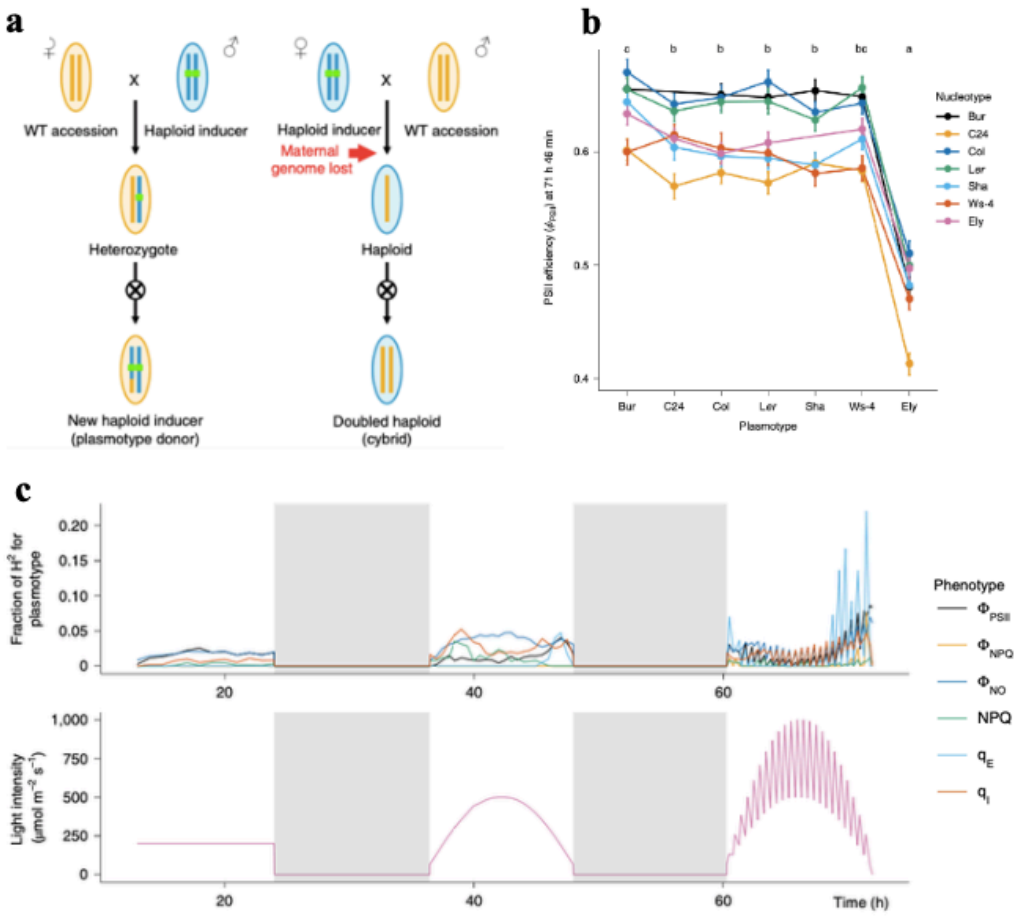

Fig. 1 | The method used to create cybrids, PSII efficiency for the cybrid panel and phenotypes under various light conditions. a, The process of creating cybrids using a haploid inducer. **b,** The bur plasmotype results in an increased PSII efficiency in comparison to the other cybrids tested. **c,** The fraction of H^2 for plasmotype is increased for several phenotypes under conditions of fluctuating light (Reproduced from Flood and Theeuwen *et al.*, 2020)

The observation of phenotypic variation due to plasmotype by Flood and Theeuwen *et al.* (2020) has prompted subsequent research efforts to encompass a broader range of genetic diversity grown under variable conditions (Theeuwen *et al.,* unpublished). Whole genome sequencing of over 1,500 *A. thaliana* accessions have enabled the analysis of genetic diversity among accessions collected from various ecoregions (1001 Genomes Consortium, 2016). Phylogenetic analysis of 622 *A. thaliana* accessions revealed that the panel used by Flood and Theeuwen *et al.* (2020) represented less than 5 percent variation of the accessions analyzed (Theeuwen, unpublished). These results also highlight that the most divergent lineages in the set were sampled from remote and isolated regions in Morocco, Tanzania, Madeira and the Iberian

Peninsula (Alonso-Blanco *et al*., 2016; Durvasula *et al*., 2017; Fulgione *et al*., 2017). Furthermore, variability in cyto-nuclear communication for accessions that have evolved in geographically isolated regions may be increased due to the wide range of growing conditions that they have evolved in.

A new cybrid panel consisting of four nucelotype donors and 60 plasmotype donors has been constructed using a selection of the aforementioned accessions and some have been whole genome sequenced to date (Fig. 2; Extended Data Table 1). The nucleotype donors include the ecotypes Columbia (Col-0), Burren (Bur-0), Cape Verde Islands (Cvi-0) and Tanzania (Tanz-1). Col-0 was selected due to its widespread use in research and availability of mutants for any subsequent investigations. Bur-0 was included due to the strong additive effects that it had on phenotypes such as elevated Φ_{PSII} in the aforementioned study by Flood and Theeuwen *et al.* (2020), potentially lowering the amount of nucleus derived variation. Cvi-0 and Tanz-1 were selected in part due to their high level of phylogenetic divergence and the substantial amount of previous research done on them (Theeuwen, unpublished). The 60 plasmotype donors were selected based on their phylogenetic diversity and availability for acquisition. The terminology regarding cybrid combinations is explained by the plasmotype listed first, then followed by an underscore and then nucleotype. For example, Tanz-1_Col-0 denotes a cybrid with a Tanz-1 plasmotype and a Bur nucleotype. The panel was phylogenetically analyzed by plasmotype and the Col-0 nucleotype cybrids were phenotyped to detect any differences in cytoplasmic variation than that of the aforementioned 7 × 7 panel by Flood and Theeuwen *et al.* (2020). In addition, the cybrids' genotypes were confirmed using KASP ™ markers and genome sequencing (Theeuwen, unpublished).

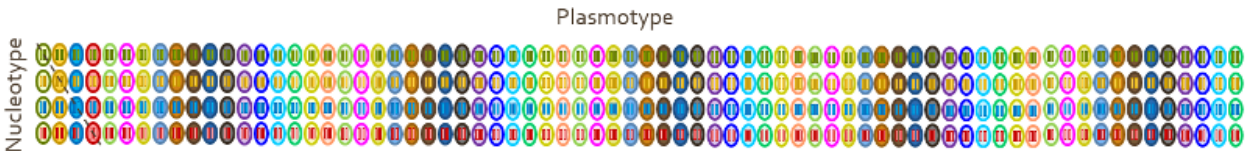

Fig. 2 | A representation of the cybrid panel of *A. thaliana* constructed by Theeuwen *et al.* (unpublished). The four nucleotypes are listed vertically while the 60 plasmotypes are listed horizontally (Reproduced from Lind, unpublished).

Crop breeding for enhanced traits is an extensive industry and is essential for meeting current and future food production demands. Modern breeding techniques including genetic

modification and gene editing have provided many of these services in a rapid and efficient manner. However, these advances have been largely restricted by agricultural regulations in regions such as Europe. Such jurisdictions are therefore dependent on traditional breeding techniques that require the identification and location of desired genes that code for desirable and heritable traits. Moreover, the lion's share of this work has historically focused on the identification and manipulation of nuclear-derived genes and the resultant plant phenotypes. Although this approach has proven to be effective, the influence of plasmotypic variation on phenotype may also be considered important for achieving goals in breeding goals and in biotechnological applications. The exploration of cyto-nuclear interactions holds great potential for crop trait enhancement as cytoplasmic genomes are already known to be responsible for fundamental plant growth processes such as metabolism and photosynthesis. An understanding of plasmotypic variation and cyto-nuclear interactions can provide plant breeders with powerful tools for crop trait enhancement. The untapped potential of this knowledge has vast applications, markedly for improving photosynthetic processes and increased crop growth efficiency.

We hypothesize that plasmotypic variation has a heritable effect on several photosynthetic phenotypes such as Φ_{PSII} and that growth in growth in variable, outdoor conditions will result in phenotypic variation patterns similar to those observed in previous experiments conducted in growth chambers. Additionally, we hypothesize that phenotyping a larger and phylogenetically broader panel of cybrids will result in novel cybrids with plasmotypic variation. Lastly, this plasmotypic variation will be represented by the measurement of additional, physiological phenotypes that have not yet been observed assessed.

The primary objective of the proposed project is to grow the new cybrid panel of 217 genotypes by Theeuwen *et al.* (unpublished) in outdoor conditions and analyze the plants for plasmotypic variation by measuring several phenotypic attributes. This will be the first time that species-wide phenotyping will take place for plasmotype-nucleotype combinations. Furthermore, we intend to sequence the lines used to later link the resultant phenotypes to underlying genetic variation. As such, we will utilize the 217 *A. thaliana* cybrids that were created with four nucleotype donors and ~60 plasmotype donors.

Methods

Outdoor cybrid experiment

Gauze tunnel. Plant growth took place in an outdoor, gauze covered tunnel at Unifarm, Wageningen University and Research, The Netherlands (51.9882583, 5.66119897). The base of the tunnel measured 8 m × 5 m and was enclosed by synthetic gauze material that was largely penetrable by rainwater, sunlight and wind so to provide conditions similar to those encountered in the field (Fig. 3). Rain gauges placed inside and outside the tunnel confirmed that all rainwater was able to penetrate the gauze. Photosynthetically active radiation (PAR) readings were also taken both inside the tunnel and at a metrological station within 500 m from the tunnel. A comparison of readings from both locations indicated that the gauze decreased the amount of PAR that penetrated through to the growing area on average by 94.3 µmol m^{-2} s^{-1}. The floor of the tunnel was covered in black landscape material. The tunnel contained access to local utilities such as water, power and a zipper door to prevent the entry of any undesired interferents.

Fig. 3 | Gauze tunnel at Unifarm, Wageningen University and Research.

Plant pots, trays and substrate. Black plastic pots measuring 7 cm × 7 cm × 18 cm were used for individual plant growth as they allowed sufficient depth for unlimited root development (Fig. 4.a). Grey plastic trays measuring 40 cm × 60 cm × 20 cm were used to hold 40 of the aforementioned pots (Fig. 4.a). The trays were organized in five rows of 11 trays and one row of 13 trays (Fig. 4.b). A small seedling tray was placed in the bottom of each large grey tray to raise the pots above the edge of the grey tray. The plant pots were filled with a mixture of 40 percent sand and 60 percent peat provided by Lensli® substrates. The substrate includes YARA PG

MIX™ which contains 15-10-20+3 of N, P_2O_5, K_2O and MgO. The added fertilizer is in powder form and results in complete substrate values of 1.0 and 5.7 for electrical conductivity and pH, respectively. No additional nutrition was applied during the experiment.

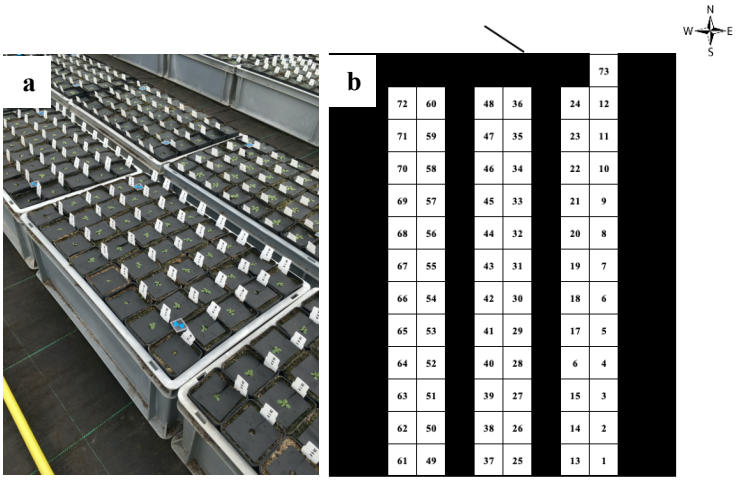

Fig. 4 | Organization of pots and trays in the growth tunnel. a, 40 pots were placed in each tray. **b,** Aerial perspective of the growth tunnel and tray placement.

Plant materials. The seeds used in this experiment were created by Theeuwen *et al.* (unpublished) and the plasmotype – nucleotype combinations are listed in Extended Data Table 1. Confirmation of the plasmotype – nucleotype combinations was completed with two KASP™ markers, one for the nuclear genome and one for the plastid genome (Theeuwen *et al.*, unpublished). Furthermore, KASP™ primers were created and assays were completed to confirm the genotypes of the cybrids. The panel was propagated simultaneously and under the same environmental conditions, however, the timeline of the project did not allow for the inclusion of this standardized panel to be utilized in the outdoor experiment. The seeds used in this experiment were propagated in several batches. The potential for a batch effect is considered in the analysis of this experiment; the standardized panel will be used for any subsequent experiments.

Seed preparation and sowing. Graphite pencil was used to mark round pieces of filter paper with the name of a cybrid from the panel (see Extended Data Table 1). Each piece of paper was placed in the bottom of large, round petri dishes and one millilitre of purified water was applied

to the filter paper using a Milli-Q® dispenser. Seeds of each cybrid were sprinkled onto the moist paper and the dishes were closed with a lid. The petri dishes were stacked in bins that contained a layer of wet paper towel in the bottom to provide moisture over an extended period of time. The bins were stored in a 4ºC refrigerated room for four days to break the seeds' dormancy. The bins were then placed in a growth chamber kept at 22 °Celsius and 16 hours day^{-1} of light for 24 hours prior to sowing them in the outdoor pots.

An R script was used to create an unbalanced, incomplete block design to randomize the cybrids among the pots resulting in the nucleotypes being randomized among the trays and the plasmotypes being randomized within the trays (Theeuwen, unpublished). Each pot was labelled with its corresponding plastic label that contained the coordinates in the tray/tunnel. The number of replicates ranged between 10-12 for the cybrid genotypes and 60-80 for the four WTs. On March 18th, 2020 the petri dishes containing the germinated cybrid seeds with a Bur nucleotype were brought to the tunnel for sowing. A fine-tipped paint brush was used to extract approximately four germinated seeds form the petri dishes and place them on the surface of the soil. The cybrids with Col and Cvi nucleotypes were sown on March 19th and the cybrids with Tanz nucleotypes were sown on March 20th. Following 20 days of growth, the healthiest looking seedling in each pot was selected to remain while the extra seedlings were removed and discarded.

Maintenance and sensors. Plastic wrapping was placed over the tunnel's gauze for the first 14 days of growth. This was to ensure that heavy rain would not disturb the establishment of the seedlings in the soil. Additionally, plastic wrapping was placed over the trays during the night for the first 14 days of growth to protect from cold temperatures. Soil covers were placed on each pot after 23 days of growth.

The pots were evenly watered as needed according to weather conditions and rainfall. Anti-slug/snail pellets were placed in small piles on the ground around the perimeter of the tunnel. Ten van Iperen® insect sticking pads were hung with string above the rows of trays to prevent herbivory damage and further infestation.

A set of remote sensors from 30MHz monitored and recorded atmospheric CO_2 concentration, PAR, soil water content (SWC), humidity, dewpoint, and temperature. The CO_2 concentration sensor was strapped to the side of the tunnel at a height of 1.5 m (Fig. 5). The

sensor for temperature, humidity and dewpoint was hung in the middle of the tunnel at a height of 1.5 m. The PAR sensor was fixed in the middle of the tunnel at the same height as the pots. The SWC sensor contained three prongs that were placed into the soil of one single pot throughout the duration of the experiment.

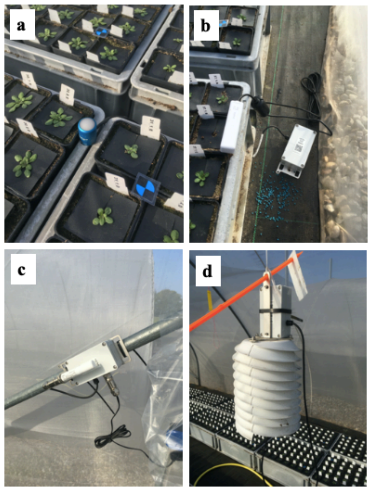

Fig. 5 | Sensors in the tunnel for recording growing conditions. a, PAR meter. **b,** SWC. **c,** CO_2. **d,** temperature etc.

Phenotyping Growth rate was intended to be measured by taking daily photos of the trays between 09:00 hrs and 11:00 hrs using a Nikon D3000 camera with a Nikon DX AF-S Nikkor 18-105 mm 1:3.5-5.6G ED lens (Fig. 6.a). The trays contained two sensing markers that were to be used for pot partitioning when the images were analyzed by a Python script (Aarts, unpublished) (Fig. 6.b). Furthermore, the script was expected to count the quantity of green pixels in each pot to extrapolate the leaf area of the plant. Regrettably, the development of this script was unsuccessful up until the end of this thesis, and growth rate was therefore excluded from the set of phenotypes analyzed.

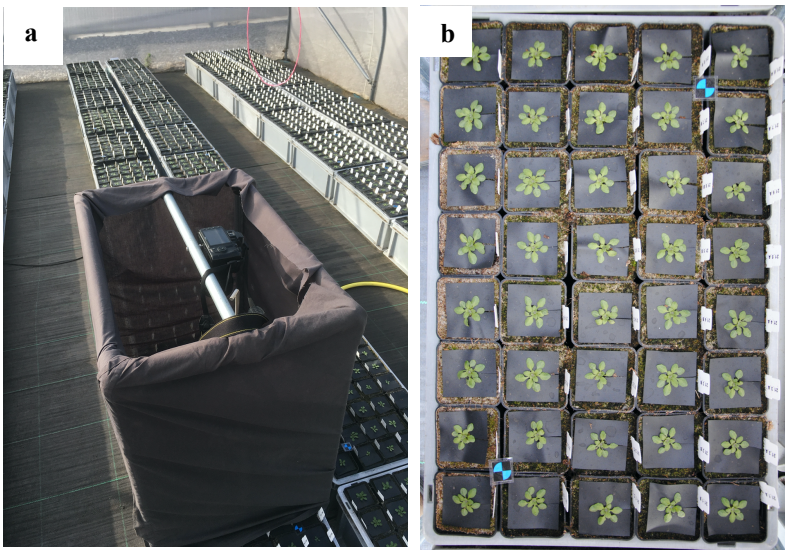

Fig. 6 | Method for recording growth rate. a, camera set up and stand for taking daily images. **b,** resulting growth rate images and partitioning markers.

Red Green Blue (RGB) and chlorophyll fluorescence imaging was completed at WUR in the Unifarm greenhouses. The trays containing nucleotypes Cvi-0, Col-0, Bur-0 and Tanz-1 were analyzed at 35, 38, 38 and 38 days of growth, respectively. The plants were brought into the greenhouse and stored in a climate-controlled room with constant conditions of 19 ºC and ~200 µmol m^{-2} s^{-1} until they were ready to be analyzed. Exposed soil was covered with rubber strips to eliminate any interfering fluorescence from the algal development. The plants were passed through a PlantScreen™ SC System supplied by Photon Systems Instruments (PSI). The software supplied by PSI for the data analysis was Plantscreen Data Analyzer Version: 3. 1. 6. 20. Trays of 20 plants each were exposed to a ~6-minute-long protocol (Fig. 7) in which fluorescence and RGB imaging took place. Digital tray masks were used to partition the individual pots/plants and were manually adjusted to ensure that they were perfectly centered for exact measurements of each individual plant. *Post hoc* adjustments were made to the RGB threshold for the Tanz nucleotype to ensure the inclusion of all relevant spectral components. Tunnel tray number 73 was excluded from the Robin analysis, reducing the number of Bur-0 replicates.

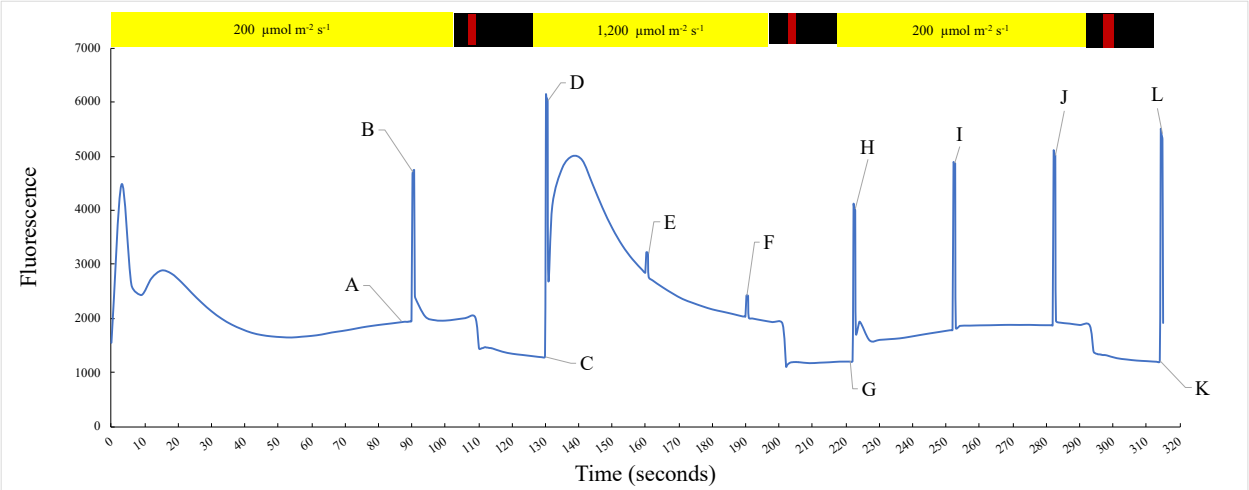

Fig. 7 | An example of the imaging protocol for one specific plant used with the Robin and time point/measurement annotations. Light input is indicated in the yellow bars at the top of the graph. Black and red bars indicate periods of dark and infrared, respectively. A-B: Actinic FqFm (Φ_{PSII}), C-D: Actinic NPQ, Φ_{NPQ}, Φ_{NO}, q_L, q_I, and q_E, E: High FqFm 1 (Φ_{PSII}), F: High FqFm 2 (Φ_{PSII}), G-H: High NPQ, Φ_{NPQ}, Φ_{NO}, q_L, q_I, and q_E, I: Low FqFm 1 (Φ_{PSII}), J: Low FqFm 2 (Φ_{PSII}), K-L: Low NPQ, Φ_{NPQ}, Φ_{NO}, q_L, q_I, and q_E.

The number of days-to-flower for each plant was recorded when the top of the highest flower bud reached 3 cm from the base of the floret. When plants reached this stage, they were harvested at the base of the floret, placed in a paper bag and dried in an oven for 48 hours. The dried plants were individually weighed, and plant material was retained for the potential of DNA extraction for further analysis. Dry weight was hence recorded when each plant reached this stage except for the Col-0 nucleotype plants which were all harvested on the same day.

Phenotypic data analysis. Fluorescence data output from the Robin analysis included size and raw fluorescence values according to the protocol. The morphological parameters included Area (Pixels), Perimeter (Pixels), Area (mm^2), Perimeter (mm), SOL, Roundness2, Isotropy, Compactness, RMS, Eccentricity and Roundness and a set of RGB parameters with various spectral inclusions (Extended data Table 2). Analysis of raw data was initiated by removing outlier plants through the use of RStudio software, version 1.2.5042 (R). The outlier removal script (Theeuwen, unpublished) analyzed each genotype separately and was based on the Robin output parameter Area (mm^2). Outlier plants were detected if they had a surface area less than two standard deviations from the genotype's mean. These plants were excluded in all phenotypes, from any subsequent analysis.

Raw fluorescence output data was analyzed using an R script (Theeuwen, unpublished) to calculate photosynthetic phenotypes according to fluorescence response in the above-mentioned protocol. Phenotypes calculated included Φ_{PSII}, non-photochemical quenching efficiency (Φ_{NPQ}), non-regulated energy losses (Φ_{NO}), NPQ, rapidly reversible NPQ (q_E) and photoinhibition of photosynthesis (q_I) under different light conditions along the protocol's time sequence. All subsequent analyses involved a total of 57 phenotypes, 11 of which were related to plant morphology, 43 were photosynthesis related and the remaining three were dry weight, number of days to flowering and specific leaf area (SLA). Individual plant data and corresponding phenotype measurements were then compiled into one dataset and all Ely_XXX plasmotype donor plants with the aforementioned mutation in the *PsbA* gene were removed. The exclusion of these plants was necessary to eliminate any influence that the large effect mutation would have on any downstream tests such as calculating H^2 and the honestly significant differences (HSD).

The combined dataset was first analyzed as a whole to determine plasmotype-nucleotype interactions. Experimental parameters such as the position of each plant in the tunnel were tested for their significance and the potential for required correction using a significance threshold of $\alpha = 0.05$; with the same threshold used for all other *post hoc* tests conducted in the analysis. Due to the significance of "Block" and "Row", the Kenward-Roger approach was incorporated into a linear mixed model for estimation of degrees of freedom (Equation 1) through the use of the lme4 package in R (Bates *et al.*, 2015; Flood and Theeuwen *et al.* 2020). The tunnel trays represent the Blocks and the longer dimension of eight pots in the trays are the Rows. The model subsequently underwent an analysis of variance (ANOVA).

$$\underline{Y} = \text{Plasmotype} + \text{Nucleotype} + (\text{Nucelotype} \times \text{Plasmotype}) + \underline{\text{Block}} + \underline{\text{Row}} + \underline{\varepsilon}$$

Equation 1. Model used for the initial ANOVA and Kenward Roger adjustment. Underlined variables are random terms.

Confirmation of normal distribution was followed by the calculation of the additive contributions of plasmotype, nucleotype and the plasmotype-nucleotype interaction to phentoypic effects by an estimation of the variation through the use of the VarCorr function from the above-mentioned package (Bates *et al.*, 2015). The sum of all variance components was then used to calculate the

fraction of explained variance for every term in the model (Theeuwen, unpublished). Broad-sense heritability (H^2) was estimated by three biologically influencing components: nucleotype, plasmotype and the plasmotype-nucleotype interaction (Theeuwen, unpublished). This analysis was only completed for plasmotypes which were present in all nucleotype sets, as some nucleoptype sets did not contain all of the plasmotype donors as the others. The model for this estimation of variance is illustrated in Equation 2 where all the fixed terms were considered random. Pairwise differences were calculated and compared between the Fisher's Least Significance Difference (LSD) test (Fisher, 1935), Tukey's test (Tukey, 1949) and the Benjamini & Hochberg test (Benjamini & Hochberg, 1995).

$$\underline{Y} = \underline{\text{Plasmotype}} + \underline{\text{Nucleotype}} + \underline{(\text{Nucelotype} \times \text{Plasmotype})} + \underline{\text{Block}} + \underline{\text{Row}} + \underline{\varepsilon}$$

Equation 2. Model used for estimation of variance. Underlined variables are random terms.

The epistatic effects of the plasmotype on the nucleotype were analyzed by using the aforementioned dataset, however, the model used analyzed each of the four nucleotype sets of separately. This model differed to the additive model by only including "Plasmotype" as the only non-random term (Equation 3).

$$\underline{Y} = \text{Plasmotype} + \underline{\text{Block}} + \underline{\text{Row}} + \underline{\varepsilon}$$

Equation 3. Model used for analyzing the four nucleotypes separately. Underlined variables are random terms.

Similar to the additive approach, the model then estimated the variance components and heritability through the use of the Equation 4.

$$\underline{Y} = \underline{\text{Plasmotype}} + \underline{\text{Block}} + \underline{\text{Row}} + \underline{\varepsilon}$$

Equation 4. Model used for estimation of variance. Underlined variables are random terms.

Subsequent *post hoc* tests were similar to the aforementioned approach except for the fact that pairwise comparisons were only made for plasmotypes within each separate set of four nucleotypes. Additionally, a Dunnett's test (1955) was conducted within each set of four nucleotypes to compare all the encompassed plasmotypes with the corresponding nucelotypes WT.

Deviant Panke-1_Bur phenotype experiment

Nearly half of the Panke-1_Bur-0 replicates displayed a deviant phenotype of the overproduction of leaves, severe upward curling of the leaves and a delay in flowering time (Figure X). Due to these observations, a separate experiment was conducted to explore the genotype's potential sensitivity to high temperatures.

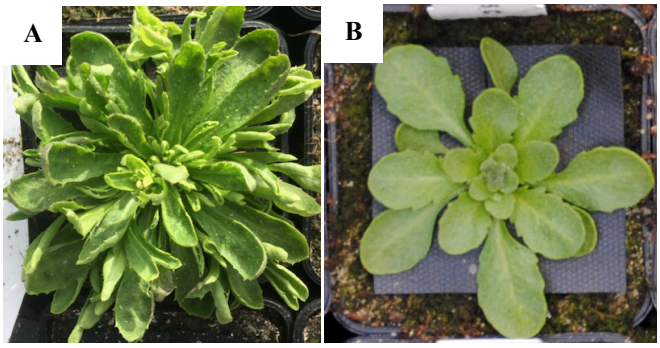

Fig. 7 | A visual comparison of a "normal" plant and a deviant pant form the Panke-1_Bur-0 replicates. a, One of the five Panke-1_Bur replicates that exhibited the deviant leaf phenotype. **b,** The leaf phenotype from the remainder of the "normal" Panke-1_Bur-0 plants.

Plant materials. Three genotypes were grown under different conditions. Seeds of Panke-1_Bur-0 and Bur WT were selected from the same batches that were used in the above-mentioned tunnel experiment. Panke-1 WT was also included; although this genotype was not used in the tunnel experiment.

Seed preparation and sowing. Graphite pencil was used to mark round pieces of filter paper with the name of a one of the three genotypes mentioned. Each piece of paper was placed in the bottom of large, round petri dishes and one millilitre of purified water was applied to the filter paper using a Milli-Q® dispenser. Seeds of each genotype were sprinkled onto the moist paper and the dishes were closed with a lid. The petri dishes were stacked in bins that contained a layer

of wet paper towel in the bottom to provide moisture over an extended period of time. The bins were stored in a 4ºC refrigerated room for four days to break the seeds' dormancy. The bins were then placed in a growth chamber kept at 22 °Celsius and 16 hours day^{-1} of light for 24 hours prior to sowing them.

Each treatment consisted of three trays. Each tray held 40, evenly spaced rockwool cubes measuring 8 cm × 8 cm × 8 cm that were pre-soaked in Hyponex nutrient solution. Rubber covers with a hole in the center we placed on top of each cube to limit algal growth. Plastic labels were placed on each cube to identify the coordinate within the three trays. The three genotypes contained 40 replicates each and were randomized across the three trays. A fine-tipped paint brush was used to place one seed on top of the corresponding rockwool cube.

Treatments and growing conditions. Two treatments were applied for the duration of this experiment. The first consisted of three trays being grown in a climate-controlled cabinet at Unifarm, WUR. The cabinet was set to 16 hours of 200 µmol m^{-2} s^{-1}, 8 hours of no light, 70 percent humidity, 25 °Celsius from 04:30 hours to 19:30 hours and 22 °Celsius from 20:00 hours to 04:00 hours. The lights used in this cabinet are light emitting diodes (LED) and emit a different spectrum than that of the second treatment. Watering of the rockwool cubes took place as needed with Hyponex nutrient solution.

The second treatment consisted of 120 rockwool cubes placed into a single tray and grown in a climate-controlled room at Klima, WUR. The room was set to 15 hours of 200 µmol m^{-2} s^{-1}, 9 hours of no light, 70 percent humidity, 19 °Celsius from 04:30 hours to 19:30 hours and 17 °Celsius from 20 hours to 4 hours. The cubes were automatically watered by bottom-up absorption with an Hyponex nutrient solution according to pre-set time intervals.

Cybrid panel standardization, DNA extraction and library preparations

The cybrid panel used in the tunnel experiment was created in several batches that grew in potentially different conditions. Consequently, variable growing conditions have the potential of effecting the genotypes of the seeds propagated. To compensate for this potential batch effect, the complete panel to-date was grown at the same time and under uniform conditions.

Additionally, DNA from these plants was extracted and library preparations were created subsequent genomic sequencing.

Panel propagation. The same germination methodology used in the tunnel experiment was used in this protocol. Rockwool cubes were presoaked in Hyponex nutrient solution and were placed in rows of four in a plastic tray for a total of 80 cubes per tray. Black rubber covers were placed on the top of each cube to prevent algal growth and each row of four cubes was labelled accordingly to the genotype assigned. A fine tipped paint brush was used to place a single seed on the cubes, resulting in the sowing of four seeds per genotype. The room (Unifarm, WUR) was set to 16 hours of natural sunlight supplemented by fluorescent light, 8 hours of no light, and ~20 °Celsius. The cubes were watered by bottom-up absorption with Hyponex nutrient solution as needed. Following 14 days of growth, two representative plants per genotype were selected to complete the propagation process and the remaining two were discarded. The plants were bound to vertical stakes as they grew.

DNA isolation and library preparation. DNA isolation of the cybrid panel took place as soon as the plants were producing flowers. One mm Zirconia beads were placed in the wells of 96 well plates. Sterile forceps were used to collect and place three terminal buds or 1 cm^2 of juvenile leaf material into the plate's wells. The plates were stored at -20°Celsius until they were needed for the library preparation. The protocols for DNA isolation and library preparation are listed in Supplementary Information (Lists 1 and 2). The verification of sufficient quantities of DNA in each sample was completed through the use of a ThermoFisher Scientific Qubit fluorometer. DNA samples from the panel were taken at random and tested using the Qubit unit's protocol.

Results

Tunnel experiment growing conditions

The seeds were sown in the gauze tunnel at a relatively cool time of the year for the experimental location. Nighttime temperatures during the first week of growth dropped down to as low as

0.5 °Celsius (Extended Data Fig. 1). Similarly, nighttime temperatures after the second week of growth regularly dropped to lows of 0.1 °Celsius. Daytime highs during the experiment were on average 16 °Celsius and the highest temperature of 28 °Celsius was on the 25th day of growth (April 11th). Percent humidity during the experiment ranged between 15.5 and 99.7 percent with an average of 59.3 percent (Extended Data Fig. 2). Ambient carbon dioxide (CO_2) concentration ranged between 331 and 660 parts per million (PPM), with an average of 421 PPM over the duration of the experiment. PAR measurements from both inside and outside the tunnel are plotted in Extended data Fig. 3. PAR fluctuations during peak intensities ranged from 1,834 μmol m^{-2} s^{-1} to 685 μmol m^{-2} s^{-1} over the course of one minute.

Continuous soil readings were taken from one pot for the duration of the experiment of which showed an average electrical conductivity of 56.3 μS cm^{-1}, average soil temperature of 12.5 °Celsius and an average volumetric water content of 8.7 percent. Hose-derived water input to the pots and the quantity of rainfall received is presented in Extended data Fig. 4.

Phenotypes

The experiment resulted in the measurement and analysis of 57 phenotypes total (Extended data Table 2). Eleven of these were related to plant morphology, 43 were photosynthesis related and the remaining three were dry weight, number of days to flowering and specific leaf area. Pearson correlation plots were used to compare phenotypes and determine how much they were correlated to each other. In figure 8 you can see these values for when plasmotype results for all four nucleotypes were combined. The photosynthetic traits such as NPQ and qE are very strongly correlated. Similarly, there is a strong correlation between surface area and dry weight. Conversely, a dry weight is not strongly correlated to "…FqFm…" (Φ_{PSII}). These plots were also made for each separate nucleotype to represent the epistatic effects (Extended data Figures 5-8). In this case there are some striking differences in correlation for the same phenotype, but between different nucleotypes. For example, surface area seems to be very strongly correlated with dry weight in the Bur-0 nucleotype but the correlation is much weaker in the Tanz-0 nucleotype, although still existent.

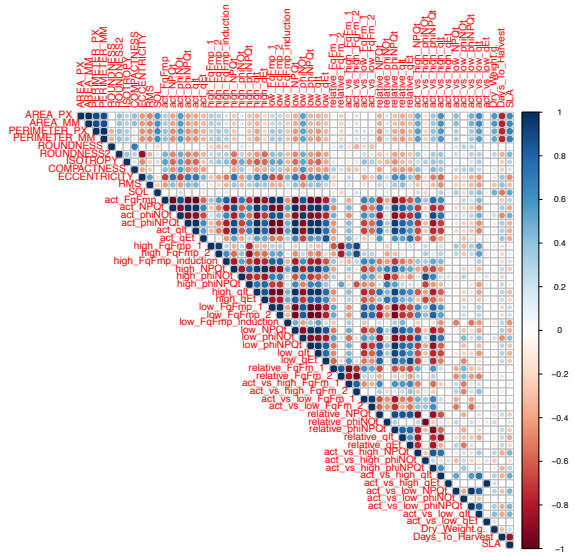

Fig. 8 | Pearson correlation plot for 57 phenotypes from the combined plasmotype from all nucleotypic backgrounds.

The average contributions, over all nucleotypes, to H^2 for the combined analysis from nucleotype, plasmotype and plasmotype-nucleotype interaction was 32.1, 0.2 and 1.8 percent, respectively (Extended data Table 2). H^2 of the phenotypic effects from the nucleotype ranged from 95 percent for dry weight to as low as 0 percent for actinic versus low q_E measurement. H^2 of phenotypes from the plasmotype ranged from 1.2 percent for leaf isotropy to zero percent for high FqFm1 (Φ_{PSII}). The phenotypic H^2 for the plasmotype-nucleotype interaction ranged from five percent for actinic Φ_{NPQ} to zero percent for high FqFm1 (Φ_{PSII}).

A comparison of the three *post hoc* tests resulted in the decision to use the Benjamini & Hochberg method for final interpretation. Over all the nucleotypes, a count of phenotypes for plasmotypes that were significantly different from each other resulted in five plasmotypes that stood out from the others (Fig. 9). The Taz-0 plasmotype resulted in 444 phenotype comparisons, the highest number out of the entire panel. Bur-0, Kas-1, Zin-9 and Yeg-1 plasmotypes also had a noticeably high number at with 427, 290, 252 and 174, respectively.

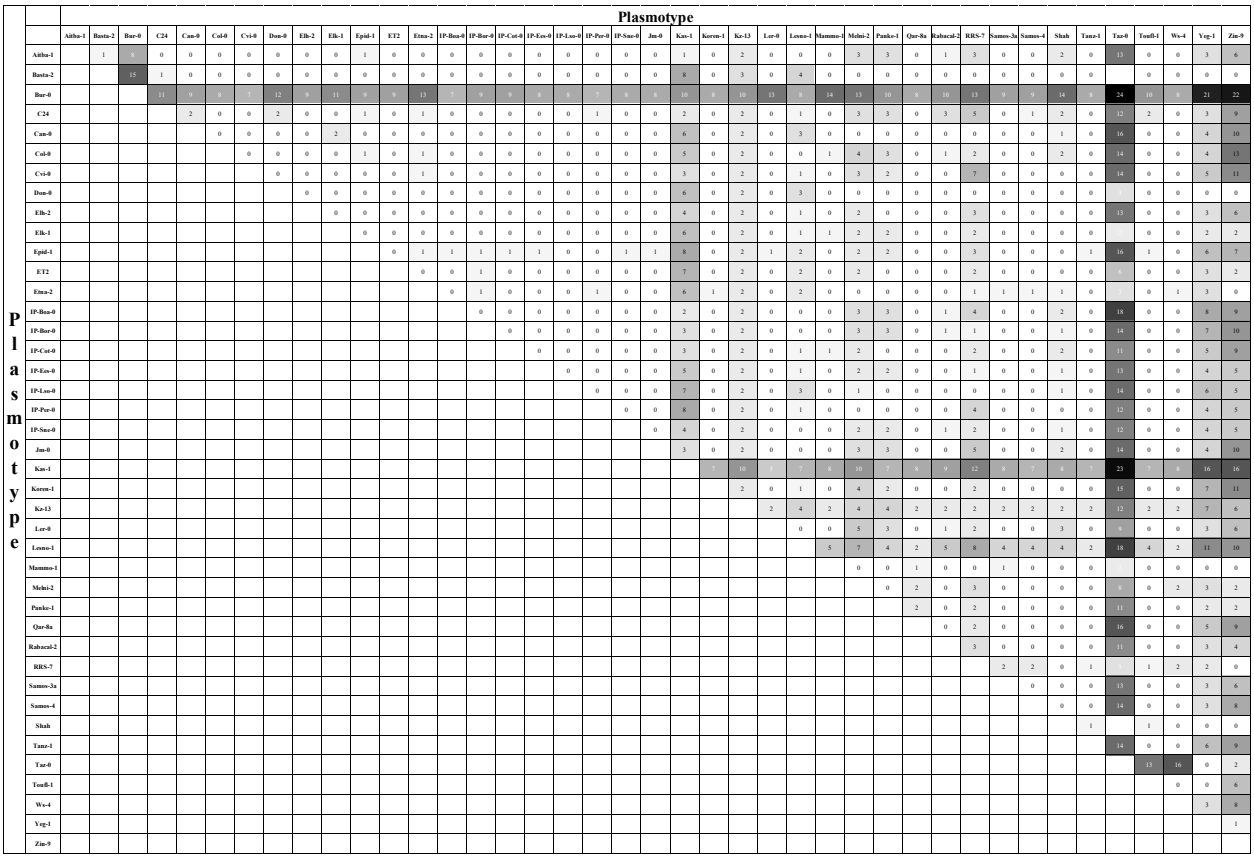

Fig. 9 The number of significantly different phenotypes if a plasmotype was swapped with another plasmotype.

Photosynthetic phenotypes from the "low…" protocol measurements were used for comparisons sake for the remainder of these results because they had the highest H^2 values. Comparisons of the plasmotypes' combined means for all the phenotypes reveal that the Bur-0 plasmotype exhibited the highest level of Φ_{PSII} in the entire panel at 0.668 (Fig. 10). These levels represent a 1.4 percent increase in Φ_{PSII} from the runner-up plasmotype C24 and a 2.3 increase from the average of all plasmotypes. Moreover, the Bur-0 plasmotype was significantly different than the Taz-0 plasmotype with a five percent difference. Furthermore, the Bur-0 plasmotype also exhibited differential levels from the rest of the panel for the photosynthetic phenotypes NPQ (0.57), Φ_{NPQ} (0.115), Φ_{NO} (0.207) and q_E (0.056) (Extended data Figures 9-12). A comparison of the Bur-0 values to the runner-up plasmotypes for the above-mentioned phenotypes resulted in percent increases of 14.2, 11.4, 1.4 and 44.8, respectively.

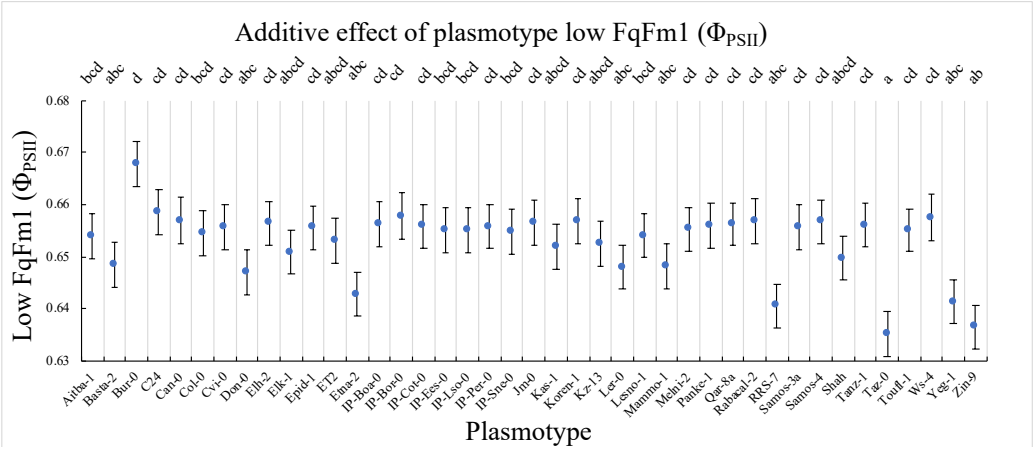

Fig. 10 | The additive effect of plasmotype on Φ_{PSII} from the low FqFm1 measurement. (Benjamini & Hochberg test; letters vary when $P < 0.05$).

The high levels for photosynthetic phenotypes from the Bur-0 plasmotype did not translate to elevated levels in plant surface area and dry weight (Figs. 11 and 12). The Bur-0 plasmotype had mediocre surface area and dry weight means at 1,690 mm^2 and 0.32 grams, respectively. The Can-0 plasmotype had the lowest dry weight of 0.29 grams and was significantly different than the IP-Ees-0 plasmotype and the highest plasmotype for dry weight Kas-1 with 0.358 grams. Although not significantly different from any of the other plasmotypes, Kas-1 still represents a 1.2 percent increase from the runner up IP-Ees-0 and a 11.6 percent increase from the photosynthetically distinct Bur-0 plasmotype. Similarly, Kas-1 was significantly different from the rest of the panel for surface area with a mean of 2,016 mm^2. This is an 11 percent increase in surface area from the runner-up plasmotype, Lesno-1. The Kas-1 plasmotype also resulted in the lowest number of days to flowering at 43.7, although not SD from the rest of the panel (Fig. 13). The plasmotype with the highest SLA was also Kas-1 at 8.04, a nine percent increase from the runner up Lesno-1 (Extended data Fig. 13).

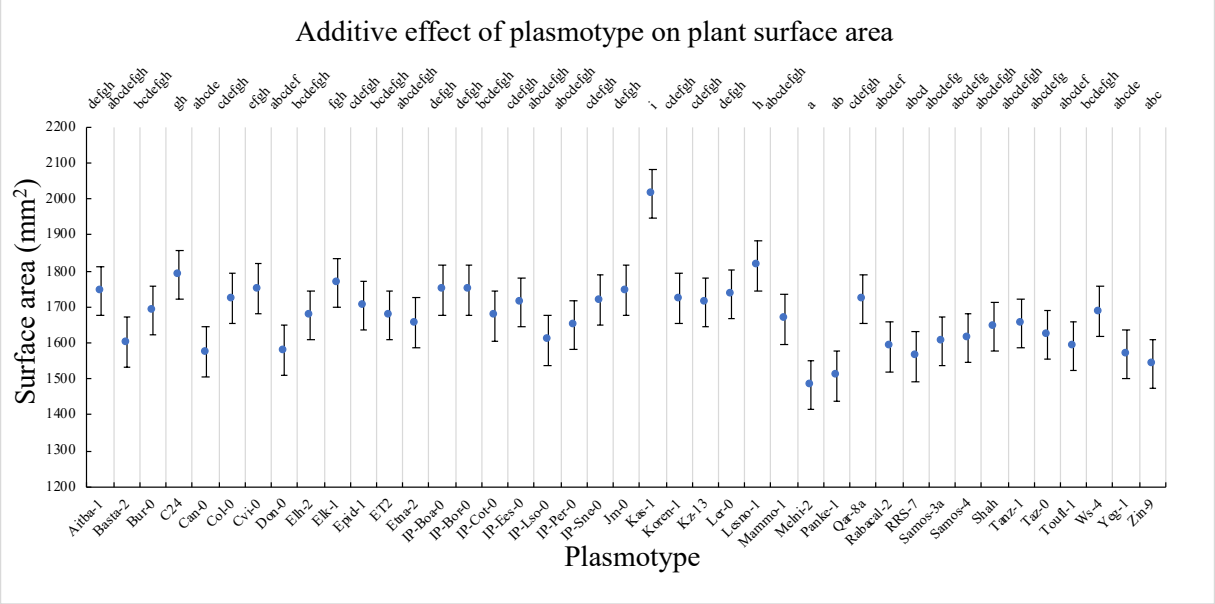

Fig. 11 | The additive effect of plasmotype on plant surface area. (Benjamini & Hochberg test; letters vary when $P < 0.05$).

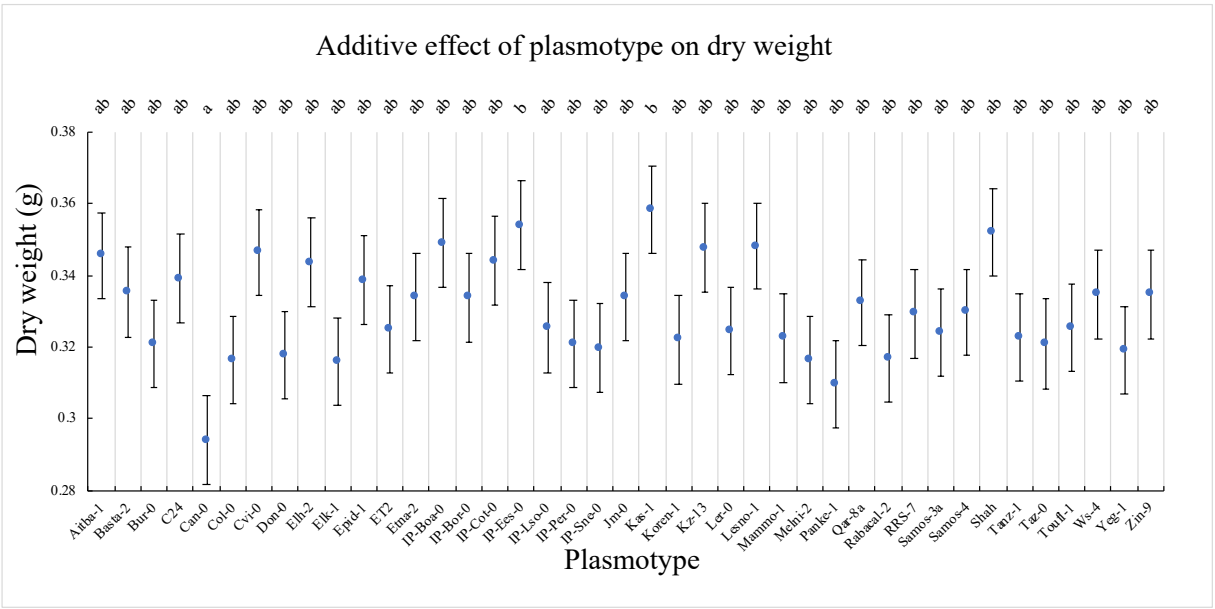

Fig. 12 | The additive effect of plasmotype on dry weight. (Benjamini & Hochberg test; letters vary when $P < 0.05$).

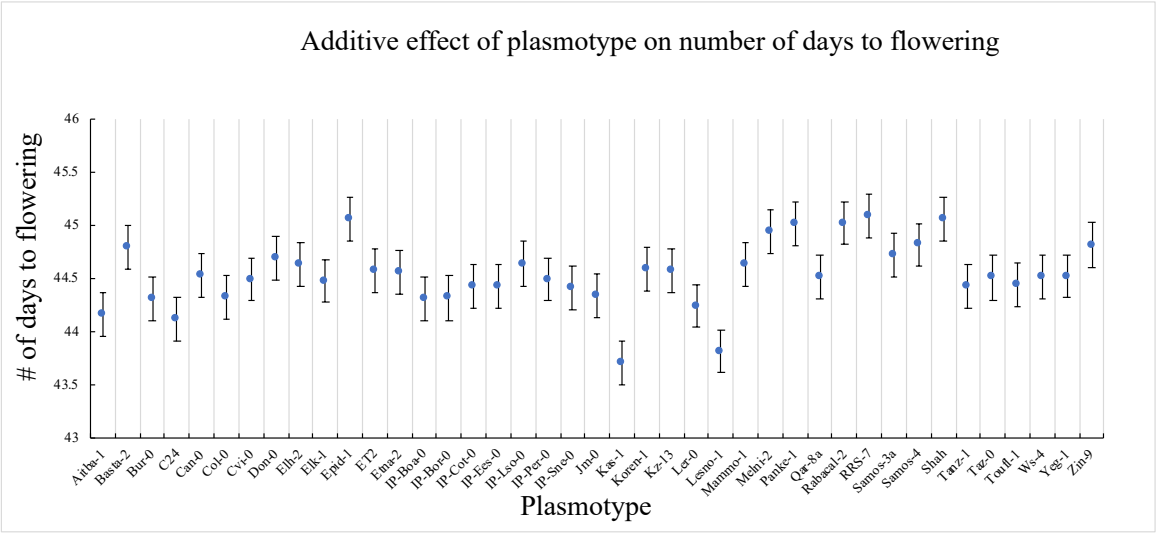

Fig. 13 | The additive effect of plasmotype on number of days to flowering. (Benjamini & Hochberg test; letters vary when $P < 0.05$).

The high phenotype count for plasmotype differences (Fig. 9) for the aforementioned Zin-9, Yeg-1 and Taz-0 plasmotypes were mainly driven by low performance in the photosynthetically related phenotypes (Extended data Figures 9-12). The Taz-0 plasmotype was the lowest for Φ_{PSII} at 0.635 and was significantly different than many other plasmotypes. Taz-0 was also noticeably high for NPQ at 0.997 and was significantly different than many other plasmotypes. This low performing plasmotype was significantly different from all plasmotypes except for three in q_E and exhibited similar differentiation for Φ_{NO}, and Φ_{NPQ} (Extended data Figures 9-12).

Epistatic effects from the plasmotype-nucleotype interaction can be visualized by looking at how each plasmotype performed within each nucleotype. Furthermore, the H^2 of the plasmotypes effect on phenotype within each nucelotype provides a basis for subsequent interpretation (Extended Table. 3). The average plasmotype derived H^2 from all the phenotypes for nucleotype donors Bur-0, Col-0, Cvi-0 and Tanz-1 was 1.82, 3.82, 5.85 and 2.52 percent, respectively. The highest H^2 for photosynthetic phenotypes across all nucleotype donors was from the "low…" measurements in the protocol. These values ranged from a H^2 of 24.73 percent for Φ_{PSII} in the Bur-0 nucleotype to 4.01 percent in the Tanz-1 nucelotype. Morphological phenotypes ranged from 17.5 percent for dry weight in the Cvi-0 nucleotype to 2.18 percent in the Tanz-1 nucleotype.

The number phenotypes for significantly different plasmotypes when compared to the nucleotypes WT can be seen in figure 14. Most of the epistatic effects occur within the Bur-0

plasmotype. Additionally, most of the epistatic changes summed over the nucleotypes arise in the Zin-9 (52), Yeg-1 (44), Taz-0 (42), IP-Bor-0 (36) and Bur-0 (27) plasmotypes.

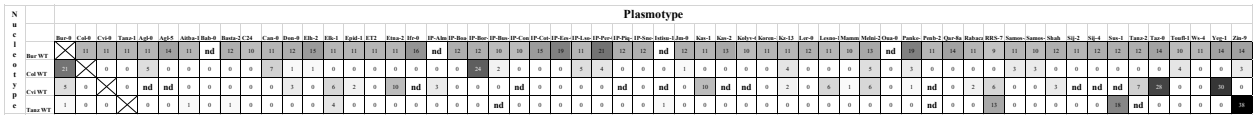

Fig. 14 | The number phenotypes for significantly different plasmotypes when compared to the nucleotypes WT. (Dunnet's test; phenotypes significantly different when $P < 0.05$).

Epistatic effects of plasmotype on Φ_{PSII} were most pronounced from measurements taken at the "low…" time points in the protocol, therefore, the remainder of the photosynthetically related epistatic results will be drawn from these measurements. Observation of epistatic effects for each individual phenotype provide a visual of how nucleotype and the plasmotype-nucleotype interaction contributes to the phenotype. For example, the high additive effects of the Kas-1 plasmotype on plant surface area can be dissected as shown in figure 15. It now becomes apparent that the majority of this Kas-1 plasmotype effect is driven by the Col-0 and Cvi-0 nucleotypes. That said, Kas-1 was also above average for plant surface area in the Bur-0 and Tanz-1 nucleotypes, showing some level of contribution from all nucleotypes. Other than Kas-1 and the occasional outliers in the Cvi-0 nucleotype, the nucleotypes seem to be relatively stable with little variation among plasmotypes for plant surface area. The results from all multiple comparison tests for nucleotype-specific phenotypes can be found in Extended Data Table 4.

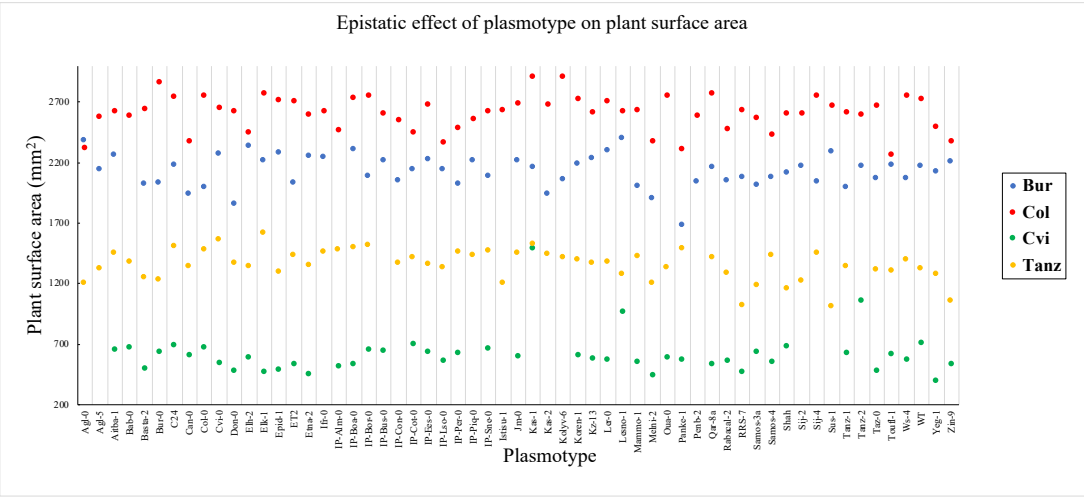

Fig. 15 | The epistatic effects of plasmotype on plant surface area.

The epistatic effect of plasmotype on dry weight is also relatively stable across nucleotypes (Fig. 16). Similar to plant surface area, Kas-1 dry weight is highly driven by the Col-0 and Cvi-0 nucleotypes with Bur-0 and Tanz-1 contributions on average and above average, respectively. Epistatic effects of plasmotype on Φ_{PSII} for the Bur-0 plasmotype are noticeable higher than all the other plasmotypes (Fig. 17). Furthermore, the highest intra-nucleotype deviations from the mean can be seen in the Col-0 and Cvi-0 nucelotypes. The Cvi-0 nucelotype shows a high level of variation among plasmotypes for Φ_{PSII} with a range from 0.676 for Bur-0 plasmotype to 0.581 for the Taz-0 plasmotype. Additionally, the Bur-0 plasmotype had the highest biomass of all plasmotypes within the Col-0 nucleotype. The IP-Bor-0_Col-0 cybrid also shows an even higher Φ_{PSII} value than Bur-0_Col-0 at 0.647.

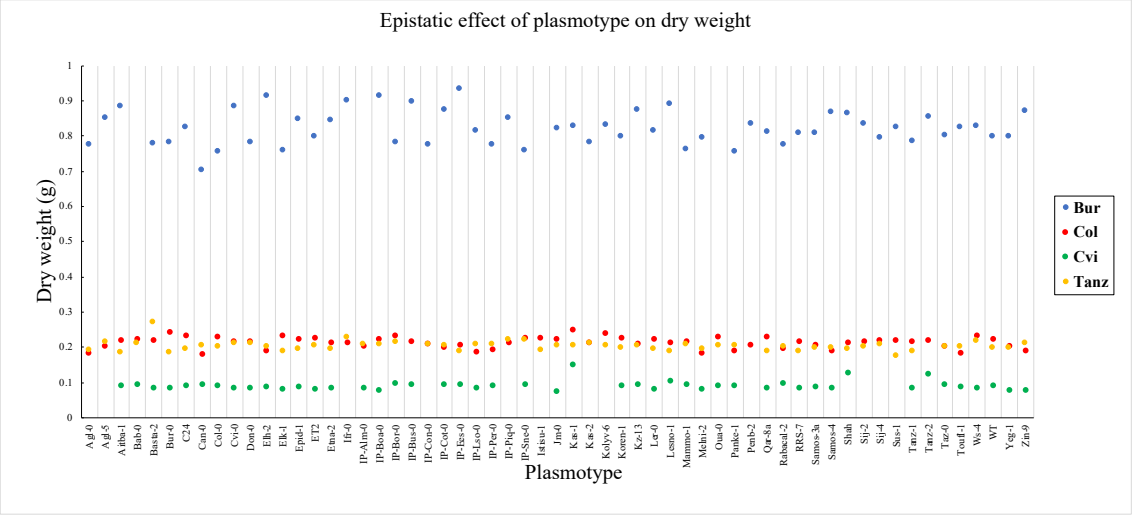

Fig. 16 | The epistatic effects of plasmotype on dry weight.

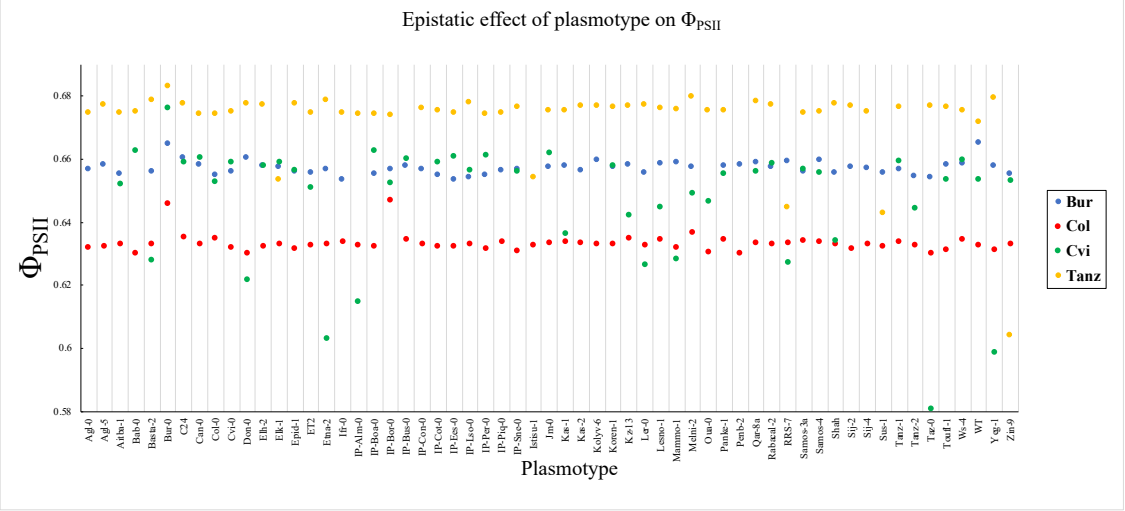

Fig. 17 | The epistatic effects of plasmotype on Φ_{PSII} .

Epistatic effects of plasmotype for NPQ, Φ_{NPQ}, Φ_{NO}, and q_E followed a similar pattern to that of Φ_{PSII} (Extended data Figures 14-17.). The Bur-0 plasmotype had consistently lower levels across all nucleotypes for these phenotypes. Similarly, XXX_Cvi-0 cybrids were highly variable for NPQ, Φ_{NPQ}, Φ_{NO}, and q_E phenotypes (Extended data Figures 14-17.)

Epistatic interactions were further analyzed through the use of a Dunnet's test to reveal any significant differences of plasmotypes compared to the WT of their nucleotype background (Extended data Table 5). A comparison of the Kas-1 plasmotype to the WT of its nucleotype backgrounds for plant surface area and dry weight reveal that it is significantly different for both phenotypes but only in the Cvi-0 nucleotype (Figs. 18-19). The Bur-0 plasmotype compared to the WT of its nucleotype background for Φ_{PSII} resulted in the only significant difference arising from the Col-0 nucleotype (Fig. 20).

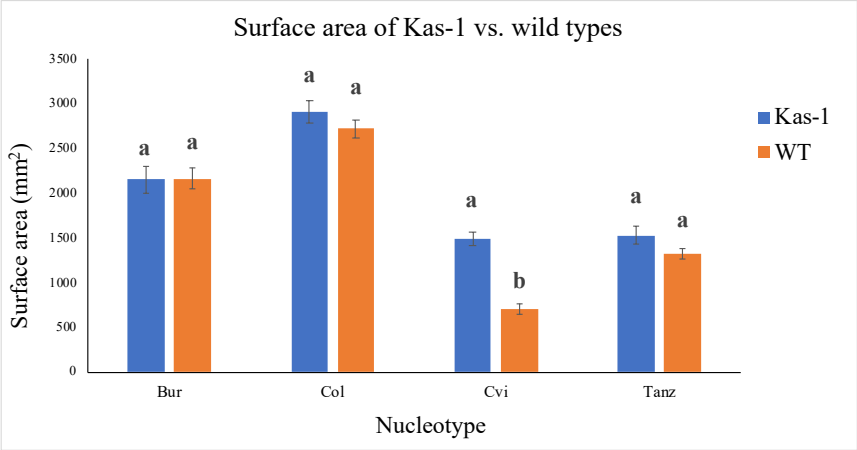

Fig. 18 | Comparison of the Kas-1 plasmotype to the WT of its nucleotype background for surface area. (Dunnet's test; letters vary when $P < 0.05$).

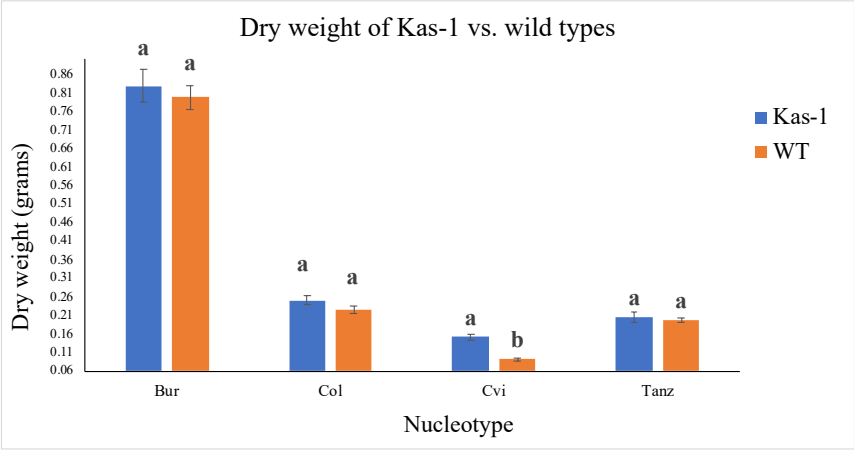

Fig. 19 | Comparison of the Kas-1 plasmotype to the WT of its nucleotype background for dry weight. (Dunnet's test; letters vary when $P < 0.05$).

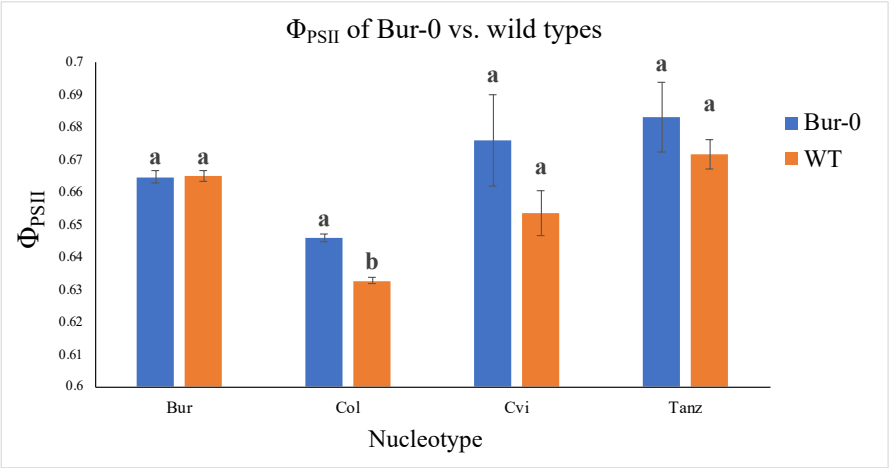

Fig. 20 | Comparison of the Bur-0 plasmotype to the WT of its nucleotype background for Φ_{PSII}. (Dunnet's test; letters vary when $P < 0.05$).

Panke-1_Bur-0 heat sensitivity experiment

The tunnel experiment resulted in 5/12 of the Panke-1_Bur-0 replicates exhibiting a deviant leaf phenotype as opposed to the rest of the Bur-0 nucleotype background plants (Fig. 7.a). A subsequent experiment occurred to test for the genotype's potential sensitivity to heat. The 26 °Celsius heat treatment resulted in 12/40 of the Pank-1_Bur-0 replicates with the curled leaf phenotype (Figs. 21 and 22). None of the WT Panke-1 or the WT Bur-0 plants had curled leaves. Moreover, the 19 °Celsius control treatment yielded similar results with 9/40 of the Pank-1_Bur-0 replicates with the curled leaf phenotype. The control treatment did not result in the curled leaf phenotype in any of the WT Panke-1 or the WT Bur-0 replicates.

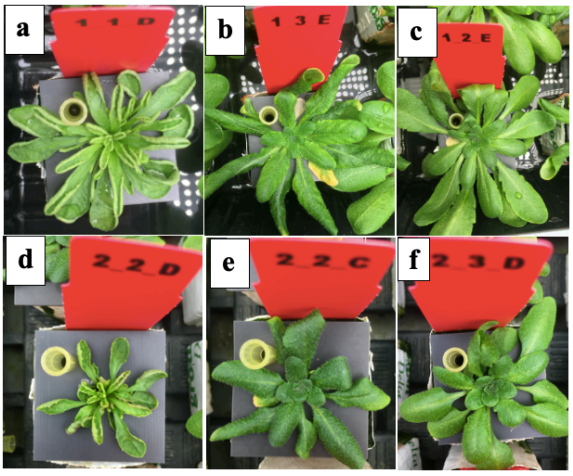

Fig. 21 | Example plants grown in two treatments. The top row are plants grown in the 26 °Celsius heat treatment and those in the bottom row are plants grown in the 19 °Celsius control treatment. **a and d,** Panke-1_Bur-0. **b and e,** WT Panke-1. **c and f,** WT Bur-0.

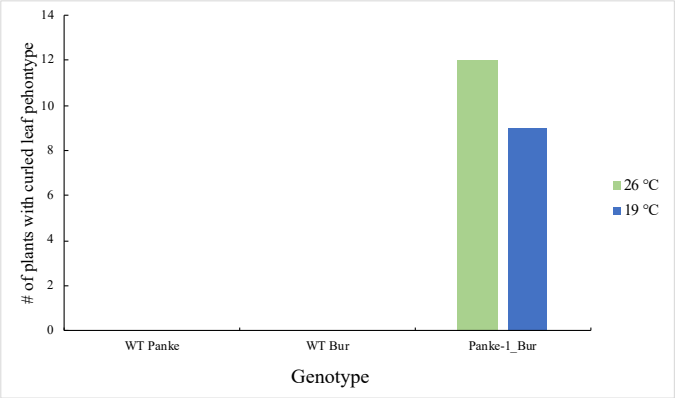

Fig. 22 | The number of WT Panke-1, WT Bur-0 and Panke-1_Bur-0 plants with the curled leaf phenotype under two temperature treatments. None of the WT plants displayed the curled leaf phenotype. 40 replicates grown for each genotype.

Cybrid panel standardization, DNA extraction and library preparations

The propagation of the cybrid panel under standard growing conditions resulted in 220 of the lines growing to maturity and producing seeds for storage. The Cvi nucleotype lines 2_Aitba-1_Cvi and 3_Panke-1_Cvi_1.2 were unsuccessful at growing to maturity and producing seeds.

DNA extraction from the 220 above mentioned lines was verified as successful following gel electrophoresis imaging. Sufficient quantities of DNA in each sample was verified through the use of the Qubit unit. The library preparations were eventually completed but remained out of the scope of this thesis project.

Discussion

Tunnel experiment

Experimental conditions in the tunnel facilitated sufficient growth and provided a high level of uniformity to all the plants. That's said, cold temperatures during the first week of growth undoubtable delayed growth of the seedlings. Although all the plants seemingly recovered uniformly, some of the plasmotype and/or nucleotype backgrounds may have been better prepared to rebound due to their phylogeny and geographic origins. For example, a cybrids

genome may be better equipped for these conditions if it originated from a colder climate. There is the possibility that this influenced some of the resulting phenotypes, particularly morphological ones such as dry weight and plant surface area. Sunlight was deemed to be uniformly distributed across the tunnel due to few exterior structures to block incoming radiation. There was no observed damage to the plants due pest interference such as slugs or thrips. The sand-soil ratio and nutrient content did not seem to limit growth in any way. The plant roots were just slightly visible around the pot edge when the soil was removed after completion of the experiment. The size of these pots seemed to be ideal for limiting root inhibition for the duration of this experiment. However, if plants are to grow to later life stages in subsequent experiments, a larger pot may be considered. Although water distribution was relatively uniform among all plants, the pots on the outer edges of the rows dried out much quicker than those closer to the center. This had a quantifiable effect on the survivability of plants in these positions during the seedling stage and was corrected for as described in the above sections. This limitation also may have limited the growth potential for plants at later stages. To prevent this issue in subsequent experiments, one may consider an unlimited, bottom-up watering method or sowing border plants there that are not intended to be included as part of the analysis.

The original methodology for measuring photosynthetically related phenotypes included the use of a handheld unit that could be used in the tunnel. Measuring these phenotypes *in situ* would have been ideal to observe photosynthesis performance in "natural conditions". This method was ultimately abandoned due to the small size of the plant leaves and the inability to fit the handheld unit around them. The use of the Robin presented a potential risk of having the plants adapt to unrepresentative temperature and PAR levels while they waited in greenhouse conditions to be measured. However, observations of how the plants performed over time did not yield any evidence for significant differences between plants that had time to adapt to greenhouse conditions and those that did not. Although the Robin was an optimal tool for measuring all the desired phenotypes, an *in situ* protocol would be advantageous for subsequent experiments and to obtain more time/adaption sensitive phenotypes. The Robin was able to account for measurements such as NPQ with short dark and infrared periods, however, longer adaption periods are needed for higher accuracy and comparability. For example, NPQ and its components need a minimum of 20 minutes dark adaption to take accurate and comparable

measurements (Harbinson, 2013). Both the lengthiness of the protocol (needed for dark adaption) and the shortness (needed to be able to analyze so many replicates over the day) of the Robin protocol limited the accuracy of these measurements for comparison to results from chamber experiments such as those from Flood and Theeuwen *et al.* (2020).

Data analysis began by identifying and removing outliers based on the threshold of greater than two standard deviations from the left of the mean weight within their genotype. This method was mainly directed to reduce variation due to the plants on the tray edge experiencing dryer conditions than those in the center. Plants that were two standard deviations to the right of the mean remained in the analysis because there were no identifiable factors that unproportionally favoured the growth over others. This initial method is necessary because the unbalanced, incomplete block design is not able to fully correct for this because it assumes that all the conditions within block (tray) are uniform, which they weren't. Future experiments of this sort may consider dealing with this border effect by sowing cybrids at random in these border positions that are not intended to be included in the analysis.

Several methods for multiple comparison tests were compared to identify which was the most appropriate for this experiment. Results from Fisher's LSD, Tukey's HSD and the Benjamini & Hochberg methods all highlighted the fact that that chances of seeing significant differences for additive effects amongst plasmotypes was greatly reduced due to the size of the cybrid panel. The comparison of 59 different cybrids for 57 different phenotypes resulted in over 20,000 comparisons per phenotype, drastically increasing the difficulty to find differences. For example, the use of a 95 percent confidence interval would result in the potential for ~1,000 false negatives with the quantity of comparisons in this experiment. Due to these observations, the Benjamini & Hochberg method was used as it was the least stringent on finding significant differences. However, even the Benjamini & Hochberg method can also be considered too stringent for this quantity of comparisons. Subsequent experiments should focus on higher replicate numbers of the most promising candidate plasmotypes from this experiment and new plasmotypes.

Mean H^2 values across all phenotypes were relatively low compared to the study by Flood and Theeuwen *et al.* (2020). As such, Theeuwen *et al.* (2020) reported plasmotype-derive additive H^2 of 91.9, 2.9 and 5.2 percent from nucleotype, plasmotype and the plasmotype-nucleotype interaction, respectively, when the Ely plasmotype was excluded. Alternatively, this

study reported H^2 values of 32.1, 0.2 and 1.8 percent from nucleotype, plasmotype and the plasmotype-nucleotype interaction, respectively. However, the set of 57 phenotypes resulted in a wide range of H^2 percentages, some of which were very low. The proportion of low-percent phenotypes was even further exacerbated by that fact that many of these phenotypes were highly correlated or redundant as indicated in the Pearson correlation plots. The analysis in this experiment included all the phenotypes for calculating mean H^2, although this data can be interpreted in many different ways. For example, by setting a minimum threshold such as 2 percent H^2, irrelevant and correlated phenotypes would not be included, hence reporting a more accurate mean. Regardless, it is always more appropriate to interpret a specific phenotypes H^2 for plasmotypes that are of particular interest and significantly different than others.

This tunnel experiment clearly supports the hypothesis of Flood and Theeuwen *et al.* (2020) of the elevated, additive potential of the Bur-0 plasmotype for photosynthetic capabilities. However, the results of this experiment do not indicate an increased effect that outdoor growth has on the phenotypes of these plasmotypes. Comparison of Φ_{PSII} levels from Flood and Theeuwen *et al.* (2020) and the tunnel experiment seem to indicate undetectable differences. The Bur-0 plasmotypes high performance in Φ_{PSII} was the highest of all plasmotypes at 0.668 but was only significantly different than a select few of the other plasmotypes. However, the Bur-0 was still 1.4 percent higher than C24, the runner-up plasmotype with 0.659 and significantly different than the Taz-0 plasmotype, with a difference of 5 percent between the two. In addition, this high photosynthetic capability of Bur-0 may have contributed to the plasmotype's notable 8.8 percent increase in dry weight when compared to the Bur-0 WT. Alternatively, differences between the two experiments began to be noticeable when the patterns from the Flood and Theeuwen *et al.* (2020) experiment were mimicked, but significantly different in the Bur-0 NPQ coefficient q_E. Although the additive effect of the Bur-0 plasmotype on q_E was comparable between the tunnel experiment and that of Flood and Theeuwen *et al.* (2020), differences between the epistatic effects were strikingly different. There were also significant differences between the two, however, these phenotypes are largely incomparable between the two experiments because NPQ and its components are highly dependent on dark adaption and timing of measurement, as explained above.

Plasmotypes with a Cvi-0 nucleotype exhibited high variation for several phenotypes including Φ_{PSII}, NPQ, Φ_{NO}, Φ_{NPQ}, q_E and number of days to flower. Although these epistatic

interactions do not contribute much to the focus of this study, it is important to recognize these patterns. The erratic behaviour of the Cvi-0 nucleotype across several phenotypes suggest that the nuclear genome has a high level of plasticity in how it interacts with other plasmotypes. Although crossing and segregating populations, Alonso-Blanco *et al.* (1998) observed similar results in Cvi-0. The introgression of Cvi-0 alleles into the Ler-0 background allowed the Ler-0 plants to be largely day length neutral for flowering compared to the WT which was highly sensitive to day length. In addition, Cvi-0 has been observed as showing high levels of variance for several phenotypes including temperature, leaf size, height, number of siliques and silique length (Suter and Widmer, 2013). Furthermore, ancestral heat treatment seemed to increase the variance of these phenotypes (Suter and Widmer, 2013). Future experiments may consider growing the Cvi-0 nucleotype background in a growth chamber as to obtain the most uniform conditions possible. This high level of "plasticity" that the nuclear genome of Cvi-0 further highlights the complexities and difficulties of unravelling cyto-nuclear interactions.

Evidence for additive effects from the Bur-0 plasmotype are now mounting and require further exploration. This is encouraging considering that the elevated Φ_{PSII} levels in the Bur-0 plasmotype are similarly high to those found from loci in the nuclear genome of *A. thaliana* (van Rooijen *et al.*, 2017). The annotation of sequence variation for previous Bur-0 lines indicated that there are no large effect mutations in the mitochondria, eliminating this as a possible explanation (Flood and Theeuwen *et al.*, 2020). Four unique missense variants and their resulting genes were, however, observed in the plastid genes (Flood and Theeuwen *et al.*, 2020). The *NAD(P)H-QUINONE OXIDOREDUCTASE SUBUNIT 6 (NDHG)* gene was particularly notable as it completes several functions for NPQ functioning in the thylakoid membrane (Strand *et al.*, 2017). Confirmation of these missenses variants and subsequent experimentation is needed though to advance the understanding of this plasmotypic variation. Sequencing of the cybrid panel used in the tunnel will help confirm the presence of previously detected and novel missense variants. In addition to reproducing the outdoor experiment again in the spring and in the fall/winter months, ensuing efforts could include chloroplast transformations of the Bur-0 plasmotype to verify the effects of knock-out lines or allelic complementation in the case that knock-out lines result in lethality.

An additional noteworthy finding from the tunnel experiment was the observation of significant, morphological phenotypes of the Kas-1 plasmotype. The 11 percent difference with

the second highest competitor for plant surface area is fascinating and calls for further investigation. Similarly, the elevated levels of dry weight from the Kas-1 plasmotype may not be significantly different than the others but is an encouraging addition to the increase in plant surface area. Although these effects are mainly driven by the Cvi-0 and Col-0 nucleotype backgrounds, they can be considered as highly additive considering their significant difference from other plasmotypes when analyzed in combination. Furthermore, correlation of surface area and dry weight is relatively strong, however, the correlation with photosynthetic parameters is quite low. Unfortunately, the scope and timeline of this project did not permit any SNP analysis to determine the presence of any missense variants with the other plasmotypes. Alternatively, literature review yielded one possible explanation for this which indicates this difference could be related to the plastid-localized, NADPH-dependent thioredoxin reductase C (NTRC) NTR enzyme. This NTR enzyme contains reductase and thioredoxin domains that, when knocked out, results in reduced leaf size and floret biomass in *A. thaliana* (Lepisto *et al.*, 2013). Similarly, the overexpression of *NTRC* genes in wild type plants resulted in increased leaf size and rosette biomass (Toivola *et al.*, 2013). Additionally, these growth-enhancing proteins are able to interact with other thioredoxin systems, increasing its utility for increased growth (Toivola *et al.*, 2013). Hence, elevated copy number variation of *NTRC* genes in the plastid genome of the Kas-1 plasmotype may explain its relatively high levels of surface area and dry weight. Dry weight and surface area phenotypes are highly complex though and are influenced by hundreds, if not thousands in *Arabidopsis*. Regardless, similar to the prospects of Bur-0, analysis of missense variants for the Kas-1 sequencing results could help in determining the genetic explanation for these extraordinary phenotypes and be advantageous for breeding initiatives.

Panke-1_Bur-0 deviant phenotype

Considering the deviant, curled leaf phenotype was not observed in the parental lines of the Panke-1_Bur-0 cybrid under both temperature treatments, it can be postulated that temperature is not the causal factor for the resulting phenotype. Therefore, the 1:4 ratio of positively observed to negatively observed phenotype in the Panke-1_Bur-0 cybrid for both the tunnel experiment and the temperature experiment indicates that there is a 1:4 segregation of the trait. Several studies point to an over deposition of secondary cell wall to explain very similar looking leaves

containing the curled phenotype (Liu *et al.,* 2013; Zhou *et al.*, 2009; Ko *et al.*, 2009; Zhong *et al.*, 2013). Transcription factors MYB46 and MYB83 are known to be master switches of secondary cell wall biosynthesis and could be over expressed in the Panke-1_Bur-0 cybrid resulting in the observed phenotype (Zhong *et al.*, 2013; Kim *et al.*, 2012). Furthermore, this could be the result of incomplete chromosome elimination during the haploid induction stage of cybrid creation, a phenomenon previously observed in similar genome modifications (Tan *et al.*, 2015). However, conformation of these hypotheses would require further analysis of segregation ratios and transcriptomics.

Conclusions

The results of this study add to the evidence that phenotypic variation exists among plasmotypes of the *A. thaliana* ecotypes. In addition, variation in physiological phenotypes is present in a panel with a broader set of cybrids. Although it remains largely inconclusive as to whether or not testing these effects in outdoor growing conditions even further enhances these differences, there is now a platform of experimentation that provides reflection for future efforts that may include the measurement of even more phenotypes and environmental conditions. The repetition of high Φ_{PSII} levels in the Bur-0 plasmotype is encouraging for future efforts to determine the underlying genetic mechanisms. The identification of genes contributing to these additive effects has the potential of being useful for breeding efforts in crop varieties. Similarly, the Kas-1 plasmotype has cautious potential for holding clues into the role of plastid genes on morphological phenotypes that increase yields. The identification of the source of this natural variation could prove to be highly applicable for both conventional and non-conventional breeding efforts.

References

1001 Genomes Consortium. (2016) 1,135 Genomes Reveal the Global Pattern of Polymorphism in *Arabidopsis thaliana*. *Cell* 166(2): 481-491.

Alonso-Blanco, C. *et al.* (2016) 1,135 genomes reveal the global pattern of polymorphism in Arabidopsis thaliana. *Cell*, 166(2): 481-491.

Alonso-Blanco *et al.* (1998) Analysis of Neutral Allelic Variation at Flowering Time Loci in the Landsberg *erecta* and Cape Verde Islands Ecotypes of *Arabidopsis thaliana. Genetics Society of America.* 149: 749-764.

Bates, D. *et al.* (2015) Fitting linear mixed-effects models using lme4. *J. Stat. Softw*. 67, 48.

Berry. J. O. *et al.* (2013) Photosynthetic gene expression in higher plants. *Photosynth. Res.* 117:91-120.

Cullis, C. A. *et al.* (2009) Transfer of genetic material between the chloroplast and nucleus: how is it related to stress in plants? *Annals of Botany* 103(4): 625-633.

Daniell, H. *et al.* (2016) Chloroplast genomes: diversity, evolution, and applications in genetic engineering. *Genome Biology* 17: 134

Douglas, A. E. and Raven J. A. (2003) Genomes at the interface between bacteria and organelles. *Phil. Trans. R. Soc. London* 358: 5-18.

Durvasula, A. *et al.* (2017). African genomes illuminate the early history and transition to selfing in *Arabidopsis thaliana. Proceedings of the National Academy of Sciences*, 114(20) : 5213-5218.

Estavillo G. M. *et al.* (2011) Evidence for a SAL1–PAP chloroplast retrograde pathway that functions in drought and high light signaling in Arabidopsis. *Plant Cell* 23: 3992–4012.

Fulgione, A. *et al.* (2017). Madeiran *Arabidopsis thaliana* reveals ancient long-range colonization and clarifies demography in Eurasia. Molecular biology and evolution, 35(3): 564-574.

Green, B. R. (2011) Chloroplast genomes of photosynthetic eukaryotes. *The Plant Journal* 66: 34-44.

Glaßer *et al*. (2014) Meta-Analysis of Retrograde Signaling in *Arabidopsis thaliana* Reveals a Core Module of Genes Embedded in Complex Cellular Signaling Networks. *Molecular Plant* 7: 1167-1190.

Gould, S. B. *et al.* (2008) Plastid evolution. *Annu Rev Plant Biol* 59:491-517.

Harbinson, J. (2013) Improving the accuracy of chlorophyll fluorescence measurements. *Plant, Cell and Environment* 36, 1751–1754.

Henze, K. and Martin, W. (2001) How do mitochondrial genes get into the nucleus? *TRENDS in Genetics* 17: 383-387.

Herrmann, R.G. (1997) Eukaryotism, Towards a New Interpretation. In: Schenk H.E.A., Herrmann R.G., Jeon K.W., Müller N.E., Schwemmler W. (eds) Eukaryotism and Symbiosis. Springer, Berlin, Heidelberg

Joseph, B. *et al.* (2103) Cytoplasmic genetic variation and extensive cytonuclear interactions influence natural variation in the metabolome. *eLife* 2, e00776.

Kim, W. *et al.* (2012) Identification of a cis-acting regulatory motif recognized by MYB46, a master transcriptional regulator of secondary wall biosynthesis. *Plant Mol Biol* 78:489-501.

Kleine, T. and Leister, D. (2016) Retrograde signalling: Organelles go networking. *Biochimica et Biophysica Acta* 1857: 1313-1325.

Ko, J. *et al.* (2009) Ectopic expression of MYB46 identifies transcriptional regulatory genes involved in secondary wall biosynthesis in *Arabidopsis. The Plant Journal* 60: 649-665.

Koussevitzky, S. (2007) Signals from chloroplasts converge to regulate nuclear gene expression. *Science* 316: 715–719.

Leister, D. (2005) Genomics-based dissection of the cross-talk of chloroplasts with the nucleus and mitochondria in *Arabidopsis. Gene* 354: 110-116.

Lepisto, A. *et al.* (2013) Deletion of chloroplast NADPH-dependent thioredoxin reductase results in inability to regulate starch synthesis and causes stunted growth under short-day photoperiods. *Journal of Experimental Botany* 64, 12: 3843–3854.

Lin, X. Y. *et al.* (1999) Sequence and analysis of chromosome 2 of the plant *Arabidopsis thaliana. Nature* 402, 761–768.

Lin, Z. *et al.* (2007) The origins and early evolution of DNA mismatch repair genes–multiple horizontal gene transfers and co-evolution. *Nucleic Acids Res*. 35: 7591–7603.

Lind, J. An exploration of the physiological effect og cytoplasmic variation on cyto-nuclear interactions in *Arabidopsis thaliana*. Masters thesis. Wageningen University and Research.

Liu, B. *et al.* Characterization, efficient transformation and regeneration of *Chirita pumila* (Gesneriaceae), a potential evo-devo model plant. *Plant Cell Tiss Organ Cult* 118: 357-371.

López-García P. *et al.* (2017) Symbiosis in eukaryotic evolution. *Journal of Theoretical Biology* 434: 20-33.

Martin, W. & Mentel, M. (2010) The Origin of Mitochondria. *Nature Education* 3(9):58.

McFaddin, G. I. (1999) Endosymbiosis and evolution of the plant cell. *Current Opinion in Plant Biology* 2:513–519.

Morley, S. A. and Nielsen B. L. (2017) Plant mitochondrial DNA. *Frontiers in Bioscience* 22: 1023-1032.

Osteryoung, K. W. and McAndrew R. S. (2001) The Plastid Division Machine. *Annu. Rev. Plant Physiol. Plant Mol. Biol.* 52: 315-33.

Parfrey, L. W. *et al.* (2011) Estimating the timing of early eukaryotic diversification with multigene molecular clocks. *PNAS* 108 (33): 13624-13629.

Raghavendra, A.S. and Padmasree, K. (2003) Beneficial interactions of mitochondrial metabolism with photosynthetic carbon assimilation. *Trends Plant Sci*. 8: 546–553.

Ramel F. (2012) Carotenoid oxidation products are stress signals that mediate gene responses to singlet oxygen in plants. *Proc. Natl. Acad. Sci.*109: 5535–5540.

Roux, F. *et al*. (2016) Cytonuclear interactions affect adaptive traits of the annual plant Arabidopsis thaliana in the field. *Proc. Natl Acad. Sci*. 113: 3687–3692.

Sato, S. *et al.* (1999) Complete Structure of the Chloroplast Genome of *Arabidopsis thaliana*. *DNA Research* 6: 283-290.

Schwartz R. M. and Dayhoff M. O. (1978) Origins of Prokaryotes, Eukaryotes, Mitochondria, and Chloroplasts. *Science* 199 (4327): 395-403.

Sloan, D.B. *et al.* (2018) Correction of Persistent Errors in *Arabidopsis* Reference Mitochondrial Genomes. *The Plant Cell* 30: 525–527.

Spang A. *et al.* (2019) Proposal of the reverse flow model for the origin of the eukaryotic cell based on comparative analyses of Asgard archaeal metabolism. *Nature Microbiology* 4: 1138-1148.

Strand, D. *et al.* (2017) The higher plant plastid NAD(P) H dehydrogenase-like complex (NDH) is a high efficiency proton pump that increases ATP production by cyclic electron flow. *Journal of Biological Chemistry* 292, 11850–11860 (2017).

Stupar, R.M. *et al.* (2001) Complex mtDNA constitutes an approximate 620-kb insertion on *Arabidopsis thaliana* chromosome 2: Implication of potential sequencing errors caused by large- unit repeats. Proc. Natl. Acad. Sci. U. S. A. 98, 5099–5103

Suter, L. and Widmer, A. (2013) Phenotypic Effects of Salt and Heat Stress over Three Generations in *Arabidopsis thaliana*. *PLOS one* 8:11.

Tan, E. H. *et al.* (2015) Catastrophic chromosomal restructuring during genome elimination in plants. *eLife* DOI: 10.7554/eLife.06516.

Tang, Z. *et al*. (2014) Potential involvement of maternal cytoplasm in the regulation of flowering time via interaction with nuclear genes in maize. *Crop Science* 54: 544–553.

The Arabidopsis Genome Initiative (2000) Analysis of the genome sequence of the flowering plant *Arabidopsis thaliana. Nature* 408: 796-815.

Toivola, J. *et al.* (2013) Overexpression of chloroplast NADPH-dependent thioredoxin reductase in *Arabidopsis* enhances leaf growth and elucidates *in vivo* function of reductase and thioredoxin domains. *Frontiers in Plant Science* 4, 389.

van Rooijen, R. *et al.* (2017) Natural variation of YELLOW SEEDLING1 affects photosynthetic acclimation of *Arabidopsis thaliana*. *Nat Commun* 8, 1421.

Woodson, J. D. *et al.* (2011) Heme synthesis by plastid ferrochelatase I regulates nuclear gene expression in plants, *Curr. Biol*. 21: 897–903.

Xiao, Y. (2012) Retrograde signaling by the plastidial metabolite MEcPP regulates expression of nuclear stress-response genes. *Cell* 149: 1525–1535.

Zhong, R. *et al.* (2013) The Poplar MYB Master Switches Bind to the SMRE Site and Activate the Secondary Wall Biosynthetic Program during Wood Formation. *PLOS one* 8:7.

Zhou, J. *et al.* (2009) MYB58 and MYB63 Are Transcriptional Activators of the Lignin Biosynthetic Pathway during Secondary Cell Wall Formation in *Arabidopsis. The Plant Cell* 21:248-266.

Acknowledgments

The author would like to extend many thanks to everyone who helped realize this project, including: Mark Aarts for his commitment to supporting and guiding students to reach their highest potential; Tom Theeuwen for his guidance, expertise and constant willingness to lend a hard working hand; Bas Zwaan for his valued input and willingness to act as examiner; Jeremy Harbinson *et al.* for their valuable input regarding experimental design and maintenance; Jan Aarts for developing the pot partitioning and green pixel count scripts; Rene Boesten, Frank Becker, Corrie Hanhart and Gema Flores Andaluz for their general help in the project and for help in the sowing process; Andre Maassen and Bert Essenstam at Unifarm for their exceptional support in setting up the experiment; and lastly all the references and previous master's students for their hard work and contributions to get the project to where it is now.

Additional information

Extended data Table 1. Genotypes and quantity of replicates sown in the tunnel experiment.

Bur-0 Nucleoptypes

Plasmotype	No. of replicates
Agl-0	11
Agl-5	11
Aitba-1	11
Basta-2	11
Bur-0	11
C24	11
Can-0	11
Col-0	11
Cvi-0	11
Don-0	11
Elh-2	11
Elk-1	11
Ely	12
Epid-1	12
ET2	12
Etna-2	12
Ifr-0	12
IP-Boa-0	12
IP-Bor-0	12
IP-Bus-0	12
IP-Con-0	12
IP-Cot-0	12
IP-Ees-0	12
IP-Lso-0	12
IP-Per-0	12
IP-Piq-0	12
IP-Sne-0	12
Jm-0	12
Kas-1	12
Kas-2	12
Kolyv-6	12
Koren-1	12
Kz-13	12
Ler-0	12
Lesno-1	12
Mammo-1	12
Melni-2	12
Panke-1	12
Penb-2	12
Qar-8a	12
Rabacal-2	12
RRS-7	12
Samos-3a	12
Samos-4	12
Shah	12
Sij-2	12
Sij-4	12
Sus-1	12
Tanz-1	12
Tanz-2	12
Taz-0	12
Toufl-1	12
Ws-4	12
Yeg-1	12
Zin-9	12
WT	72

Col-0 Nucleotypes

Plasmotype	No. of replicates
Agl-0	12
Agl-5	12
Aitba-1	12
Bab-0	12
Basta-2	12
Bur-0	12
C24	12
Can-0	12
Col-0	12
Cvi-0	12
Don-0	12
Elh-2	12
Elk-1	12
Ely	12
Epid-1	12
ET2	12
Etna-2	12
Ifr-0	12
IP-Alm-0	12
IP-Boa-0	12
IP-Bor-0	12
IP-Bus-0	12
IP-Con-0	12
IP-Cot-0	12
IP-Ees-0	12
IP-Lso-0	12
IP-Per-0	12
IP-Piq-0	12
IP-Sne-0	12
Istisu-1	12
Jm-0	12
Kas-1	12
Kas-2	12
Kolyv-6	12
Koren-1	12
Kz-13	12
Ler-0	12
Lesno-1	12
Mammo-1	12
Melni-2	12
Oua-0	12
Panke-1	12
Penb-2	12
Qar-8a	12
Rabacal-2	12
RRS-7	12
Samos-3a	12
Samos-4	13
Shah	13
Sij-2	13
Sij-4	13
Sus-1	13
Tanz-1	13
Tanz-2	13
Taz-0	13
Toufl-1	13
Ws-4	13
Yeg-1	13
Zin-9	13
WT	80

Cvi-0 Nucleotypes

Plasmotype	No. of replicates
Aitba-1	12
Bab-0	12
Basta-2	12
Bur-0	12
C24	12
Can-0	12
Col-0	12
Cvi-0	12
Don-0	12
Elh-2	12
Elk-1	12
Ely	12
Epid-1	12
ET2	12
Etna-2	12
IP-Alm-0	12
IP-Boa-0	12
IP-Bor-0	12
IP-Bus-0	12
IP-Cot-0	12
IP-Ees-0	12
IP-Lso-0	12
IP-Per-0	12
IP-Sne-0	12
Jm-0	12
Kas-1	12
Koren-1	12
Kz-13	12
Ler-0	12
Lesno-1	12
Mammo-1	12
Melni-2	12
Oua-0	12
Panke-1	12
Qar-8a	12
Rabacal-2	13
RRS-7	13
Samos-3a	13
Samos-4	13
Shah	13
Tanz-1	13
Tanz-2	13
Taz-0	13
Toufl-1	13
Ws-4	13
Yeg-1	13
Zin-9	13
WT	64

Tanz-1 Nucleotypes

Plasmotype	No. of replicates
Agl-0	12
Agl-5	12
Aitba-1	12
Bab-0	12
Basta-2	12
Bur-0	12
C24	12
Can-0	12
Col-0	12
Cvi-0	12
Don-0	12
Elh-2	12
Elk-1	12
Ely	12
Epid-1	12
ET2	12
Etna-2	12
Ifr-0	12
IP-Alm-0	12
IP-Boa-0	12
IP-Bor-0	12
IP-Con-0	12
IP-Cot-0	12
IP-Ees-0	12
IP-Lso-0	12
IP-Per-0	12
IP-Piq-0	12
IP-Sne-0	12
Istisu-1	12
Jm-0	12
Kas-1	12
Kas-2	12
Kolyv-6	12
Koren-1	12
Kz-13	12
Ler-0	12
Lesno-1	12
Mammo-1	12
Melni-2	12
Oua-0	12
Panke-1	12
Qar-8a	12
Rabacal-2	12
RRS-7	12
Samos-3a	12
Samos-4	12
Shah	12
Sij-2	12
Sij-4	12
Sus-1	12
Tanz-1	12
Taz-0	12
Toufl-1	12
Ws-4	12
Yeg-1	12
Zin-9	12
WT	12
WT	76

Extended data Table 2. Additive H^2 values for the phenotypes of the combined analysis of all cybrids.

Phenotype	Nucleotype:Plasmotype	Block	Plasmotype	Row	Nucleotype	Residual
Surface area (px)	1.10%	6.61%	0.33%	1.03%	81.74%	9.19%
Surface area (mm^2)	1.10%	6.61%	0.33%	1.03%	81.75%	9.19%
Perimeter (px)	1.52%	8.05%	0.27%	0.56%	68.98%	20.62%
Perimeter (mm^2)	1.52%	8.05%	0.27%	0.56%	68.98%	20.62%
Roundness	0.92%	3.74%	0.00%	0.00%	41.21%	54.13%
Roundness 2	0.01%	3.04%	0.01%	0.00%	34.52%	62.42%
Isotropy	0.64%	0.00%	1.16%	0.38%	5.81%	92.00%
Compactness	1.79%	1.79%	0.03%	0.00%	50.95%	45.45%
Eccentricity	1.22%	2.48%	0.13%	0.21%	23.24%	72.72%
RMS	0.00%	2.67%	0.07%	0.29%	13.75%	83.22%
SOL	0.32%	7.54%	0.64%	1.61%	44.43%	45.46%
Act. FqFm (Φ_{PSII})	3.32%	20.13%	0.11%	0.00%	16.98%	59.47%
Act. NPQ	4.87%	8.87%	0.09%	0.04%	7.77%	78.36%
Act. Φ_{NO}	1.57%	18.31%	0.11%	0.14%	62.55%	17.32%
Act. Φ_{NPQ}	5.07%	14.19%	0.22%	0.04%	8.16%	72.32%
Act. Φ_{NPQ}	4.93%	6.05%	0.00%	0.00%	6.61%	82.41%
Act. q_E	2.16%	44.17%	0.00%	0.77%	14.45%	38.45%
High FqFm 1 (Φ_{PSII})	0.00%	28.34%	0.00%	0.66%	59.80%	11.20%
High FqFm 2 (Φ_{PSII})	0.00%	30.70%	0.00%	0.46%	51.96%	16.88%
High FqFm induction (Φ_{PSII})	2.08%	18.21%	0.00%	0.43%	35.32%	43.96%
High NPQ	1.07%	24.40%	0.00%	0.61%	16.18%	57.74%
High Φ_{NO}	0.68%	34.94%	0.17%	0.75%	46.98%	16.48%
High Φ_{NPQ}	0.51%	35.63%	0.00%	0.22%	28.21%	35.42%
High q_I	3.79%	4.97%	0.09%	0.15%	17.78%	73.21%
High q_E	0.27%	31.53%	0.00%	0.67%	14.62%	52.90%
Low FqFm 1 (Φ_{PSII})	3.95%	5.58%	0.45%	0.13%	24.20%	65.69%
Low FqFm 2 (Φ_{PSII})	3.96%	7.13%	0.43%	0.00%	25.69%	62.79%
Low FqFm induction (Φ_{PSII})	0.70%	29.35%	0.34%	1.32%	31.96%	36.33%
Low NPQ	4.74%	6.63%	0.11%	0.06%	10.20%	78.25%
Low Φ_{NO}	1.67%	22.40%	0.17%	0.11%	60.51%	15.14%
Low Φ_{NPQ}	5.02%	7.57%	0.41%	0.07%	17.90%	69.02%
Low q_I	4.40%	5.84%	0.06%	0.00%	8.07%	81.64%
Low q_E	5.08%	12.02%	0.19%	1.19%	21.92%	59.60%
Relative FqFm 1 (Φ_{PSII})	0.08%	29.47%	0.06%	0.55%	64.28%	5.55%
Relative FqFm 2 (Φ_{PSII})	0.01%	31.75%	0.05%	0.50%	60.01%	7.69%
Act. vs. High FqFm 1 (Φ_{PSII})	0.02%	29.28%	0.06%	0.97%	60.56%	9.12%
Act. vs. High FqFmp 2 (Φ_{PSII})	0.00%	32.94%	0.05%	0.72%	53.32%	12.98%
Act. vs. Low FqFmp 1 (Φ_{PSII})	0.94%	24.78%	0.37%	0.36%	52.10%	21.46%
Act. vs. Low FqFmp 2 (Φ_{PSII})	1.49%	26.45%	0.86%	0.06%	50.35%	20.79%
Relative NPQ	2.46%	39.15%	0.98%	0.21%	11.95%	45.25%
Relative Φ_{NO}	0.12%	40.49%	0.15%	1.06%	35.85%	22.34%
Relative Φ_{NPQ}	4.42%	13.81%	0.86%	0.23%	29.59%	51.10%
Relative q_I	0.44%	33.34%	0.10%	1.54%	45.17%	19.42%
Relative q_E	3.52%	13.47%	1.15%	3.42%	46.65%	31.78%
Act. vs. High NPQ	0.34%	53.92%	0.58%	1.25%	13.87%	30.04%
Act. vs. High Φ_{NO}	0.06%	45.48%	0.26%	1.31%	31.68%	21.21%
Act. vs. High Φ_{NPQ}	1.69%	36.77%	0.80%	0.34%	36.89%	23.50%
Act. vs. High q_I	0.17%	39.01%	0.13%	1.92%	39.12%	19.65%
Act. vs. High q_E	0.05%	0.00%	0.00%	0.03%	0.03%	99.88%
Act. vs. Low NPQ	0.82%	75.05%	0.64%	1.89%	3.52%	18.07%
Act. vs. Low Φ_{NO}	0.80%	52.34%	0.00%	1.93%	9.72%	35.21%
Act. vs. Low Φ_{NPQ}	1.06%	67.68%	0.80%	1.17%	13.39%	15.89%
Act. vs. Low q_I	1.55%	38.64%	0.38%	0.44%	8.87%	50.12%
Act. vs. Low q_E	0.05%	0.00%	0.00%	0.02%	0.03%	99.90%
Dry Weight (g)	0.25%	1.25%	0.00%	0.13%	94.73%	3.64%
Days to harvest	0.59%	1.90%	0.11%	0.32%	92.92%	4.16%
Specific leaf area (mm^{-2} mg^{-1})	1.01%	2.61%	0.00%	0.33%	88.36%	7.69%

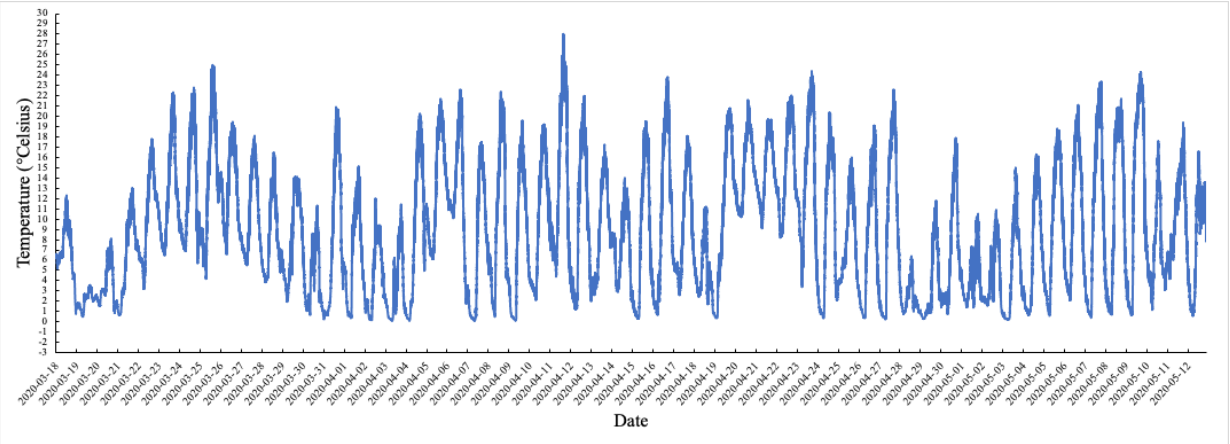

Extended data Fig. 1 Temperature recorded in the tunnel for the duration of the experiment.

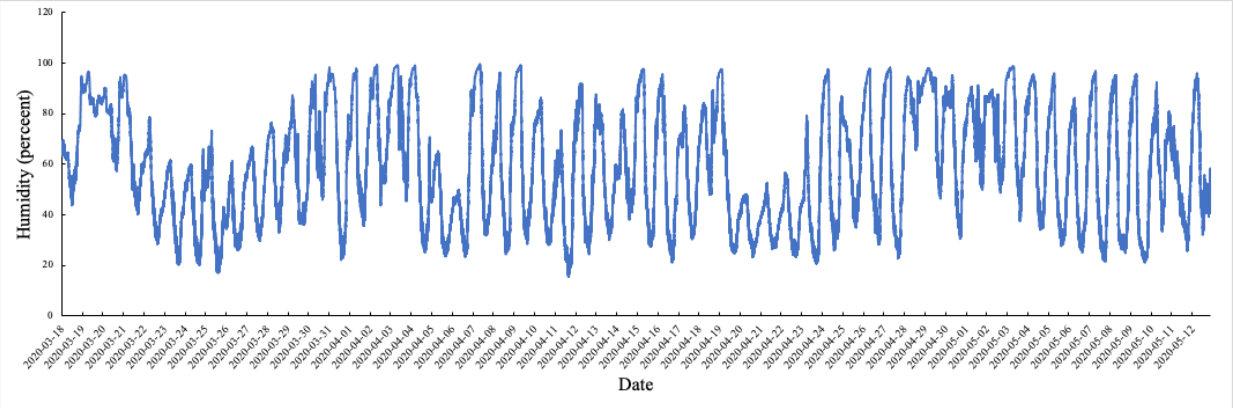

Extended data Fig. 2 Humidity recorded in the tunnel for the duration of the experiment.

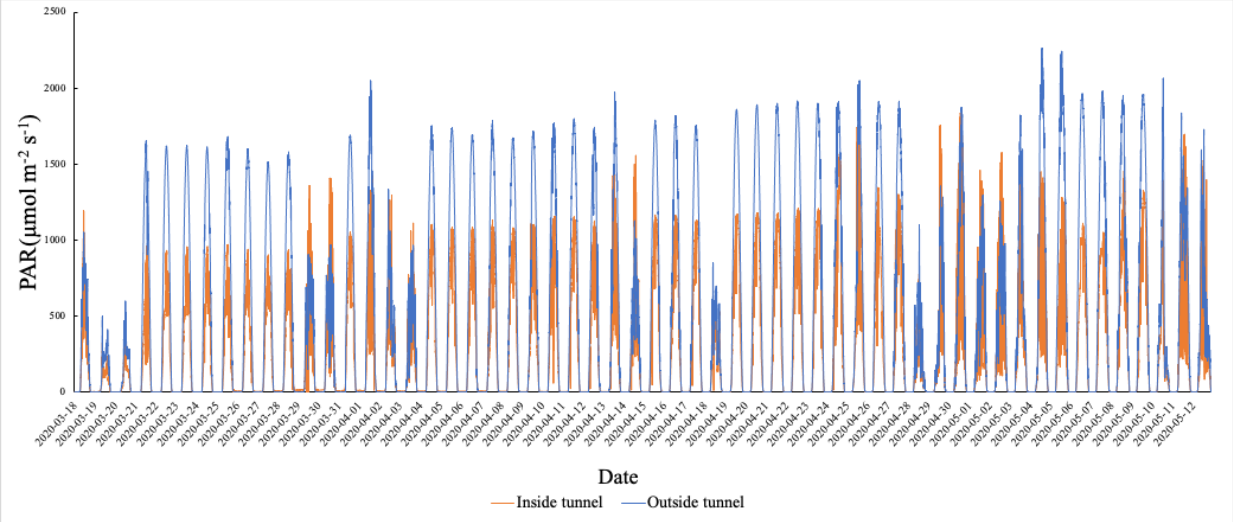

Extended data Fig. 3 PAR recorded inside and outside tunnel for the duration of the experiment.

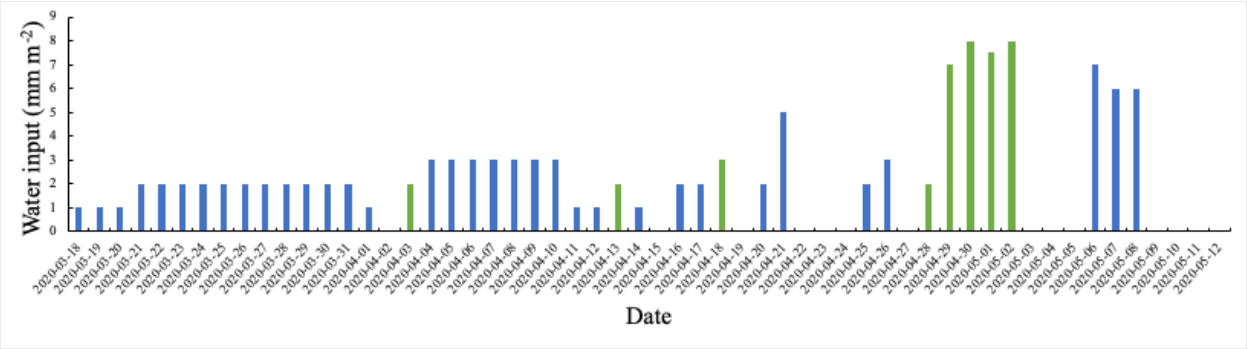

Extended data Fig. 4 The water input that the plants in the tunnel experienced for the duration of the experiment. Blue lines indicate hose derived water and green lines indicate rainwater.

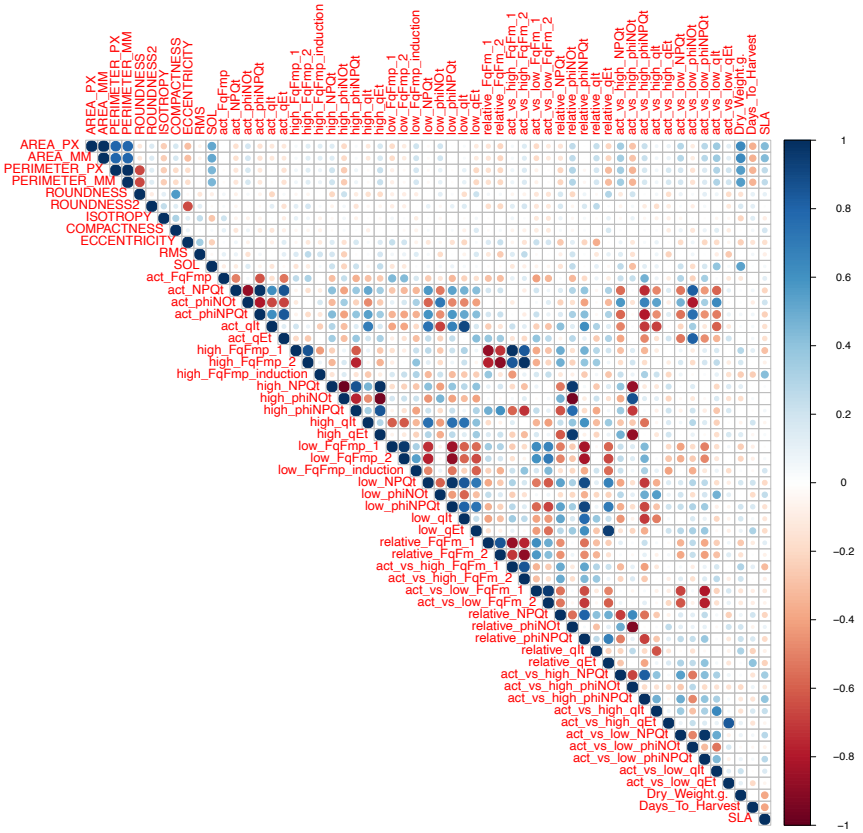

Extended data Fig. 5 Pearson correlation plot for the phenotypes within the Bur-0 nucleotype donor.

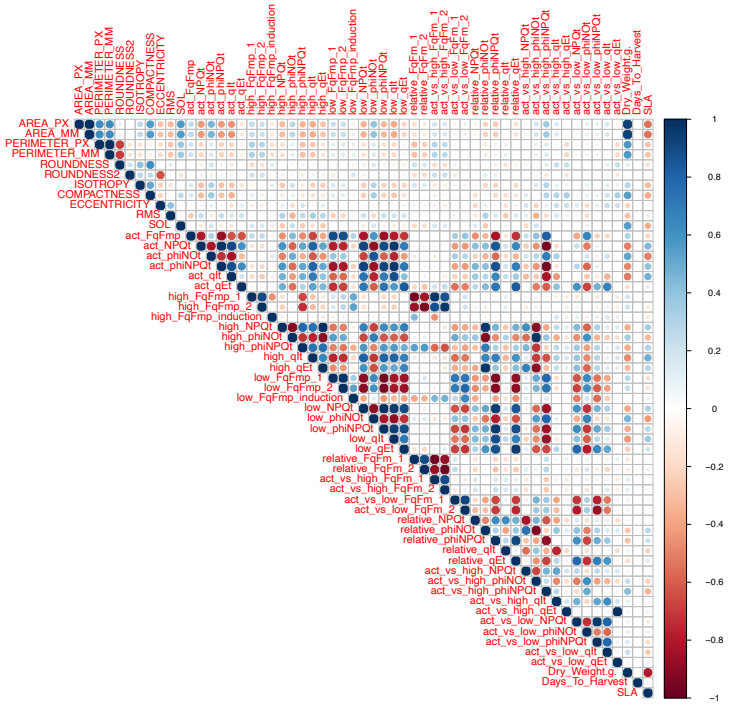

Extended data Fig. 6 Pearson correlation plot for the phenotypes within the Col-0 nucleotype donor.

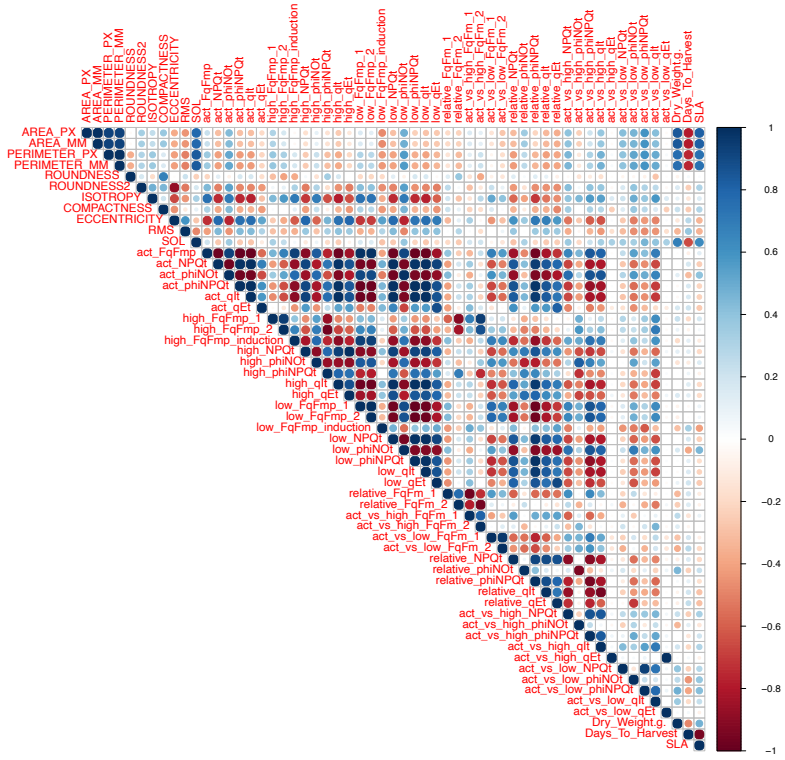

Extended data Fig. 7 Pearson correlation plot for the phenotypes within the Cvi-0 nucleotype donor.

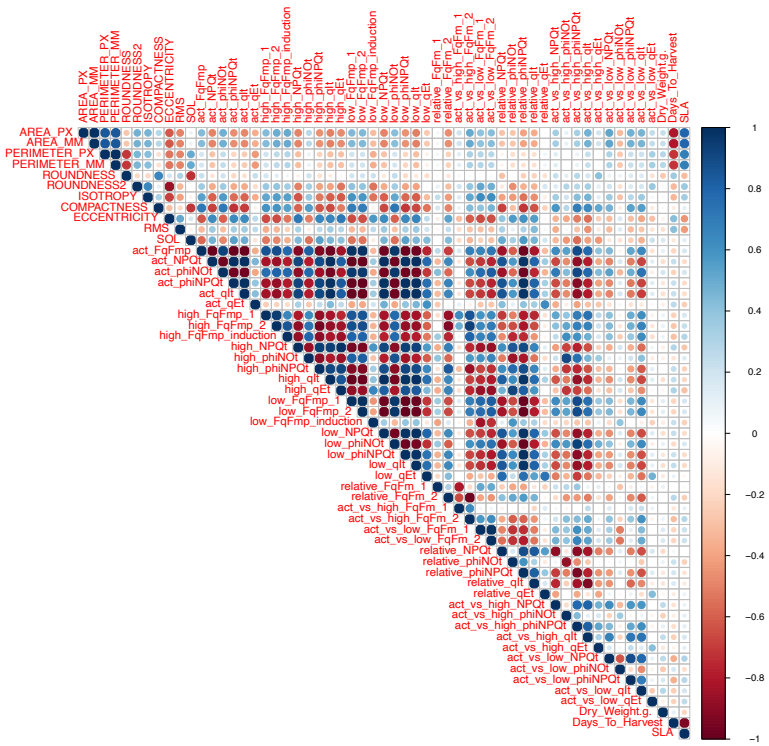

Extended data Fig. 8 Pearson correlation plot for the phenotypes within the Cvi-0 nucleotype donor.

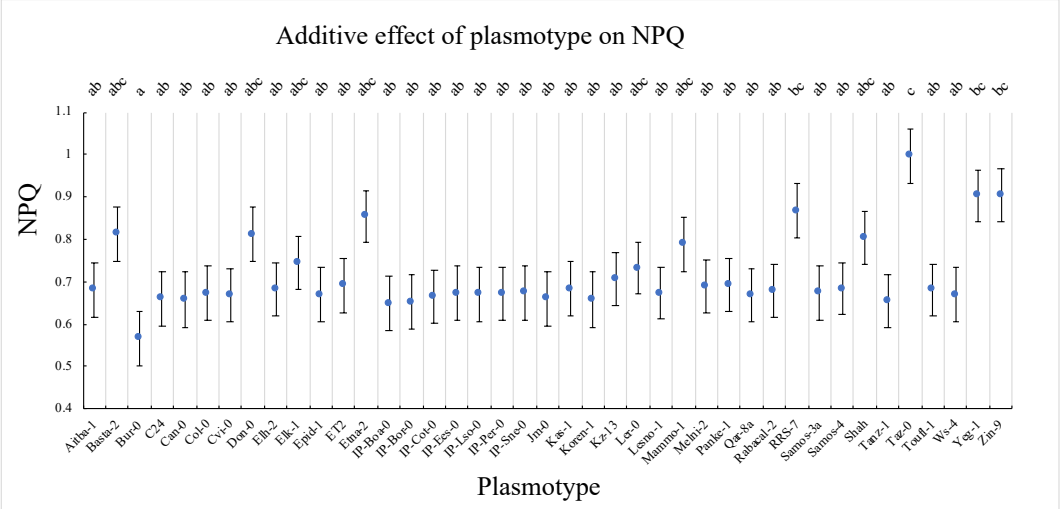

Extended data Fig. 9 Additive effects of plasmotype on NPQ. (Benjamini & Hochberg test; letters vary when $P < 0.05$).

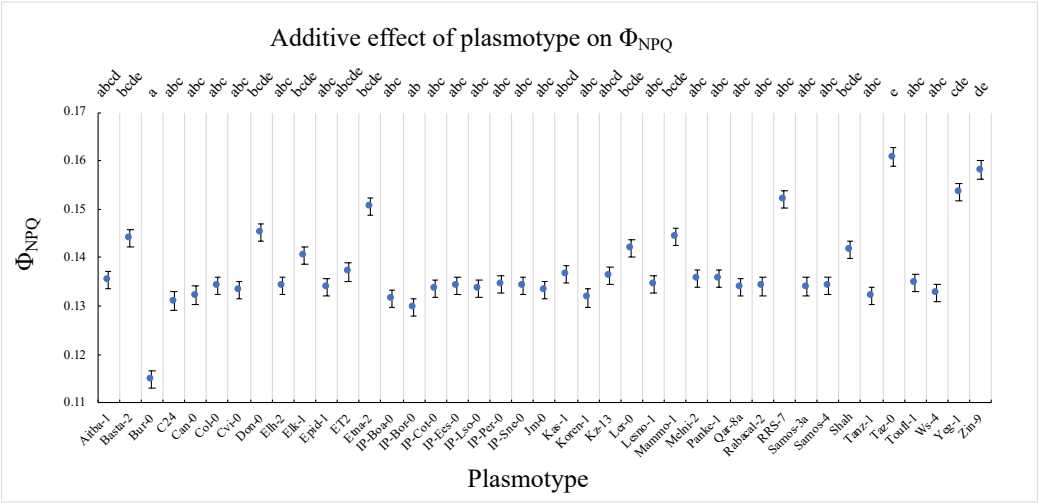

Extended data Fig. 10 Additive effects of plasmotype on Φ_{NPQ}. (Benjamini & Hochberg test; letters vary when $P < 0.05$).

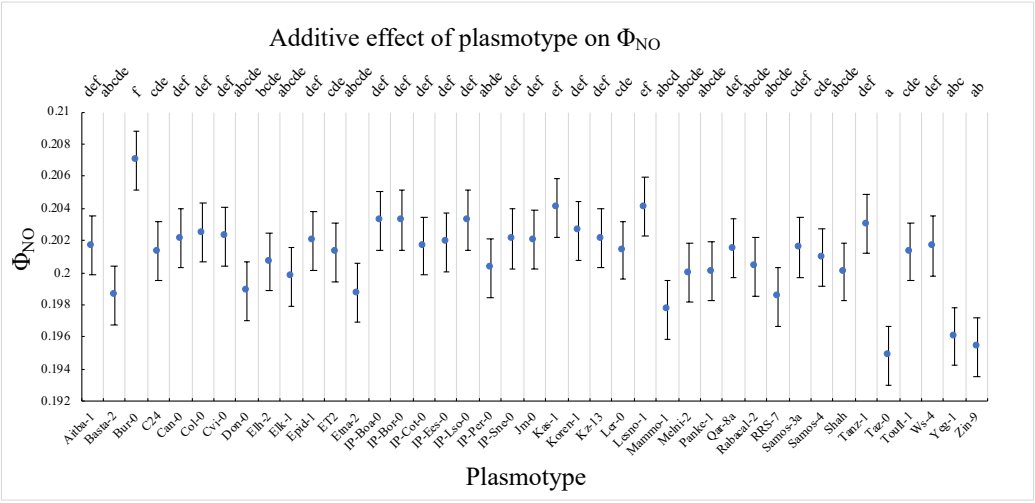

Extended data Fig. 11 Additive effects of plasmotype on Φ_{NO}. (Benjamini & Hochberg test; letters vary when $P < 0.05$).

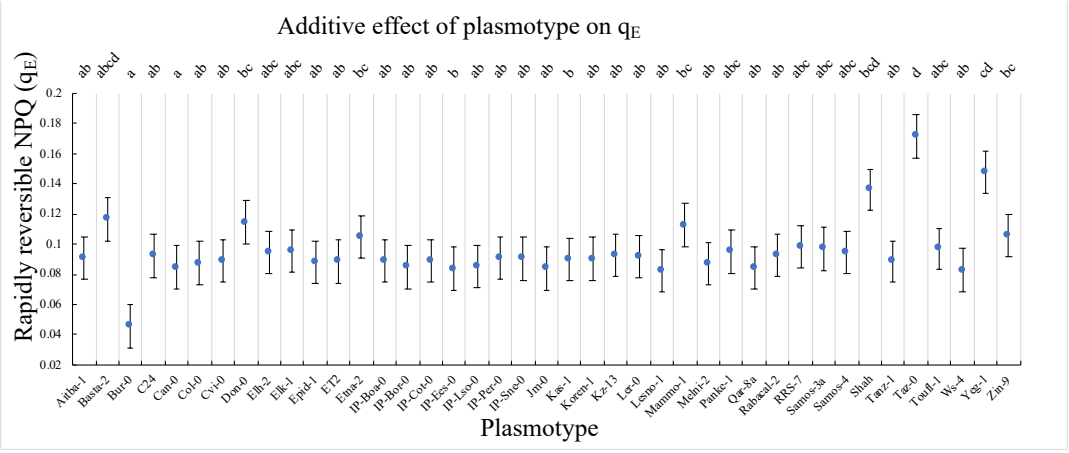

Extended data Fig. 12 Additive effects of plasmotype on q_E. (Benjamini & Hochberg test; letters vary when $P < 0.05$).

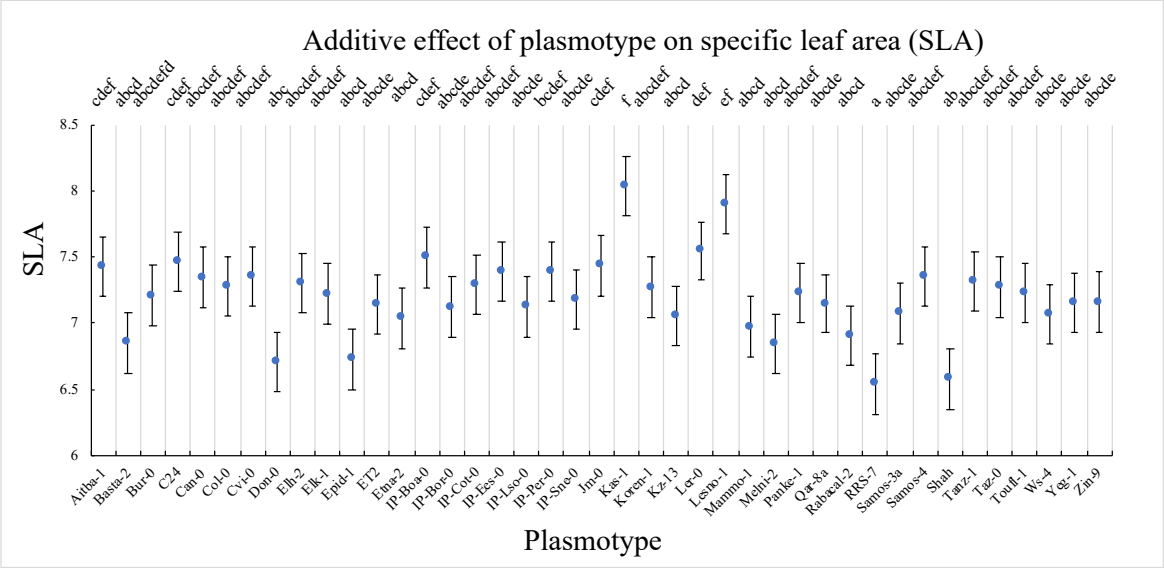

Extended data Fig. 13 Additive effects of plasmotype on specific leaf area. (Benjamini & Hochberg test; letters vary when $P < 0.05$).

Extended data Table 3. Epistatic H^2 values for the phenotypes of plasmotypes within each nucelotype.

Phenotype	Nucelotype donor															
	Bur				Col				Cvi				Tanz			
	Plasmotype	Block	Row	Residual	Plasmotype	Block	Row	Residual	Plasmotype	Block	Row	Residual	Plasmotype	Block	Row	Residual
Surface area (px)	2.26%	38.64%	10.53%	48.58%	6.48%	42.68%	9.08%	41.76%	27.62%	22.02%	5.68%	44.68%	7.62%	28.84%	4.56%	58.98%
Surface area (mm^2)	2.26%	38.64%	10.53%	48.58%	6.48%	42.68%	9.08%	41.76%	27.62%	22.02%	5.68%	44.68%	7.62%	28.84%	4.56%	58.98%
Perimeter (px)	2.06%	28.22%	2.97%	66.76%	1.44%	27.01%	2.64%	68.90%	13.30%	24.09%	4.45%	58.17%	4.95%	23.99%	0.23%	70.83%
Perimeter (mm^2)	2.06%	28.22%	2.97%	66.76%	1.44%	27.01%	2.64%	68.90%	13.30%	24.09%	4.45%	58.17%	4.95%	23.99%	0.23%	70.83%
Roundness	0.00%	1.42%	1.04%	97.54%	0.00%	4.40%	0.00%	95.60%	4.86%	6.93%	1.77%	86.44%	0.00%	10.63%	1.21%	88.17%
Roundness 2	0.00%	4.59%	1.96%	93.45%	0.09%	12.67%	0.00%	87.24%	1.32%	1.76%	0.00%	96.92%	0.00%	0.44%	0.00%	99.56%
Isotropy	0.58%	0.00%	0.00%	99.42%	2.87%	0.00%	0.33%	96.80%	2.73%	0.00%	0.00%	97.27%	0.28%	0.14%	3.36%	96.22%
Compactness	0.00%	2.12%	3.46%	94.42%	2.64%	4.66%	3.42%	89.28%	4.49%	3.40%	3.20%	88.91%	3.56%	3.58%	0.03%	92.83%
Eccentricity	0.00%	3.41%	0.39%	96.20%	0.00%	6.17%	0.34%	93.50%	2.40%	4.30%	0.00%	93.30%	2.18%	0.00%	2.38%	95.44%
RMS	0.00%	1.14%	0.57%	98.28%	0.00%	1.47%	0.32%	98.20%	0.22%	7.59%	0.00%	92.19%	0.00%	2.27%	1.88%	95.86%
SOL	0.00%	13.70%	3.49%	82.82%	1.96%	23.39%	4.98%	69.67%	1.97%	3.56%	0.20%	94.26%	2.11%	3.06%	7.33%	87.50%
Act. FqFm (Φ_{PSII})	0.08%	92.28%	0.26%	7.38%	4.73%	59.57%	0.62%	35.08%	5.32%	16.34%	0.00%	78.34%	3.63%	4.30%	1.96%	90.11%
Act. NPQ	0.85%	64.65%	3.09%	31.40%	5.31%	76.16%	1.67%	16.86%	6.01%	10.60%	0.00%	83.39%	4.35%	1.49%	1.90%	92.25%
Act. Φ_{NO}	0.93%	75.39%	2.06%	21.63%	0.55%	87.58%	1.18%	10.69%	7.18%	28.09%	0.00%	64.73%	7.56%	10.86%	2.24%	79.34%
Act. Φ_{NPQ}	0.68%	73.94%	2.54%	22.84%	10.03%	60.35%	1.84%	27.78%	6.58%	12.68%	0.00%	80.74%	5.16%	3.27%	2.20%	89.37%
Act. Φ_{NPQ}	1.43%	74.78%	3.69%	20.10%	4.09%	55.97%	3.95%	35.99%	5.65%	7.83%	0.00%	86.52%	4.62%	1.63%	1.47%	92.27%
Act. q_E	0.12%	80.03%	1.19%	18.67%	1.87%	62.46%	7.54%	28.13%	5.53%	19.22%	1.27%	73.98%	0.00%	29.67%	8.42%	61.91%
High FqFm 1 (Φ_{PSII})	0.02%	93.44%	0.66%	5.88%	0.00%	76.18%	4.07%	19.75%	0.00%	45.74%	3.23%	51.03%	0.00%	36.87%	1.33%	61.80%
High FqFm 2 (Φ_{PSII})	0.00%	92.66%	1.01%	6.34%	0.00%	79.74%	2.71%	17.55%	0.00%	40.05%	2.13%	57.82%	0.89%	24.56%	0.02%	74.53%
High FqFm induction (Φ_{PSII})	1.90%	55.03%	0.93%	42.14%	0.08%	28.10%	2.70%	69.12%	6.34%	6.69%	0.00%	86.97%	1.84%	36.44%	5.38%	56.34%
High NPQ	1.39%	67.66%	0.91%	30.05%	0.52%	81.33%	1.74%	16.41%	2.40%	7.11%	0.00%	90.50%	0.49%	18.93%	2.01%	78.57%
High Φ_{NO}	2.26%	47.66%	1.06%	49.02%	0.62%	85.89%	1.93%	11.55%	2.25%	36.54%	1.03%	60.19%	2.65%	63.90%	3.90%	29.55%
High Φ_{NPQ}	0.25%	88.94%	1.04%	9.77%	0.00%	60.45%	1.46%	38.09%	0.36%	25.32%	0.61%	73.70%	2.21%	34.75%	1.40%	61.64%
High q_I	3.67%	71.49%	0.60%	24.24%	6.29%	61.52%	1.79%	30.40%	5.81%	4.02%	0.00%	90.17%	3.01%	3.19%	1.97%	91.83%
High q_E	1.16%	64.68%	1.02%	33.14%	0.28%	81.51%	1.67%	16.53%	0.84%	9.64%	0.00%	89.51%	0.00%	25.78%	1.89%	72.33%
Low FqFm 1 (Φ_{PSII})	6.92%	73.07%	0.36%	19.64%	24.73%	29.09%	6.31%	39.88%	6.43%	7.90%	0.00%	85.67%	4.01%	2.21%	2.78%	91.00%
Low FqFm 2 (Φ_{PSII})	5.55%	77.74%	1.92%	14.79%	20.49%	55.64%	1.99%	21.88%	6.25%	8.64%	0.00%	85.11%	4.31%	2.87%	2.80%	90.02%
Low FqFm induction (Φ_{PSII})	1.83%	82.15%	5.37%	10.65%	1.13%	82.68%	2.24%	13.95%	3.92%	35.08%	7.18%	53.83%	0.00%	2.42%	0.34%	97.24%
Low NPQ	5.56%	77.11%	2.01%	15.32%	6.81%	85.77%	0.24%	7.18%	6.29%	7.54%	0.00%	86.17%	3.38%	1.99%	1.72%	92.92%
Low Φ_{NO}	0.72%	95.39%	0.12%	3.77%	1.30%	93.08%	0.39%	5.22%	8.38%	25.60%	0.30%	65.73%	6.06%	20.44%	1.08%	72.43%
Low Φ_{NPQ}	12.41%	49.34%	5.21%	33.04%	14.03%	75.30%	0.21%	10.46%	6.98%	8.50%	0.00%	84.51%	4.97%	3.74%	2.30%	88.99%
Low q_I	1.54%	82.47%	3.98%	12.02%	4.60%	82.92%	0.95%	11.52%	5.51%	6.72%	0.00%	87.76%	3.76%	1.37%	1.15%	93.72%
Low q_E	8.90%	47.74%	6.41%	36.95%	7.46%	58.96%	9.88%	23.70%	8.13%	10.15%	0.79%	80.93%	0.00%	21.75%	4.94%	73.31%
Relative FqFm 1 (Φ_{PSII})	0.23%	93.82%	0.69%	5.27%	0.00%	78.00%	3.61%	18.38%	2.34%	54.64%	3.30%	39.72%	0.00%	46.12%	8.62%	45.26%
Relative FqFm 2 (Φ_{PSII})	0.21%	92.54%	1.28%	5.97%	0.00%	79.69%	2.75%	17.56%	0.52%	54.59%	2.07%	42.82%	0.00%	36.50%	1.80%	61.70%
Act. vs. High FqFm 1 (Φ_{PSII})	0.08%	93.02%	0.72%	6.18%	0.00%	74.67%	4.30%	21.02%	2.18%	48.35%	5.07%	44.40%	0.00%	52.89%	7.05%	40.06%
Act. vs. High FqFmp 2 (Φ_{PSII})	0.00%	92.01%	1.17%	6.81%	0.00%	78.29%	2.84%	18.87%	0.00%	46.94%	3.85%	49.21%	0.00%	35.67%	1.43%	62.91%
Act. vs. Low FqFmp 1 (Φ_{PSII})	1.53%	90.41%	0.16%	7.90%	1.57%	63.30%	5.69%	29.45%	4.92%	34.29%	0.47%	60.32%	2.22%	3.13%	2.54%	92.11%
Act. vs. Low FqFmp 2 (Φ_{PSII})	2.64%	88.56%	0.00%	8.79%	7.29%	55.33%	2.88%	34.50%	7.44%	32.22%	1.04%	59.31%	3.31%	6.89%	3.60%	86.20%
Relative NPQ	1.46%	86.20%	0.51%	11.84%	0.11%	58.40%	2.40%	39.09%	6.14%	30.06%	0.00%	63.80%	3.21%	25.31%	3.63%	67.85%
Relative Φ_{NO}	0.95%	70.39%	0.40%	28.27%	0.20%	78.70%	3.07%	18.03%	0.53%	32.06%	0.67%	66.74%	0.28%	49.67%	3.88%	46.17%
Relative Φ_{NPQ}	3.30%	86.21%	0.83%	9.66%	7.87%	70.93%	0.57%	20.63%	8.87%	13.44%	0.00%	77.69%	5.62%	2.30%	3.83%	88.25%
Relative q_I	0.10%	91.60%	1.66%	6.64%	0.00%	52.72%	5.22%	42.07%	2.31%	34.79%	2.12%	60.78%	2.87%	20.28%	6.79%	70.06%
Relative q_E	9.28%	41.34%	9.16%	40.22%	18.44%	27.20%	16.08%	38.28%	9.35%	16.89%	5.92%	67.83%	0.00%	41.19%	10.53%	48.28%
Act. vs. High NPQ	0.84%	83.54%	1.85%	13.76%	0.00%	64.47%	4.48%	31.05%	3.31%	43.19%	0.37%	53.13%	1.56%	49.47%	8.44%	40.53%
Act. vs. High Φ_{NO}	0.89%	68.57%	1.09%	29.45%	0.41%	78.96%	3.03%	17.59%	0.00%	42.73%	0.96%	56.32%	0.84%	68.26%	4.57%	26.33%
Act. vs. High Φ_{NPQ}	0.84%	84.44%	1.66%	13.06%	3.62%	60.53%	2.63%	33.22%	7.88%	31.34%	0.45%	60.32%	6.07%	15.86%	7.19%	70.88%
Act. vs. High q_I	0.00%	88.42%	1.81%	9.77%	0.00%	26.97%	10.85%	62.18%	2.17%	40.60%	1.88%	55.34%	2.66%	24.27%	7.78%	65.29%
Act. vs. High q_E	0.15%	0.00%	0.30%	99.55%	0.00%	0.00%	0.07%	99.93%	0.20%	0.05%	0.08%	99.67%	0.00%	16.32%	3.21%	80.47%
Act. vs. Low NPQ	0.48%	87.29%	1.01%	11.22%	4.27%	52.19%	9.85%	33.70%	7.66%	46.81%	0.13%	45.40%	1.80%	44.28%	16.63%	37.29%
Act. vs. Low Φ_{NO}	0.46%	64.67%	2.72%	32.14%	0.96%	64.94%	2.11%	32.00%	3.72%	38.70%	2.49%	55.09%	0.15%	45.90%	4.73%	49.22%
Act. vs. Low Φ_{NPQ}	0.83%	88.58%	0.61%	9.98%	5.21%	44.11%	11.96%	38.72%	8.20%	48.58%	1.21%	42.00%	1.56%	38.09%	16.36%	43.98%
Act. vs. Low q_I	0.40%	52.35%	0.07%	47.18%	2.66%	50.39%	3.44%	43.51%	3.55%	33.65%	0.57%	62.24%	1.90%	29.54%	5.60%	62.95%
Act. vs. Low q_E	0.00%	2.51%	0.00%	97.49%	0.00%	0.00%	0.09%	99.91%	0.20%	0.05%	0.08%	99.67%	0.00%	27.87%	3.07%	69.06%
Dry Weight (g)	4.64%	22.46%	12.15%	60.76%	8.00%	44.96%	8.50%	38.53%	17.50%	17.57%	5.31%	59.62%	2.18%	8.03%	0.23%	89.57%
Days to harvest	4.95%	21.50%	8.52%	65.02%	16.50%	50.51%	16.50%	16.49%	13.84%	26.91%	6.30%	52.94%	5.87%	27.91%	7.18%	59.03%
Specific leaf area (mm^{-2} mg^{-1})	2.19%	23.72%	8.64%	65.46%	2.26%	34.94%	3.77%	59.02%	14.91%	15.85%	3.80%	65.44%	5.13%	21.29%	7.67%	65.91%

Extended data Table 4. Phenotype HSD values from the combined analysis of all cybrids.

| | | |

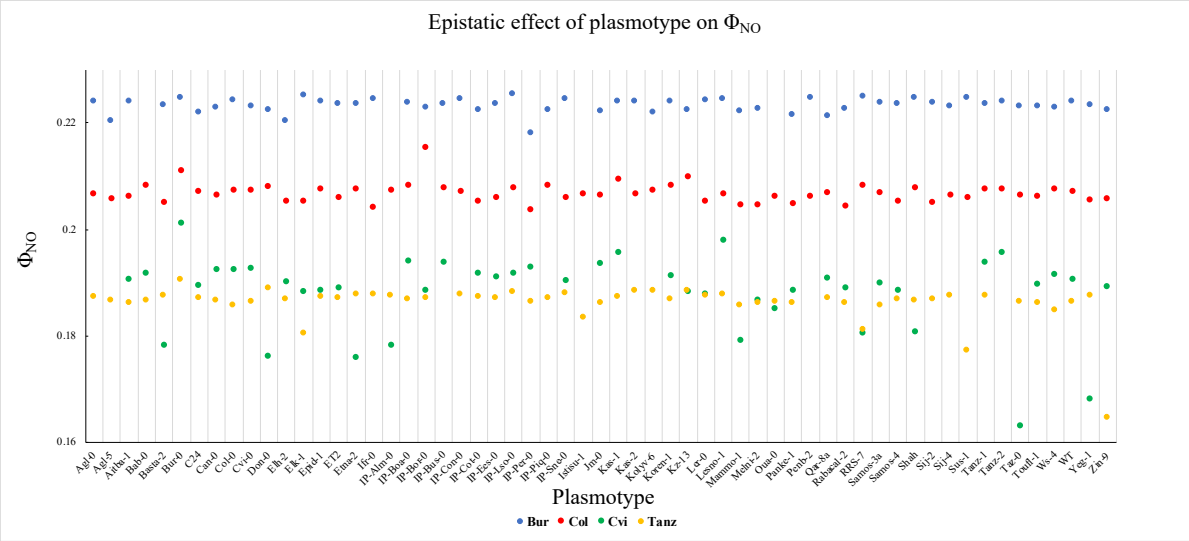

Extended data Fig. 15 Epistatic effects of plasmotype on Φ_{NO}.

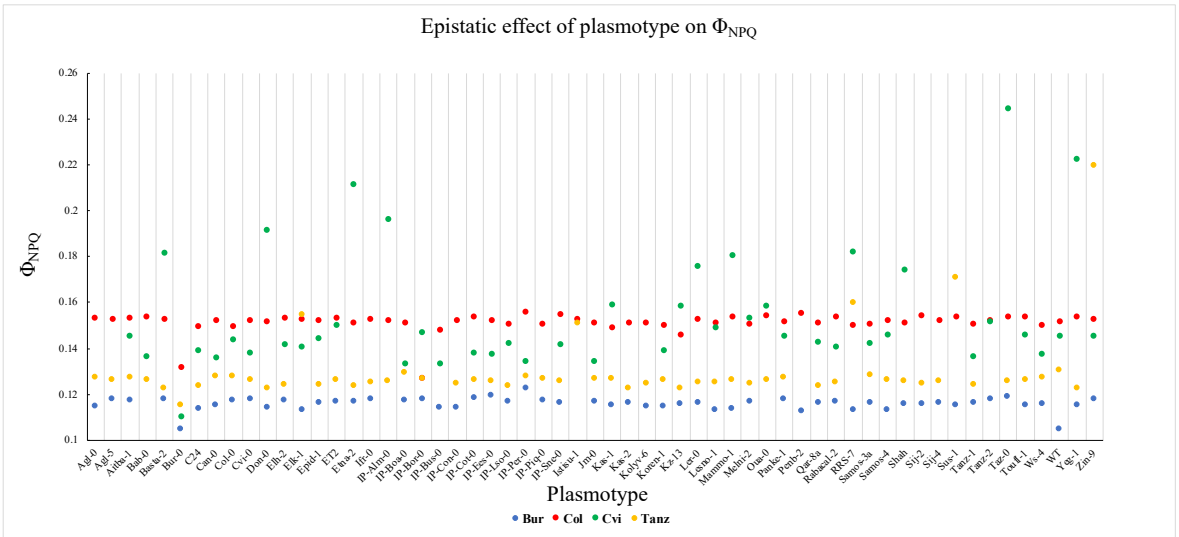

Extended data Fig. 16 Epistatic effects of plasmotype on Φ_{NPQ}.

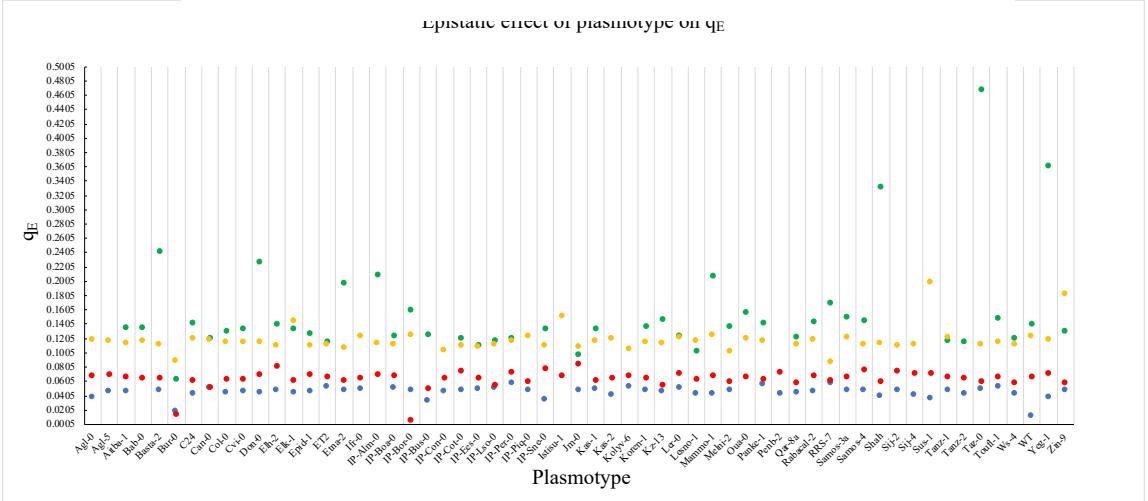

Extended data Fig. 17 Epistatic effects of plasmotype on q_E.

Extended data Table 5. Comparisons of plasmotypes against the WT of its nucleotype donor for three phenotypes. Cells highlighted in green are significantly different then the WT of the nucelotype donor. Red cells are not significantly different than the WT of the WT nucelotype donor (Dunnet's test, significant differences if $P < 0.05$).

Bur				Col				Cvi				Tanz			
Comparison	Surface area (mm^2)	Φ_{PSII}	Dry weight (g)	Comparison	Surface area (mm^2)	Φ_{PSII}	Dry weight (g)	Comparison	Surface area (mm^2)	Φ_{PSII}	Dry weight (g)	Comparison	Surface area (mm^2)	Φ_{PSII}	Dry weight (g)
Agl-0 - WT-Bur	0.852	0.000	1.000	Agl-0 - WT-Col	0.001	1.000	0.001	Aitba-1 - WT-Cvi	0.999	1.000	1.000	Agl-0 - WT-Tanz	0.961	1.000	1.000
Agl-5 - WT-Bur	1.000	0.000	0.960	Agl-5 - WT-Col	0.930	1.000	0.460	Bab-0 - WT-Cvi	1.000	1.000	1.000	Agl-5 - WT-Tanz	1.000	1.000	0.973
Aitba-1 - WT-Bur	1.000	0.000	0.579	Aitba-1 - WT-Col	0.995	1.000	1.000	Basta-2 - WT-Cvi	0.131	0.849	0.998	Aitba-1 - WT-Tanz	0.918	1.000	0.999
Basta-2 - WT-Bur	0.983	0.000	1.000	Bab-0 - WT-Col	0.958	0.378	1.000	Bur-0 - WT-Cvi	0.988	0.910	0.999	Bab-0 - WT-Tanz	1.000	1.000	0.996
Bur-0 - WT-Bur	0.987	1.000	1.000	Basta-2 - WT-Col	0.999	1.000	1.000	C24 - WT-Cvi	1.000	1.000	1.000	Basta-2 - WT-Tanz	0.999	1.000	0.000
C24 - WT-Bur	1.000	0.005	1.000	Bur-0 - WT-Col	0.914	0.000	0.628	Can-0 - WT-Cvi	0.891	1.000	1.000	Bur-0 - WT-Tanz	0.994	0.988	0.992
Can-0 - WT-Bur	0.826	0.000	0.497	C24 - WT-Col	1.000	0.308	0.997	Col-0 - WT-Cvi	1.000	1.000	1.000	C24 - WT-Tanz	0.551	1.000	1.000
Col-0 - WT-Bur	0.957	0.000	0.992	Can-0 - WT-Col	0.009	1.000	0.000	Cvi-0 - WT-Cvi	0.295	1.000	0.986	Can-0 - WT-Tanz	1.000	1.000	1.000
Cvi-0 - WT-Bur	0.999	0.000	0.519	Col-0 - WT-Col	1.000	0.640	1.000	Don-0 - WT-Cvi	0.033	0.542	0.993	Col-0 - WT-Tanz	0.786	1.000	1.000
Don-0 - WT-Bur	0.286	0.004	1.000	Cvi-0 - WT-Col	1.000	1.000	0.999	Elh-2 - WT-Cvi	0.782	1.000	1.000	Cvi-0 - WT-Tanz	0.204	1.000	0.997
Elh-2 - WT-Bur	0.938	0.000	0.113	Don-0 - WT-Col	0.996	0.442	1.000	Elk-1 - WT-Cvi	0.020	1.000	0.969	Don-0 - WT-Tanz	1.000	1.000	0.993
Elk-1 - WT-Bur	1.000	0.000	0.992	Elh-2 - WT-Col	0.162	1.000	0.021	Epid-1 - WT-Cvi	0.052	1.000	1.000	Elh-2 - WT-Tanz	1.000	1.000	1.000
Epid-1 - WT-Bur	0.997	0.000	0.972	Elk-1 - WT-Col	1.000	1.000	0.992	ET2 - WT-Cvi	0.288	1.000	0.909	Elk-1 - WT-Tanz	0.036	0.821	1.000
ET2 - WT-Bur	0.987	0.000	1.000	Epid-1 - WT-Col	1.000	0.998	1.000	Etna-2 - WT-Cvi	0.016	0.052	0.998	Epid-1 - WT-Tanz	1.000	1.000	1.000
Etna-2 - WT-Bur	1.000	0.000	0.976	ET2 - WT-Col	1.000	1.000	1.000	IP-Alm-0 - WT-Cvi	0.182	0.304	0.999	ET2 - WT-Tanz	0.984	1.000	1.000
Ifr-0 - WT-Bur	1.000	0.000	0.265	Etna-2 - WT-Col	0.971	1.000	0.991	IP-Boa-0 - WT-Cvi	0.313	1.000	0.569	Etna-2 - WT-Tanz	1.000	1.000	1.000
IP-Boa-0 - WT-Bur	0.987	0.000	0.096	Ifr-0 - WT-Col	0.994	0.978	0.992	IP-Bor-0 - WT-Cvi	0.999	1.000	0.999	Ifr-0 - WT-Tanz	0.847	1.000	0.332
IP-Bor-0 - WT-Bur	1.000	0.000	1.000	IP-Alm-0 - WT-Col	0.190	1.000	0.564	IP-Bus-0 - WT-Cvi	0.999	1.000	1.000	IP-Alm-0 - WT-Tanz	0.775	1.000	1.000
IP-Bus-0 - WT-Bur	1.000	0.000	0.310	IP-Boa-0 - WT-Col	1.000	1.000	1.000	IP-Cot-0 - WT-Cvi	1.000	1.000	1.000	IP-Boa-0 - WT-Tanz	0.630	1.000	1.000
IP-Con-0 - WT-Bur	0.995	0.000	1.000	IP-Bor-0 - WT-Col	1.000	0.000	0.992	IP-Ees-0 - WT-Cvi	0.993	1.000	1.000	IP-Bor-0 - WT-Tanz	0.482	1.000	0.961
IP-Cot-0 - WT-Bur	1.000	0.000	0.691	IP-Bus-0 - WT-Col	0.985	0.744	0.999	IP-Lso-0 - WT-Cvi	0.558	1.000	0.993	IP-Con-0 - WT-Tanz	1.000	1.000	1.000
IP-Ees-0 - WT-Bur	1.000	0.000	0.025	IP-Con-0 - WT-Col	0.740	1.000	0.957	IP-Per-0 - WT-Cvi	0.987	1.000	1.000	IP-Cot-0 - WT-Tanz	0.995	1.000	1.000
IP-Lso-0 - WT-Bur	1.000	0.000	1.000	IP-Cot-0 - WT-Col	0.144	1.000	0.229	IP-Sne-0 - WT-Cvi	1.000	1.000	1.000	IP-Ees-0 - WT-Tanz	1.000	1.000	1.000
IP-Per-0 - WT-Bur	0.980	0.000	1.000	IP-Ees-0 - WT-Col	1.000	1.000	0.758	Jm-0 - WT-Cvi	0.946	1.000	0.647	IP-Lso-0 - WT-Tanz	1.000	1.000	1.000
IP-Piq-0 - WT-Bur	1.000	0.000	0.967	IP-Lso-0 - WT-Col	0.009	1.000	0.014	Kas-1 - WT-Cvi	0.000	0.977	0.000	IP-Per-0 - WT-Tanz	0.891	1.000	0.999
IP-Sne-0 - WT-Bur	1.000	0.000	0.992	IP-Per-0 - WT-Col	0.304	0.999	0.068	Koren-1 - WT-Cvi	0.926	1.000	1.000	IP-Piq-0 - WT-Tanz	0.959	1.000	0.782
Jm-0 - WT-Bur	1.000	0.000	1.000	IP-Piq-0 - WT-Col	0.834	0.991	0.997	Kz-13 - WT-Cvi	0.667	0.999	1.000	IP-Sne-0 - WT-Tanz	0.880	1.000	0.791
Kas-1 - WT-Bur	1.000	0.000	0.999	IP-Sne-0 - WT-Col	0.992	0.918	1.000	Ler-0 - WT-Cvi	0.603	0.754	0.862	Istisu-1 - WT-Tanz	0.956	0.824	1.000
Kas-2 - WT-Bur	0.669	0.000	1.000	Istisu-1 - WT-Col	0.997	1.000	1.000	Lesno-1 - WT-Cvi	0.007	1.000	0.680	Jm-0 - WT-Tanz	0.925	1.000	1.000
Kolyv-6 - WT-Bur	0.997	0.000	0.999	Jm-0 - WT-Col	1.000	0.999	1.000	Mammo-1 - WT-Cvi	0.511	0.853	1.000	Kas-1 - WT-Tanz	0.485	1.000	1.000
Koren-1 - WT-Bur	1.000	0.000	1.000	Kas-1 - WT-Col	0.603	0.988	0.138	Melni-2 - WT-Cvi	0.007	1.000	0.943	Kas-2 - WT-Tanz	0.963	1.000	0.983
Kz-13 - WT-Bur	1.000	0.000	0.697	Kas-2 - WT-Col	1.000	1.000	0.995	Oua-0 - WT-Cvi	0.879	1.000	1.000	Kolyv-6 - WT-Tanz	0.988	1.000	1.000
Ler-0 - WT-Bur	0.985	0.000	1.000	Kolyv-6 - WT-Col	0.695	1.000	0.931	Panke-1 - WT-Cvi	0.640	1.000	1.000	Koren-1 - WT-Tanz	0.999	1.000	1.000
Lesno-1 - WT-Bur	0.646	0.000	0.355	Koren-1 - WT-Col	1.000	1.000	1.000	Qar-8a - WT-Cvi	0.207	1.000	0.989	Kz-13 - WT-Tanz	1.000	1.000	1.000
Mammo-1 - WT-Bur	0.959	0.000	0.997	Kz-13 - WT-Col	0.984	0.456	0.921	Rabacal-2 - WT-Cvi	0.551	1.000	0.998	Ler-0 - WT-Tanz	1.000	1.000	1.000
Melni-2 - WT-Bur	0.368	0.000	1.000	Ler-0 - WT-Col	1.000	1.000	1.000	RRS-7 - WT-Cvi	0.038	0.828	0.999	Lesno-1 - WT-Tanz	1.000	1.000	0.999
Panke-1 - WT-Bur	0.003	0.000	0.991	Lesno-1 - WT-Col	0.993	0.815	0.991	Samos-3a - WT-Cvi	0.995	1.000	1.000	Mammo-1 - WT-Tanz	0.976	1.000	0.999
Penb-2 - WT-Bur	0.994	0.000	0.997	Mammo-1 - WT-Col	0.998	1.000	1.000	Samos-4 - WT-Cvi	0.330	1.000	0.999	Melni-2 - WT-Tanz	0.966	1.000	1.000
Qar-8a - WT-Bur	1.000	0.000	1.000	Melni-2 - WT-Col	0.007	0.007	0.001	Shah - WT-Cvi	1.000	0.963	0.000	Oua-0 - WT-Tanz	1.000	1.000	1.000
Rabacal-2 - WT-Bur	0.996	0.000	1.000	Oua-0 - WT-Col	1.000	0.574	1.000	Tanz-1 - WT-Cvi	0.977	1.000	0.999	Panke-1 - WT-Tanz	0.695	1.000	1.000
RRS-7 - WT-Bur	1.000	0.000	1.000	Panke-1 - WT-Col	0.000	0.676	0.007	Tanz-2 - WT-Cvi	0.000	1.000	0.000	Qar-8a - WT-Tanz	0.991	1.000	1.000
Samos-3a - WT-Bur	0.970	0.000	1.000	Penb-2 - WT-Col	0.953	0.346	0.686	Taz-0 - WT-Cvi	0.044	0.000	1.000	Rabacal-2 - WT-Tanz	1.000	1.000	1.000
Samos-4 - WT-Bur	1.000	0.001	0.817	Qar-8a - WT-Col	1.000	1.000	1.000	Toufl-1 - WT-Cvi	0.916	1.000	1.000	RRS-7 - WT-Tanz	0.020	0.219	1.000
Shah - WT-Bur	1.000	0.000	0.850	Rabacal-2 - WT-Col	0.221	1.000	0.089	Ws-4 - WT-Cvi	0.712	1.000	0.993	Samos-3a - WT-Tanz	0.898	1.000	1.000
Sij-2 - WT-Bur	1.000	0.000	0.996	RRS-7 - WT-Col	0.997	1.000	1.000	Yeg-1 - WT-Cvi	0.000	0.005	0.683	Samos-4 - WT-Tanz	0.981	1.000	1.000
Sij-4 - WT-Bur	0.998	0.000	1.000	Samos-3a - WT-Col	0.848	0.925	0.753	Zin-9 - WT-Cvi	0.306	1.000	0.672	Shah - WT-Tanz	0.691	1.000	1.000
Sus-1 - WT-Bur	0.993	0.000	1.000	Samos-4 - WT-Col	0.047	0.974	0.007					Sij-2 - WT-Tanz	0.989	1.000	1.000
Tanz-1 - WT-Bur	0.927	0.000	1.000	Shah - WT-Col	0.966	1.000	0.984					Sij-4 - WT-Tanz	0.938	1.000	0.999
Tanz-2 - WT-Bur	1.000	0.000	0.921	Sij-2 - WT-Col	0.967	0.996	1.000					Sus-1 - WT-Tanz	0.011	0.142	0.879
Taz-0 - WT-Bur	0.999	0.000	1.000	Sij-4 - WT-Col	1.000	1.000	1.000					Tanz-1 - WT-Tanz	1.000	1.000	1.000
Toufl-1 - WT-Bur	1.000	0.000	1.000	Sus-1 - WT-Col	1.000	1.000	1.000					Taz-0 - WT-Tanz	1.000	1.000	1.000
Ws-4 - WT-Bur	0.999	0.000	1.000	Tanz-1 - WT-Col	0.989	0.995	1.000					Toufl-1 - WT-Tanz	1.000	1.000	1.000
Yeg-1 - WT-Bur	1.000	0.000	1.000	Tanz-2 - WT-Col	0.981	1.000	1.000					Ws-4 - WT-Tanz	0.999	1.000	0.932
Zin-9 - WT-Bur	1.000	0.000	0.622	Taz-0 - WT-Col	1.000	0.544	0.663					Yeg-1 - WT-Tanz	1.000	1.000	1.000
				Toufl-1 - WT-Col	0.000	0.909	0.001					Zin-9 - WT-Tanz	0.095	0.000	0.997
				Ws-4 - WT-Col	1.000	0.824	0.999								
				Yeg-1 - WT-Col	0.283	0.970	0.340								
				Zin-9 - WT-Col	0.014	1.000	0.023								

Extended data Table 6. Phenotype means from the combined analysis of all cybrids.

Plasmotype	Aitba-1	Basta-2	Bur-0	C24	Can-0	Col-0	Cvi-0	Don-0	Elh-2	Elk-1	Epid-1	ET2	Etna-2	IP-Boa-0	IP-Bor-0	IP-Cot-0	IP-Ees-0	IP-Lso-0	IP-Per-0
Surface area (px)	36669	33668	35534	37617	33088	36239	36804	33193	35228	37120	35804	35239	34807	36743	36756	35214	35999	33808	34701
Surface area (mm^2)	1744	1601	1690	1789	1574	1724	1751	1579	1676	1766	1703	1676	1656	1748	1748	1675	1712	1608	1651
Perimeter (px)	1374	1287	1364	1371	1293	1350	1399	1304	1368	1341	1295	1325	1316	1364	1377	1382	1340	1267	1332
Perimeter (mm^2)	300	281	298	299	282	294	305	284	298	292	282	289	287	297	300	301	292	276	291
Roundness	0.23	0.24	0.23	0.24	0.24	0.24	0.23	0.23	0.22	0.24	0.25	0.24	0.25	0.24	0.23	0.23	0.24	0.25	0.24
Roundness 2	0.90	0.90	0.90	0.90	0.90	0.90	0.90	0.89	0.90	0.90	0.90	0.90	0.89	0.90	0.90	0.91	0.90	0.90	0.90
Isotropy	0.77	0.74	0.79	0.80	0.78	0.80	0.77	0.78	0.77	0.77	0.81	0.80	0.72	0.78	0.81	0.79	0.80	0.77	0.75
Compactness	0.73	0.73	0.73	0.74	0.74	0.73	0.73	0.73	0.73	0.73	0.75	0.74	0.74	0.73	0.73	0.73	0.74	0.74	0.73
Eccentricity	0.17	0.18	0.17	0.17	0.17	0.16	0.17	0.19	0.17	0.16	0.17	0.18	0.20	0.17	0.16	0.16	0.16	0.17	0.16
RMS	0.45	0.47	0.48	0.45	0.46	0.45	0.42	0.47	0.46	0.47	0.48	0.49	0.51	0.46	0.44	0.47	0.46	0.45	0.47
SOL	32.2	24.8	28.6	30.6	27.1	26.5	30.9	28.1	27.8	29.2	27.4	27.0	27.4	31.9	28.2	28.8	28.9	27.4	26.1
Act. FqFm (Φ_{PSII})	0.66	0.66	0.67	0.67	0.67	0.67	0.66	0.66	0.67	0.66	0.66	0.66	0.65	0.67	0.67	0.67	0.67	0.67	0.66
Act. NPQ	0.48	0.57	0.42	0.46	0.46	0.46	0.47	0.57	0.47	0.53	0.47	0.49	0.60	0.45	0.46	0.46	0.46	0.47	0.47
Act. Φ_{NO}	0.23	0.23	0.23	0.23	0.23	0.23	0.23	0.23	0.23	0.23	0.23	0.23	0.23	0.23	0.23	0.23	0.23	0.23	0.23
Act. Φ_{NPQ}	0.11	0.12	0.10	0.10	0.10	0.10	0.11	0.12	0.11	0.11	0.11	0.11	0.12	0.10	0.10	0.10	0.11	0.11	0.11
Act. Φ_{NPQ}	0.41	0.50	0.37	0.39	0.40	0.41	0.40	0.50	0.41	0.47	0.41	0.42	0.54	0.39	0.40	0.40	0.41	0.41	0.40
Act. q_E	0.07	0.07	0.05	0.06	0.05	0.06	0.06	0.07	0.07	0.06	0.06	0.07	0.05	0.06	0.06	0.06	0.06	0.06	0.07
High FqFm 1 (Φ_{PSII})	0.21	0.22	0.21	0.22	0.21	0.21	0.21	0.21	0.21	0.22	0.21	0.21	0.21	0.21	0.22	0.22	0.22	0.21	0.21
High FqFm 2 (Φ_{PSII})	0.28	0.28	0.27	0.28	0.28	0.28	0.27	0.27	0.28	0.28	0.28	0.27	0.27	0.28	0.28	0.28	0.28	0.27	0.28
High FqFm induction (Φ_{PSII})	1.30	1.28	1.30	1.29	1.30	1.30	1.30	1.29	1.30	1.29	1.29	1.30	1.28	1.30	1.30	1.30	1.30	1.29	1.30
High NPQ	4.53	4.81	4.28	4.30	4.33	4.42	4.54	4.88	4.60	4.55	4.49	4.56	5.09	4.51	4.33	4.53	4.47	4.50	4.69
High Φ_{NO}	0.14	0.13	0.14	0.14	0.14	0.14	0.14	0.14	0.13	0.14	0.14	0.14	0.13	0.14	0.14	0.14	0.14	0.14	0.13
High Φ_{NPQ}	0.59	0.59	0.59	0.58	0.58	0.59	0.59	0.59	0.59	0.58	0.59	0.59	0.60	0.59	0.58	0.59	0.58	0.59	0.59
High q_I	1.05	1.17	0.95	1.01	1.04	1.05	1.05	1.17	1.07	1.12	1.04	1.08	1.24	1.04	1.02	1.05	1.05	1.05	1.07
High q_E	3.48	3.64	3.33	3.29	3.30	3.37	3.49	3.71	3.53	3.44	3.45	3.48	3.86	3.47	3.30	3.48	3.41	3.44	3.62
Low FqFm 1 (Φ_{PSII})	0.65	0.65	0.67	0.66	0.66	0.65	0.66	0.65	0.66	0.65	0.66	0.65	0.64	0.66	0.66	0.66	0.66	0.66	0.66
Low FqFm 2 (Φ_{PSII})	0.66	0.66	0.68	0.67	0.67	0.66	0.66	0.66	0.67	0.66	0.66	0.66	0.65	0.66	0.67	0.66	0.66	0.66	0.66
Low FqFm induction (Φ_{PSII})	1.01	1.01	1.02	1.01	1.01	1.01	1.01	1.01	1.01	1.01	1.01	1.01	1.01	1.01	1.01	1.01	1.01	1.01	1.01
Low NPQ	0.68	0.81	0.57	0.66	0.66	0.67	0.67	0.81	0.68	0.75	0.67	0.69	0.85	0.65	0.65	0.66	0.67	0.67	0.67
Low Φ_{NO}	0.20	0.20	0.21	0.20	0.20	0.20	0.20	0.20	0.20	0.20	0.20	0.20	0.20	0.20	0.20	0.20	0.20	0.20	0.20
Low Φ_{NPQ}	0.14	0.14	0.11	0.13	0.13	0.13	0.13	0.15	0.13	0.14	0.13	0.14	0.15	0.13	0.13	0.13	0.13	0.13	0.13
Low q_I	0.59	0.69	0.52	0.57	0.57	0.58	0.58	0.70	0.59	0.65	0.58	0.60	0.75	0.56	0.57	0.57	0.59	0.59	0.58
Low q_E	0.09	0.12	0.05	0.09	0.08	0.09	0.09	0.11	0.09	0.10	0.09	0.09	0.11	0.09	0.08	0.09	0.08	0.09	0.09
Relative FqFm 1 (Φ_{PSII})	3.21	3.16	3.31	3.13	3.21	3.19	3.25	3.17	3.19	3.14	3.19	3.24	3.19	3.21	3.16	3.16	3.17	3.21	3.19
Relative FqFm 2 (Φ_{PSII})	2.48	2.48	2.56	2.44	2.48	2.48	2.52	2.48	2.49	2.45	2.49	2.52	2.52	2.48	2.46	2.47	2.47	2.50	2.47
Act. vs. High FqFm 1 (Φ_{PSII})	0.32	0.33	0.31	0.33	0.32	0.32	0.31	0.32	0.32	0.33	0.32	0.32	0.32	0.32	0.32	0.32	0.32	0.32	0.32
Act. vs. High FqFmp 2 (Φ_{PSII})	0.41	0.42	0.40	0.42	0.41	0.41	0.41	0.41	0.41	0.42	0.41	0.41	0.41	0.41	0.42	0.42	0.42	0.41	0.42
Act. vs. Low FqFmp 1 (Φ_{PSII})	0.99	0.98	1.00	0.99	0.98	0.98	0.99	0.98	0.99	0.98	0.99	0.99	0.98	0.99	0.99	0.98	0.98	0.98	0.99
Act. vs. Low FqFmp 2 (Φ_{PSII})	1.00	1.00	1.01	1.00	1.00	1.00	1.00	1.00	1.00	1.00	1.00	1.00	0.99	1.00	1.00	1.00	1.00	1.00	1.00
Relative NPQ	0.15	0.16	0.14	0.16	0.16	0.16	0.15	0.16	0.15	0.16	0.15	0.15	0.16	0.15	0.15	0.15	0.16	0.15	0.15
Relative Φ_{NO}	1.53	1.52	1.49	1.48	1.48	1.50	1.53	1.53	1.54	1.50	1.53	1.53	1.57	1.54	1.49	1.54	1.52	1.52	1.57
Relative Φ_{NPQ}	0.23	0.24	0.20	0.23	0.23	0.23	0.23	0.24	0.23	0.24	0.23	0.23	0.24	0.23	0.22	0.23	0.23	0.23	0.23
Relative q_I	0.57	0.56	0.55	0.57	0.56	0.56	0.56	0.57	0.56	0.57	0.56	0.56	0.57	0.55	0.56	0.56	0.56	0.56	0.56
Relative q_E	0.03	0.03	0.01	0.03	0.03	0.03	0.03	0.03	0.03	0.03	0.03	0.03	0.02	0.03	0.03	0.03	0.02	0.03	0.03
Act. vs. High NPQ	9.78	9.51	10.56	9.58	9.57	9.73	9.96	9.36	9.86	9.40	9.89	9.54	9.74	10.13	9.73	9.90	9.63	9.89	9.95
Act. vs. High Φ_{NO}	0.59	0.59	0.61	0.61	0.61	0.60	0.59	0.60	0.59	0.60	0.59	0.59	0.58	0.59	0.61	0.59	0.60	0.60	0.58
Act. vs. High Φ_{NPQ}	5.65	5.55	6.29	5.70	5.71	5.72	5.73	5.51	5.67	5.55	5.69	5.53	5.56	5.77	5.78	5.67	5.61	5.79	5.58
Act. vs. High q_I	2.60	2.62	2.62	2.63	2.62	2.65	2.65	2.59	2.64	2.61	2.63	2.61	2.58	2.71	2.63	2.61	2.64	2.65	2.62
Act. vs. High q_E	147	-203	88	201	-132	-70	257	-13	-11	52	-151	-90	224	67	401	56	-100	173	59
Act. vs. Low NPQ	1.45	1.45	1.37	1.46	1.45	1.46	1.45	1.43	1.44	1.44	1.45	1.43	1.45	1.46	1.44	1.46	1.45	1.46	1.45
Act. vs. Low Φ_{NO}	0.88	0.88	0.89	0.88	0.88	0.88	0.88	0.88	0.88	0.88	0.88	0.88	0.88	0.88	0.89	0.88	0.88	0.88	0.88
Act. vs. Low Φ_{NPQ}	1.28	1.27	1.21	1.28	1.28	1.28	1.28	1.26	1.27	1.27	1.27	1.26	1.27	1.28	1.27	1.28	1.28	1.29	1.27
Act. vs. Low q_I	1.45	1.44	1.41	1.46	1.43	1.45	1.44	1.43	1.44	1.44	1.44	1.42	1.42	1.45	1.44	1.44	1.45	1.44	1.44
Act. vs. Low q_E	4.90	-9.54	1.22	6.76	-0.36	-0.29	10.25	-2.37	-1.42	3.54	-2.75	-0.72	1.79	2.38	2.74	1.95	-3.42	6.41	0.69
Dry Weight (g)	0.35	0.34	0.32	0.34	0.29	0.32	0.35	0.32	0.34	0.32	0.34	0.32	0.33	0.35	0.33	0.34	0.35	0.33	0.32
Days to harvest	44.16	44.79	44.30	44.12	44.53	44.32	44.49	44.69	44.62	44.47	45.06	44.57	44.55	44.31	44.31	44.42	44.42	44.63	44.49
Specific leaf area (mm^{-2} mg^{-1})	7.43	6.85	7.21	7.46	7.34	7.28	7.35	6.70	7.30	7.22	6.73	7.14	7.04	7.50	7.12	7.29	7.39	7.12	7.40

Plasmotype	IP-Sne-0	Jm-0	Kas-1	Koren-1	Kz-13	Ler-0	Lesno-1	Mammo-1	Melni-2	Panke-1	Qar-8a	Rabacal-2	RRS-7	Samos-3a	Samos-4	Shah	Tanz-1	Taz-0	Toufl-1	Ws-4	Yeg-1	Zin-9
Surface area (px)	36129	36682	42375	36229	35981	36459	38142	35032	31184	31694	36179	33402	32832	33718	33951	34598	34770	34116	33450	35468	32958	32425
Surface area (mm^2)	1719	1745	2016	1723	1711	1734	1814	1666	1483	1508	1721	1589	1562	1604	1615	1646	1654	1623	1591	1687	1568	1542
Perimeter (px)	1357	1362	1507	1338	1351	1377	1357	1340	1250	1258	1351	1330	1235	1329	1333	1296	1324	1311	1318	1354	1263	1286
Perimeter (mm^2)	296	297	329	292	295	300	296	292	273	274	295	290	269	290	291	283	289	286	288	295	275	281
Roundness	0.24	0.24	0.24	0.24	0.24	0.23	0.26	0.23	0.24	0.24	0.24	0.23	0.26	0.24	0.23	0.24	0.24	0.23	0.23	0.23	0.24	0.23
Roundness 2	0.90	0.90	0.90	0.90	0.90	0.91	0.91	0.89	0.90	0.90	0.91	0.90	0.90	0.91	0.90	0.90	0.90	0.89	0.90	0.90	0.90	0.90
Isotropy	0.80	0.80	0.77	0.78	0.78	0.80	0.80	0.77	0.76	0.79	0.78	0.78	0.73	0.78	0.80	0.78	0.79	0.77	0.78	0.78	0.75	0.77
Compactness	0.74	0.74	0.74	0.75	0.73	0.73	0.76	0.71	0.73	0.73	0.74	0.73	0.74	0.73	0.72	0.73	0.73	0.72	0.72	0.73	0.73	0.71
Eccentricity	0.17	0.17	0.16	0.17	0.17	0.16	0.16	0.22	0.18	0.18	0.16	0.17	0.19	0.16	0.17	0.18	0.18	0.20	0.17	0.17	0.19	0.18
RMS	0.45	0.48	0.44	0.48	0.46	0.49	0.44	0.50	0.49	0.49	0.43	0.46	0.47	0.47	0.47	0.48	0.46	0.47	0.49	0.44	0.49	0.50
SOL	29.3	29.2	34.0	32.2	29.8	28.1	30.0	29.6	24.9	26.3	29.0	26.9	24.3	28.6	27.6	28.1	27.5	28.8	26.7	29.2	27.5	34.2
Act. FqFm (Φ_{PSII})	0.66	0.67	0.66	0.67	0.66	0.66	0.66	0.66	0.66	0.66	0.67	0.66	0.65	0.66	0.66	0.66	0.67	0.65	0.66	0.67	0.65	0.65
Act. NPQ	0.47	0.45	0.47	0.45	0.49	0.51	0.46	0.56	0.50	0.48	0.47	0.48	0.63	0.48	0.47	0.57	0.46	0.72	0.48	0.46	0.65	0.66
Act. Φ_{NO}	0.23	0.23	0.23	0.23	0.23	0.23	0.23	0.23	0.23	0.23	0.23	0.23	0.22	0.23	0.23	0.23	0.23	0.22	0.23	0.23	0.22	0.22
Act. Φ_{NPQ}	0.11	0.10	0.11	0.10	0.11	0.11	0.10	0.12	0.11	0.11	0.11	0.11	0.12	0.11	0.11	0.11	0.10	0.13	0.11	0.10	0.12	0.13
Act. Φ_{NPQ}	0.40	0.40	0.41	0.39	0.43	0.45	0.41	0.48	0.43	0.42	0.40	0.41	0.55	0.40	0.41	0.48	0.40	0.61	0.41	0.41	0.56	0.60
Act. q_E	0.06	0.06	0.06	0.06	0.06	0.05	0.05	0.08	0.07	0.06	0.06	0.07	0.08	0.07	0.07	0.09	0.07	0.10	0.07	0.06	0.09	0.06
High FqFm 1 (Φ_{PSII})	0.21	0.21	0.21	0.21	0.21	0.21	0.21	0.22	0.21	0.21	0.21	0.21	0.21	0.21	0.21	0.21	0.21	0.21	0.21	0.22	0.21	0.21
High FqFm 2 (Φ_{PSII})	0.28	0.27	0.27	0.28	0.27	0.27	0.27	0.28	0.27	0.27	0.27	0.27	0.26	0.27	0.27	0.27	0.27	0.27	0.28	0.28	0.27	0.27
High FqFm induction (Φ_{PSII})	1.30	1.30	1.29	1.30	1.29	1.28	1.29	1.29	1.29	1.29	1.30	1.30	1.27	1.29	1.29	1.29	1.29	1.27	1.30	1.30	1.29	1.28
High NPQ	4.44	4.48	4.73	4.44	4.53	4.70	4.47	5.00	4.40	4.59	4.47	4.53	5.21	4.57	4.63	4.65	4.53	5.38	4.44	4.41	4.78	5.01
High Φ_{NO}	0.14	0.14	0.13	0.14	0.14	0.13	0.14	0.13	0.14	0.14	0.14	0.14	0.13	0.14	0.13	0.14	0.14	0.13	0.14	0.14	0.14	0.13
High Φ_{NPQ}	0.58	0.59	0.59	0.59	0.59	0.59	0.59	0.59	0.59	0.59	0.59	0.59	0.60	0.59	0.59	0.59	0.59	0.60	0.59	0.58	0.59	0.60
High q_I	1.05	1.04	1.08	1.03	1.07	1.13	1.05	1.14	1.07	1.07	1.07	1.05	1.25	1.05	1.05	1.12	1.05	1.30	1.05	1.03	1.22	1.28
High q_E	3.39	3.45	3.64	3.42	3.46	3.58	3.41	3.86	3.34	3.51	3.40	3.47	3.96	3.52	3.57	3.53	3.48	4.08	3.39	3.38	3.57	3.74
Low FqFm 1 (Φ_{PSII})	0.65	0.66	0.65	0.66	0.65	0.65	0.65	0.65	0.66	0.66	0.66	0.66	0.64	0.66	0.66	0.65	0.66	0.64	0.66	0.66	0.64	0.64
Low FqFm 2 (Φ_{PSII})	0.66	0.67	0.66	0.67	0.66	0.66	0.66	0.66	0.66	0.66	0.66	0.67	0.65	0.66	0.67	0.66	0.66	0.64	0.66	0.67	0.65	0.65
Low FqFm induction (Φ_{PSII})	1.01	1.01	1.01	1.01	1.01	1.01	1.01	1.02	1.01	1.01	1.01	1.01	1.02	1.01	1.01	1.01	1.01	1.01	1.01	1.01	1.01	1.01
Low NPQ	0.67	0.66	0.68	0.66	0.70	0.73	0.67	0.79	0.69	0.69	0.67	0.68	0.87	0.67	0.68	0.80	0.65	1.00	0.68	0.67	0.90	0.91
Low Φ_{NO}	0.20	0.20	0.20	0.20	0.20	0.20	0.20	0.20	0.20	0.20	0.20	0.20	0.20	0.20	0.20	0.20	0.20	0.19	0.20	0.20	0.20	0.20
Low Φ_{NPQ}	0.13	0.13	0.14	0.13	0.14	0.14	0.13	0.14	0.14	0.14	0.13	0.13	0.15	0.13	0.13	0.14	0.13	0.16	0.13	0.13	0.15	0.16
Low q_I	0.58	0.58	0.60	0.57	0.61	0.64	0.59	0.68	0.60	0.60	0.58	0.59	0.77	0.58	0.59	0.67	0.57	0.83	0.58	0.59	0.75	0.80
Low q_E	0.09	0.08	0.09	0.09	0.09	0.09	0.08	0.11	0.09	0.10	0.08	0.09	0.10	0.10	0.09	0.14	0.09	0.17	0.10	0.08	0.15	0.11
Relative FqFm 1 (Φ_{PSII})	3.18	3.22	3.17	3.19	3.19	3.15	3.23	3.13	3.24	3.22	3.25	3.22	3.20	3.21	3.20	3.15	3.26	3.15	3.21	3.18	3.15	3.16
Relative FqFm 2 (Φ_{PSII})	2.47	2.50	2.48	2.48	2.49	2.47	2.53	2.44	2.53	2.51	2.52	2.51	2.54	2.50	2.50	2.48	2.54	2.51	2.48	2.46	2.48	2.50
Act. vs. High FqFm 1 (Φ_{PSII})	0.32	0.32	0.32	0.32	0.32	0.32	0.32	0.33	0.32	0.32	0.32	0.32	0.32	0.32	0.32	0.32	0.31	0.33	0.32	0.32	0.32	0.32
Act. vs. High FqFmp 2 (Φ_{PSII})	0.42	0.41	0.41	0.41	0.41	0.41	0.40	0.42	0.41	0.41	0.41	0.41	0.40	0.41	0.41	0.41	0.40	0.41	0.41	0.42	0.42	0.41
Act. vs. Low FqFmp 1 (Φ_{PSII})	0.99	0.99	0.98	0.99	0.98	0.98	0.98	0.98	0.99	0.99	0.99	0.99	0.98	0.99	0.99	0.98	0.99	0.98	0.99	0.99	0.98	0.98
Act. vs. Low FqFmp 2 (Φ_{PSII})	1.00	1.00	0.99	1.00	1.00	0.99	1.00	1.00	1.00	1.00	1.00	1.00	0.99	1.00	1.00	1.00	1.00	1.00	1.00	1.00	1.00	0.99
Relative NPQ	0.16	0.15	0.15	0.15	0.16	0.16	0.15	0.16	0.16	0.16	0.15	0.15	0.16	0.15	0.15	0.16	0.15	0.17	0.16	0.16	0.17	0.17
Relative Φ_{NO}	1.51	1.52	1.59	1.52	1.50	1.56	1.52	1.55	1.48	1.52	1.51	1.52	1.58	1.54	1.55	1.49	1.53	1.55	1.50	1.50	1.50	1.54
Relative Φ_{NPQ}	0.23	0.23	0.23	0.23	0.23	0.24	0.23	0.24	0.23	0.23	0.23	0.23	0.25	0.23	0.23	0.24	0.22	0.26	0.23	0.23	0.25	0.26
Relative q_I	0.57	0.56	0.55	0.56	0.57	0.56	0.56	0.58	0.57	0.56	0.56	0.56	0.57	0.56	0.56	0.58	0.55	0.58	0.57	0.57	0.58	0.58
Relative q_E	0.03	0.02	0.02	0.03	0.03	0.03	0.02	0.03	0.03	0.03	0.02	0.03	0.03	0.03	0.03	0.03	0.03	0.03	0.03	0.03	0.03	0.03
Act. vs. High NPQ	9.61	9.86	10.29	10.03	9.66	9.93	9.91	9.47	9.28	9.73	9.69	9.70	9.62	9.87	10.04	9.44	9.90	9.12	9.49	9.65	9.15	9.23
Act. vs. High Φ_{NO}	0.60	0.59	0.58	0.60	0.61	0.58	0.60	0.59	0.61	0.60	0.60	0.60	0.59	0.59	0.59	0.61	0.60	0.59	0.61	0.61	0.60	0.58
Act. vs. High Φ_{NPQ}	5.62	5.69	5.76	5.81	5.72	5.65	5.79	5.50	5.58	5.64	5.66	5.62	5.54	5.68	5.71	5.60	5.78	5.30	5.60	5.65	5.41	5.32
Act. vs. High q_I	2.62	2.62	2.73	2.68	2.63	2.63	2.63	2.60	2.55	2.63	2.64	2.62	2.59	2.64	2.68	2.60	2.67	2.53	2.62	2.62	2.55	2.55
Act. vs. High q_E	97	73	355	139	64667	34	56	84	72	171	112	184	226	-8786	244	-72	131	141	-208	122	23	75
Act. vs. Low NPQ	1.45	1.46	1.48	1.47	1.44	1.47	1.47	1.45	1.42	1.45	1.45	1.44	1.43	1.45	1.45	1.45	1.45	1.43	1.44	1.44	1.44	1.44
Act. vs. Low Φ_{NO}	0.88	0.88	0.88	0.88	0.88	0.88	0.88	0.88	0.89	0.88	0.88	0.88	0.89	0.88	0.88	0.88	0.89	0.88	0.88	0.88	0.88	0.88
Act. vs. Low Φ_{NPQ}	1.28	1.28	1.30	1.29	1.27	1.29	1.29	1.27	1.25	1.28	1.28	1.26	1.26	1.27	1.27	1.28	1.28	1.25	1.27	1.27	1.26	1.26
Act. vs. Low q_I	1.45	1.45	1.47	1.45	1.44	1.44	1.45	1.44	1.42	1.44	1.44	1.43	1.42	1.44	1.45	1.45	1.44	1.42	1.44	1.44	1.43	1.42
Act. vs. Low q_E	1.96	2.36	9.62	4.23	#####	1.64	2.58	1.46	3.53	4.53	4.50	4.75	6.42	-98.86	5.68	-3.72	6.49	4.95	-5.44	3.51	0.84	1.50
Dry Weight (g)	0.32	0.33	0.36	0.32	0.35	0.32	0.35	0.32	0.32	0.31	0.33	0.32	0.33	0.32	0.33	0.35	0.32	0.32	0.33	0.33	0.32	0.33
Days to harvest	44.41	44.33	43.70	44.58	44.57	44.24	43.81	44.63	44.94	45.02	44.51	45.02	45.08	44.72	44.82	45.06	44.42	44.50	44.44	44.52	44.52	44.81
Specific leaf area (mm^{-2} mg^{-1})	7.18	7.44	8.04	7.27	7.06	7.55	7.90	6.97	6.84	7.23	7.15	6.91	6.54	7.07	7.35	6.58	7.32	7.27	7.24	7.07	7.15	7.16

Extended data Table 7. Phenotype standard errors from the combined analysis of all cybrids.

Plasmotype	Aitba-1	Basta-2	Bur-0	C24	Can-0	Col-0	Cvi-0	Don-0	Elh-2	Elk-1	Epid-1	ET2	Etna-2	IP-Boa-0	IP-Bor-0	IP-Cot-0	IP-Ees-0	IP-Lso-0	IP-Per-0
Surface area (px)	1444	1462	1447	1454	1469	1450	1442	1447	1440	1439	1454	1455	1435	1455	1471	1447	1458	1454	1440
Surface area (mm^2)	68.68	69.54	68.85	69.14	69.88	68.99	68.58	68.84	68.48	68.47	69.16	69.20	68.24	69.21	69.95	68.84	69.36	69.18	68.48
Perimeter (px)	38.70	39.48	38.85	39.11	39.79	38.98	38.61	38.84	38.52	38.51	39.13	39.17	38.29	39.18	39.85	38.84	39.31	39.15	38.51
Perimeter (mm^2)	8.440	8.609	8.473	8.531	8.678	8.501	8.421	8.471	8.401	8.398	8.534	8.543	8.351	8.545	8.692	8.471	8.574	8.539	8.399
Roundness	0.0074	0.0076	0.0075	0.0075	0.0077	0.0075	0.0074	0.0075	0.0074	0.0074	0.0075	0.0076	0.0073	0.0076	0.0077	0.0075	0.0076	0.0075	0.0074
Roundness 2	0.0038	0.0039	0.0038	0.0039	0.0040	0.0039	0.0038	0.0038	0.0038	0.0038	0.0039	0.0039	0.0038	0.0039	0.0040	0.0038	0.0039	0.0039	0.0038
Isotropy	0.0141	0.0145	0.0142	0.0143	0.0146	0.0142	0.0140	0.0142	0.0140	0.0140	0.0143	0.0143	0.0139	0.0143	0.0147	0.0141	0.0144	0.0143	0.0140
Compactness	0.0069	0.0071	0.0069	0.0070	0.0072	0.0070	0.0069	0.0069	0.0068	0.0068	0.0070	0.0070	0.0068	0.0070	0.0072	0.0069	0.0070	0.0070	0.0068
Eccentricity	0.0104	0.0107	0.0104	0.0105	0.0108	0.0105	0.0103	0.0104	0.0103	0.0103	0.0105	0.0105	0.0102	0.0105	0.0108	0.0104	0.0106	0.0105	0.0103
RMS	0.0191	0.0197	0.0192	0.0194	0.0199	0.0193	0.0191	0.0192	0.0190	0.0190	0.0194	0.0195	0.0188	0.0195	0.0199	0.0192	0.0195	0.0194	0.0190
SOL	2.2592	2.3060	2.2682	2.2842	2.3248	2.2760	2.2537	2.2677	2.2483	2.2476	2.2851	2.2874	2.2345	2.2879	2.3285	2.2677	2.2959	2.2865	2.2477
Act. FqFm (Φ_{PSII})	0.0041	0.0042	0.0041	0.0041	0.0042	0.0041	0.0041	0.0041	0.0040	0.0040	0.0041	0.0041	0.0040	0.0041	0.0042	0.0041	0.0041	0.0041	0.0040
Act. NPQ	0.0482	0.0495	0.0484	0.0489	0.0500	0.0487	0.0480	0.0484	0.0479	0.0478	0.0489	0.0490	0.0475	0.0490	0.0501	0.0484	0.0492	0.0490	0.0478
Act. Φ_{NO}	0.0020	0.0020	0.0020	0.0020	0.0020	0.0020	0.0020	0.0020	0.0020	0.0020	0.0020	0.0020	0.0020	0.0020	0.0020	0.0020	0.0020	0.0020	0.0020
Act. Φ_{NPQ}	0.0053	0.0054	0.0053	0.0054	0.0055	0.0054	0.0053	0.0053	0.0053	0.0053	0.0054	0.0054	0.0052	0.0054	0.0055	0.0053	0.0054	0.0054	0.0053
Act. Φ_{NPQ}	0.0439	0.0452	0.0442	0.0446	0.0457	0.0444	0.0438	0.0442	0.0437	0.0436	0.0446	0.0447	0.0433	0.0447	0.0458	0.0442	0.0449	0.0447	0.0436
Act. q_E	0.0105	0.0107	0.0106	0.0106	0.0108	0.0106	0.0105	0.0106	0.0105	0.0105	0.0106	0.0106	0.0104	0.0106	0.0108	0.0106	0.0107	0.0106	0.0105
High FqFm 1 (Φ_{PSII})	0.0039	0.0040	0.0040	0.0040	0.0040	0.0040	0.0039	0.0040	0.0039	0.0039	0.0040	0.0040	0.0039	0.0040	0.0040	0.0040	0.0040	0.0040	0.0039
High FqFm 2 (Φ_{PSII})	0.0051	0.0051	0.0051	0.0051	0.0052	0.0051	0.0051	0.0051	0.0051	0.0050	0.0051	0.0051	0.0050	0.0051	0.0052	0.0051	0.0051	0.0051	0.0050
High FqFm induction (Φ_{PSII})	0.0070	0.0072	0.0070	0.0071	0.0072	0.0071	0.0070	0.0070	0.0070	0.0070	0.0071	0.0071	0.0069	0.0071	0.0072	0.0070	0.0071	0.0071	0.0070
High NPQ	0.2369	0.2421	0.2379	0.2397	0.2442	0.2388	0.2363	0.2378	0.2357	0.2356	0.2398	0.2401	0.2341	0.2401	0.2447	0.2379	0.2410	0.2400	0.2356
High Φ_{NO}	0.0030	0.0030	0.0030	0.0030	0.0030	0.0030	0.0030	0.0030	0.0030	0.0030	0.0030	0.0030	0.0029	0.0030	0.0030	0.0030	0.0030	0.0030	0.0030
High Φ_{NPQ}	0.0059	0.0060	0.0059	0.0060	0.0061	0.0060	0.0059	0.0059	0.0059	0.0059	0.0060	0.0060	0.0059	0.0060	0.0061	0.0059	0.0060	0.0060	0.0059
High q_I	0.0561	0.0576	0.0564	0.0569	0.0583	0.0566	0.0559	0.0563	0.0557	0.0557	0.0569	0.0570	0.0552	0.0570	0.0584	0.0563	0.0573	0.0570	0.0557
High q_E	0.1935	0.1974	0.1943	0.1956	0.1990	0.1949	0.1930	0.1942	0.1926	0.1925	0.1957	0.1959	0.1914	0.1959	0.1993	0.1942	0.1966	0.1958	0.1926
Low FqFm 1 (Φ_{PSII})	0.0042	0.0044	0.0043	0.0043	0.0044	0.0043	0.0042	0.0043	0.0042	0.0042	0.0043	0.0043	0.0042	0.0043	0.0044	0.0043	0.0043	0.0043	0.0042
Low FqFm 2 (Φ_{PSII})	0.0042	0.0044	0.0043	0.0043	0.0044	0.0043	0.0042	0.0043	0.0042	0.0042	0.0043	0.0043	0.0042	0.0043	0.0044	0.0043	0.0043	0.0043	0.0042
Low FqFm induction (Φ_{PSII})	0.0011	0.0011	0.0011	0.0011	0.0011	0.0011	0.0011	0.0011	0.0011	0.0011	0.0011	0.0011	0.0011	0.0011	0.0011	0.0011	0.0011	0.0011	0.0011
Low NPQ	0.0629	0.0647	0.0633	0.0639	0.0654	0.0636	0.0627	0.0633	0.0625	0.0625	0.0639	0.0640	0.0620	0.0640	0.0655	0.0632	0.0643	0.0640	0.0625
Low Φ_{NO}	0.0018	0.0019	0.0018	0.0018	0.0019	0.0018	0.0018	0.0018	0.0018	0.0018	0.0018	0.0018	0.0018	0.0018	0.0019	0.0018	0.0018	0.0018	0.0018
Low Φ_{NPQ}	0.0055	0.0056	0.0055	0.0056	0.0057	0.0055	0.0055	0.0055	0.0054	0.0054	0.0056	0.0056	0.0054	0.0056	0.0057	0.0055	0.0056	0.0056	0.0054
Low q_I	0.0524	0.0539	0.0527	0.0532	0.0545	0.0530	0.0523	0.0527	0.0521	0.0521	0.0533	0.0533	0.0516	0.0533	0.0546	0.0527	0.0536	0.0533	0.0521
Low q_E	0.0140	0.0144	0.0141	0.0142	0.0145	0.0142	0.0140	0.0141	0.0140	0.0140	0.0142	0.0142	0.0139	0.0142	0.0145	0.0141	0.0143	0.0142	0.0140
Relative FqFm 1 (Φ_{PSII})	0.0609	0.0613	0.0610	0.0611	0.0614	0.0611	0.0609	0.0610	0.0608	0.0608	0.0611	0.0611	0.0607	0.0612	0.0615	0.0610	0.0612	0.0611	0.0608
Relative FqFm 2 (Φ_{PSII})	0.0424	0.0427	0.0425	0.0426	0.0428	0.0425	0.0424	0.0425	0.0423	0.0423	0.0426	0.0426	0.0422	0.0426	0.0429	0.0425	0.0426	0.0426	0.0423
Act. vs. High FqFm 1 (Φ_{PSII})	0.0054	0.0054	0.0054	0.0054	0.0055	0.0054	0.0054	0.0054	0.0054	0.0054	0.0054	0.0054	0.0054	0.0054	0.0055	0.0054	0.0054	0.0054	0.0054
Act. vs. High FqFmp 2 (Φ_{PSII})	0.0066	0.0067	0.0066	0.0066	0.0067	0.0066	0.0066	0.0066	0.0066	0.0066	0.0066	0.0066	0.0066	0.0066	0.0067	0.0066	0.0067	0.0066	0.0066
Act. vs. Low FqFmp 1 (Φ_{PSII})	0.0025	0.0026	0.0025	0.0026	0.0026	0.0026	0.0025	0.0025	0.0025	0.0025	0.0026	0.0026	0.0025	0.0026	0.0026	0.0025	0.0026	0.0026	0.0025
Act. vs. Low FqFmp 2 (Φ_{PSII})	0.0021	0.0021	0.0021	0.0021	0.0021	0.0021	0.0021	0.0021	0.0021	0.0021	0.0021	0.0021	0.0021	0.0021	0.0022	0.0021	0.0021	0.0021	0.0021
Relative NPQ	0.0046	0.0046	0.0046	0.0046	0.0047	0.0046	0.0046	0.0046	0.0045	0.0045	0.0046	0.0046	0.0045	0.0046	0.0047	0.0046	0.0046	0.0046	0.0045
Relative Φ_{NO}	0.0357	0.0361	0.0357	0.0359	0.0362	0.0358	0.0356	0.0357	0.0356	0.0356	0.0359	0.0359	0.0354	0.0359	0.0363	0.0357	0.0360	0.0359	0.0356
Relative Φ_{NPQ}	0.0063	0.0065	0.0063	0.0064	0.0065	0.0064	0.0063	0.0063	0.0063	0.0063	0.0064	0.0064	0.0062	0.0064	0.0065	0.0063	0.0064	0.0064	0.0063
Relative q_I	0.0108	0.0109	0.0108	0.0108	0.0109	0.0108	0.0108	0.0108	0.0107	0.0107	0.0108	0.0108	0.0107	0.0108	0.0109	0.0108	0.0109	0.0108	0.0107
Relative q_E	0.0022	0.0022	0.0022	0.0022	0.0022	0.0022	0.0022	0.0022	0.0022	0.0022	0.0022	0.0022	0.0021	0.0022	0.0022	0.0022	0.0022	0.0022	0.0022
Act. vs. High NPQ	0.3084	0.3120	0.3091	0.3103	0.3135	0.3097	0.3080	0.3090	0.3075	0.3075	0.3104	0.3106	0.3065	0.3106	0.3138	0.3090	0.3112	0.3105	0.3075
Act. vs. High Φ_{NO}	0.0121	0.0122	0.0121	0.0122	0.0123	0.0122	0.0121	0.0121	0.0121	0.0121	0.0122	0.0122	0.0121	0.0122	0.0123	0.0121	0.0122	0.0122	0.0121
Act. vs. High Φ_{NPQ}	0.1122	0.1138	0.1125	0.1131	0.1145	0.1128	0.1120	0.1125	0.1118	0.1118	0.1131	0.1132	0.1114	0.1132	0.1146	0.1125	0.1135	0.1132	0.1118
Act. vs. High q_I	0.0573	0.0578	0.0574	0.0576	0.0580	0.0575	0.0572	0.0574	0.0571	0.0571	0.0576	0.0576	0.0570	0.0576	0.0581	0.0574	0.0577	0.0576	0.0571
Act. vs. High q_E	9216	9484	9267	9359	9591	9315	9183	9266	9153	9151	9363	9375	9072	9376	9608	9262	9422	9368	9147
Act. vs. Low NPQ	0.0198	0.0199	0.0198	0.0198	0.0199	0.0198	0.0197	0.0198	0.0197	0.0197	0.0198	0.0198	0.0197	0.0198	0.0199	0.0198	0.0199	0.0198	0.0197
Act. vs. Low Φ_{NO}	0.0040	0.0041	0.0040	0.0040	0.0041	0.0040	0.0040	0.0040	0.0040	0.0040	0.0040	0.0041	0.0040	0.0041	0.0041	0.0040	0.0041	0.0040	0.0040
Act. vs. Low Φ_{NPQ}	0.0145	0.0146	0.0145	0.0145	0.0146	0.0145	0.0145	0.0145	0.0145	0.0145	0.0145	0.0145	0.0144	0.0146	0.0146	0.0145	0.0146	0.0145	0.0145
Act. vs. Low q_I	0.0106	0.0108	0.0106	0.0107	0.0108	0.0106	0.0105	0.0106	0.0105	0.0105	0.0107	0.0107	0.0105	0.0107	0.0109	0.0106	0.0107	0.0107	0.0105
Act. vs. Low q_E	336	346	338	342	350	340	335	338	334	334	342	342	331	342	351	338	344	342	334
Dry Weight (g)	0.0121	0.0125	0.0122	0.0123	0.0126	0.0122	0.0121	0.0122	0.0123	0.0122	0.0123	0.0123	0.0122	0.0124	0.0125	0.0123	0.0123	0.0126	0.0121
Days to harvest	0.2032	0.2079	0.2038	0.2048	0.2091	0.2043	0.2028	0.2037	0.2051	0.2037	0.2049	0.2050	0.2043	0.2062	0.2078	0.2062	0.2056	0.2089	0.2024
Specific leaf area (mm^{-2} mg^{-1})	0.2246	0.2311	0.2255	0.2269	0.2328	0.2262	0.2241	0.2254	0.2273	0.2254	0.2270	0.2272	0.2262	0.2288	0.2310	0.2269	0.2280	0.2325	0.2236

Plasmotype	IP-Sne-0	Jm-0	Kas-1	Koren-1	Kz-13	Ler-0	Lesno-1	Mammo-1	Melni-2	Panke-1	Qar-8a	Rabacal-2	RRS-7	Samos-3a	Samos-4	Shah	Tanz-1	Taz-0	Toufl-1	Ws-4	Yeg-1	Zin-9
Surface area (px)	1463	1456	1441	1468	1442	1434	1434	1455	1433	1447	1427	1440	1455	1458	1430	1436	1434	1454	1422	1467	1422	1440
Surface area (mm^2)	69.59	69.24	68.55	69.84	68.57	68.19	68.19	69.23	68.16	68.84	67.87	68.48	69.22	69.34	68.01	68.29	68.21	69.14	67.66	69.77	67.64	68.48
Perimeter (px)	39.53	39.20	38.58	39.74	38.60	38.25	38.25	39.20	38.23	38.84	37.96	38.51	39.19	39.29	38.09	38.34	38.27	39.12	37.76	39.69	37.75	38.51
Perimeter (mm^2)	8.621	8.550	8.415	8.668	8.418	8.342	8.343	8.549	8.337	8.472	8.278	8.400	8.547	8.570	8.307	8.363	8.347	8.532	8.236	8.656	8.232	8.399
Roundness	0.0077	0.0076	0.0074	0.0077	0.0074	0.0073	0.0073	0.0076	0.0073	0.0075	0.0072	0.0074	0.0076	0.0076	0.0073	0.0073	0.0073	0.0075	0.0072	0.0077	0.0072	0.0074
Roundness 2	0.0039	0.0039	0.0038	0.0040	0.0038	0.0038	0.0038	0.0039	0.0038	0.0038	0.0037	0.0038	0.0039	0.0039	0.0037	0.0038	0.0038	0.0039	0.0037	0.0040	0.0037	0.0038
Isotropy	0.0145	0.0143	0.0140	0.0146	0.0140	0.0138	0.0138	0.0143	0.0138	0.0141	0.0137	0.0140	0.0143	0.0144	0.0138	0.0139	0.0138	0.0143	0.0136	0.0146	0.0136	0.0140
Compactness	0.0071	0.0070	0.0068	0.0071	0.0069	0.0068	0.0068	0.0070	0.0068	0.0069	0.0067	0.0068	0.0070	0.0070	0.0067	0.0068	0.0068	0.0070	0.0066	0.0071	0.0066	0.0068
Eccentricity	0.0107	0.0106	0.0103	0.0108	0.0103	0.0102	0.0102	0.0106	0.0102	0.0104	0.0101	0.0103	0.0105	0.0106	0.0101	0.0102	0.0102	0.0105	0.0100	0.0107	0.0100	0.0103
RMS	0.0197	0.0195	0.0190	0.0199	0.0191	0.0188	0.0188	0.0195	0.0188	0.0192	0.0186	0.0190	0.0195	0.0195	0.0187	0.0189	0.0188	0.0194	0.0185	0.0198	0.0185	0.0190
SOL	2.3089	2.2894	2.2520	2.3221	2.2530	2.2319	2.2321	2.2890	2.2305	2.2678	2.2142	2.2478	2.2886	2.2949	2.2221	2.2376	2.2332	2.2844	2.2025	2.3187	2.2015	2.2478
Act. FqFm (Φ_{PSII})	0.0042	0.0041	0.0041	0.0042	0.0041	0.0040	0.0040	0.0041	0.0040	0.0041	0.0040	0.0040	0.0041	0.0041	0.0040	0.0040	0.0040	0.0041	0.0039	0.0042	0.0039	0.0040
Act. NPQ	0.0496	0.0490	0.0480	0.0500	0.0480	0.0474	0.0474	0.0490	0.0474	0.0484	0.0469	0.0478	0.0490	0.0492	0.0471	0.0476	0.0474	0.0489	0.0465	0.0499	0.0465	0.0478
Act. Φ_{NO}	0.0020	0.0020	0.0020	0.0020	0.0020	0.0020	0.0020	0.0020	0.0020	0.0020	0.0020	0.0020	0.0020	0.0020	0.0020	0.0020	0.0020	0.0020	0.0020	0.0020	0.0020	0.0020
Act. Φ_{NPQ}	0.0055	0.0054	0.0053	0.0055	0.0053	0.0052	0.0052	0.0054	0.0052	0.0053	0.0052	0.0053	0.0054	0.0054	0.0052	0.0052	0.0052	0.0054	0.0051	0.0055	0.0051	0.0053
Act. Φ_{NPQ}	0.0453	0.0447	0.0437	0.0456	0.0438	0.0432	0.0432	0.0447	0.0432	0.0442	0.0427	0.0436	0.0447	0.0449	0.0429	0.0434	0.0432	0.0446	0.0424	0.0455	0.0424	0.0436
Act. q_E	0.0107	0.0106	0.0105	0.0108	0.0105	0.0104	0.0104	0.0106	0.0104	0.0106	0.0104	0.0105	0.0106	0.0107	0.0104	0.0105	0.0104	0.0106	0.0103	0.0107	0.0103	0.0105
High FqFm 1 (Φ_{PSII})	0.0040	0.0040	0.0039	0.0040	0.0039	0.0039	0.0039	0.0040	0.0039	0.0040	0.0039	0.0039	0.0040	0.0040	0.0039	0.0039	0.0039	0.0040	0.0039	0.0040	0.0039	0.0039
High FqFm 2 (Φ_{PSII})	0.0051	0.0051	0.0051	0.0052	0.0051	0.0050	0.0050	0.0051	0.0050	0.0051	0.0050	0.0050	0.0051	0.0051	0.0050	0.0050	0.0050	0.0051	0.0050	0.0051	0.0050	0.0050
High FqFm induction (Φ_{PSII})	0.0072	0.0071	0.0070	0.0072	0.0070	0.0069	0.0069	0.0071	0.0069	0.0070	0.0068	0.0070	0.0071	0.0071	0.0069	0.0069	0.0069	0.0071	0.0068	0.0072	0.0068	0.0070
High NPQ	0.2425	0.2403	0.2361	0.2440	0.2362	0.2338	0.2339	0.2402	0.2337	0.2379	0.2319	0.2356	0.2402	0.2409	0.2327	0.2345	0.2340	0.2397	0.2305	0.2436	0.2304	0.2356
High Φ_{NO}	0.0030	0.0030	0.0030	0.0030	0.0030	0.0029	0.0029	0.0030	0.0029	0.0030	0.0029	0.0030	0.0030	0.0030	0.0029	0.0029	0.0029	0.0030	0.0029	0.0030	0.0029	0.0030
High Φ_{NPQ}	0.0060	0.0060	0.0059	0.0061	0.0059	0.0059	0.0059	0.0060	0.0059	0.0059	0.0058	0.0059	0.0060	0.0060	0.0058	0.0059	0.0059	0.0060	0.0058	0.0061	0.0058	0.0059
High q_I	0.0577	0.0571	0.0558	0.0582	0.0558	0.0551	0.0551	0.0571	0.0551	0.0563	0.0545	0.0557	0.0570	0.0572	0.0548	0.0553	0.0552	0.0569	0.0541	0.0581	0.0541	0.0557
High q_E	0.1977	0.1960	0.1929	0.1988	0.1930	0.1912	0.1913	0.1960	0.1911	0.1942	0.1898	0.1926	0.1960	0.1965	0.1904	0.1917	0.1913	0.1956	0.1888	0.1985	0.1887	0.1926
Low FqFm 1 (Φ_{PSII})	0.0044	0.0043	0.0042	0.0044	0.0042	0.0042	0.0042	0.0043	0.0042	0.0043	0.0041	0.0042	0.0043	0.0043	0.0042	0.0042	0.0042	0.0043	0.0041	0.0044	0.0041	0.0042
Low FqFm 2 (Φ_{PSII})	0.0044	0.0043	0.0042	0.0044	0.0042	0.0042	0.0042	0.0043	0.0042	0.0043	0.0041	0.0042	0.0043	0.0043	0.0041	0.0042	0.0042	0.0043	0.0041	0.0044	0.0041	0.0042
Low FqFm induction (Φ_{PSII})	0.0011	0.0011	0.0011	0.0011	0.0011	0.0011	0.0011	0.0011	0.0011	0.0011	0.0011	0.0011	0.0011	0.0011	0.0011	0.0011	0.0011	0.0011	0.0011	0.0011	0.0011	0.0011
Low NPQ	0.0648	0.0641	0.0626	0.0653	0.0627	0.0619	0.0619	0.0641	0.0618	0.0632	0.0612	0.0625	0.0640	0.0643	0.0615	0.0621	0.0619	0.0639	0.0608	0.0652	0.0607	0.0625
Low Φ_{NO}	0.0019	0.0018	0.0018	0.0019	0.0018	0.0018	0.0018	0.0018	0.0018	0.0018	0.0018	0.0018	0.0018	0.0018	0.0018	0.0018	0.0018	0.0018	0.0018	0.0019	0.0018	0.0018
Low Φ_{NPQ}	0.0056	0.0056	0.0054	0.0057	0.0055	0.0054	0.0054	0.0056	0.0054	0.0055	0.0053	0.0054	0.0056	0.0056	0.0053	0.0054	0.0054	0.0056	0.0053	0.0057	0.0053	0.0054
Low q_I	0.0540	0.0534	0.0522	0.0544	0.0522	0.0516	0.0516	0.0534	0.0515	0.0527	0.0510	0.0521	0.0534	0.0536	0.0512	0.0517	0.0516	0.0532	0.0506	0.0543	0.0506	0.0521
Low q_E	0.0144	0.0143	0.0140	0.0145	0.0140	0.0139	0.0139	0.0143	0.0138	0.0141	0.0137	0.0140	0.0143	0.0143	0.0138	0.0139	0.0139	0.0142	0.0137	0.0145	0.0136	0.0140
Relative FqFm 1 (Φ_{PSII})	0.0613	0.0612	0.0609	0.0614	0.0609	0.0607	0.0607	0.0612	0.0607	0.0610	0.0606	0.0608	0.0612	0.0612	0.0607	0.0608	0.0607	0.0611	0.0605	0.0614	0.0605	0.0608
Relative FqFm 2 (Φ_{PSII})	0.0427	0.0426	0.0423	0.0428	0.0424	0.0422	0.0422	0.0426	0.0422	0.0425	0.0421	0.0423	0.0426	0.0426	0.0422	0.0423	0.0422	0.0426	0.0420	0.0428	0.0420	0.0423
Act. vs. High FqFm 1 (Φ_{PSII})	0.0054	0.0054	0.0054	0.0055	0.0054	0.0054	0.0054	0.0054	0.0054	0.0054	0.0054	0.0054	0.0054	0.0054	0.0054	0.0054	0.0054	0.0054	0.0053	0.0055	0.0053	0.0054
Act. vs. High FqFmp 2 (Φ_{PSII})	0.0067	0.0066	0.0066	0.0067	0.0066	0.0066	0.0066	0.0066	0.0066	0.0066	0.0065	0.0066	0.0066	0.0067	0.0066	0.0066	0.0066	0.0066	0.0065	0.0067	0.0065	0.0066
Act. vs. Low FqFmp 1 (Φ_{PSII})	0.0026	0.0026	0.0025	0.0026	0.0025	0.0025	0.0025	0.0026	0.0025	0.0025	0.0025	0.0025	0.0026	0.0026	0.0025	0.0025	0.0025	0.0026	0.0025	0.0026	0.0025	0.0025
Act. vs. Low FqFmp 2 (Φ_{PSII})	0.0021	0.0021	0.0021	0.0021	0.0021	0.0021	0.0021	0.0021	0.0021	0.0021	0.0021	0.0021	0.0021	0.0021	0.0021	0.0021	0.0021	0.0021	0.0021	0.0021	0.0021	0.0021
Relative NPQ	0.0047	0.0046	0.0045	0.0047	0.0046	0.0045	0.0045	0.0046	0.0045	0.0046	0.0045	0.0045	0.0046	0.0046	0.0045	0.0045	0.0045	0.0046	0.0045	0.0047	0.0045	0.0045
Relative Φ_{NO}	0.0361	0.0359	0.0356	0.0362	0.0356	0.0354	0.0354	0.0359	0.0354	0.0357	0.0353	0.0356	0.0359	0.0360	0.0353	0.0355	0.0354	0.0359	0.0352	0.0362	0.0352	0.0356
Relative Φ_{NPQ}	0.0065	0.0064	0.0063	0.0065	0.0063	0.0062	0.0062	0.0064	0.0062	0.0063	0.0061	0.0063	0.0064	0.0064	0.0062	0.0062	0.0062	0.0064	0.0061	0.0065	0.0061	0.0063
Relative q_I	0.0109	0.0108	0.0107	0.0109	0.0107	0.0107	0.0107	0.0108	0.0107	0.0108	0.0107	0.0107	0.0108	0.0109	0.0107	0.0107	0.0107	0.0108	0.0106	0.0109	0.0106	0.0107
Relative q_E	0.0022	0.0022	0.0022	0.0022	0.0022	0.0021	0.0021	0.0022	0.0021	0.0022	0.0021	0.0022	0.0022	0.0022	0.0021	0.0021	0.0021	0.0022	0.0021	0.0022	0.0021	0.0022
Act. vs. High NPQ	0.3123	0.3107	0.3078	0.3133	0.3079	0.3063	0.3063	0.3107	0.3062	0.3091	0.3049	0.3075	0.3107	0.3112	0.3055	0.3067	0.3064	0.3103	0.3040	0.3130	0.3039	0.3075
Act. vs. High Φ_{NO}	0.0123	0.0122	0.0121	0.0123	0.0121	0.0121	0.0121	0.0122	0.0120	0.0121	0.0120	0.0121	0.0122	0.0122	0.0120	0.0121	0.0121	0.0122	0.0120	0.0123	0.0120	0.0121
Act. vs. High Φ_{NPQ}	0.1139	0.1132	0.1120	0.1144	0.1120	0.1113	0.1113	0.1132	0.1112	0.1125	0.1107	0.1118	0.1132	0.1134	0.1110	0.1115	0.1113	0.1131	0.1103	0.1143	0.1103	0.1118
Act. vs. High q_I	0.0578	0.0576	0.0572	0.0580	0.0572	0.0569	0.0569	0.0576	0.0569	0.0574	0.0567	0.0571	0.0576	0.0577	0.0568	0.0570	0.0570	0.0576	0.0566	0.0580	0.0566	0.0571
Act. vs. High q_E	9496	9386	9171	9572	9178	9058	9057	9382	9048	9262	8954	9148	9381	9415	8999	9089	9063	9358	8887	9553	8880	9148
Act. vs. Low NPQ	0.0199	0.0198	0.0197	0.0199	0.0197	0.0197	0.0197	0.0198	0.0197	0.0198	0.0196	0.0197	0.0198	0.0199	0.0197	0.0197	0.0197	0.0198	0.0196	0.0199	0.0196	0.0197
Act. vs. Low Φ_{NO}	0.0041	0.0041	0.0040	0.0041	0.0040	0.0040	0.0040	0.0041	0.0040	0.0040	0.0040	0.0040	0.0041	0.0041	0.0040	0.0040	0.0040	0.0040	0.0040	0.0041	0.0040	0.0040
Act. vs. Low Φ_{NPQ}	0.0146	0.0146	0.0145	0.0146	0.0145	0.0144	0.0144	0.0146	0.0144	0.0145	0.0144	0.0145	0.0146	0.0146	0.0144	0.0144	0.0144	0.0145	0.0144	0.0146	0.0144	0.0145
Act. vs. Low q_I	0.0108	0.0107	0.0105	0.0108	0.0105	0.0104	0.0104	0.0107	0.0104	0.0106	0.0104	0.0105	0.0107	0.0107	0.0104	0.0105	0.0104	0.0107	0.0103	0.0108	0.0103	0.0105
Act. vs. Low q_E	347	343	335	349	335	331	331	343	330	338	327	334	342	344	329	332	331	342	324	349	324	334
Dry Weight (g)	0.0124	0.0123	0.0122	0.0125	0.0122	0.0121	0.0120	0.0124	0.0121	0.0122	0.0120	0.0121	0.0125	0.0123	0.0120	0.0123	0.0120	0.0126	0.0121	0.0124	0.0121	0.0125
Days to harvest	0.2065	0.2052	0.2038	0.2074	0.2039	0.2027	0.2014	0.2068	0.2024	0.2037	0.2027	0.2024	0.2079	0.2056	0.2007	0.2047	0.2026	0.2098	0.2030	0.2071	0.2028	0.2088
Specific leaf area (mm^{-2} mg^{-1})	0.2292	0.2274	0.2255	0.2304	0.2256	0.2240	0.2222	0.2296	0.2236	0.2254	0.2221	0.2236	0.2311	0.2279	0.2213	0.2268	0.2223	0.2337	0.2245	0.2301	0.2241	0.2305

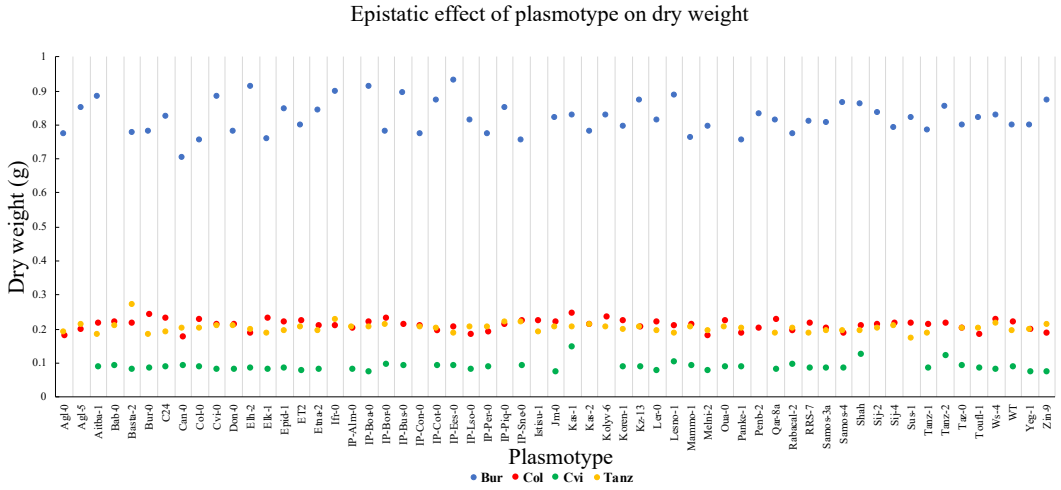

Extended data Fig. 7 Epistatic effects of plasmotype on dry weight.

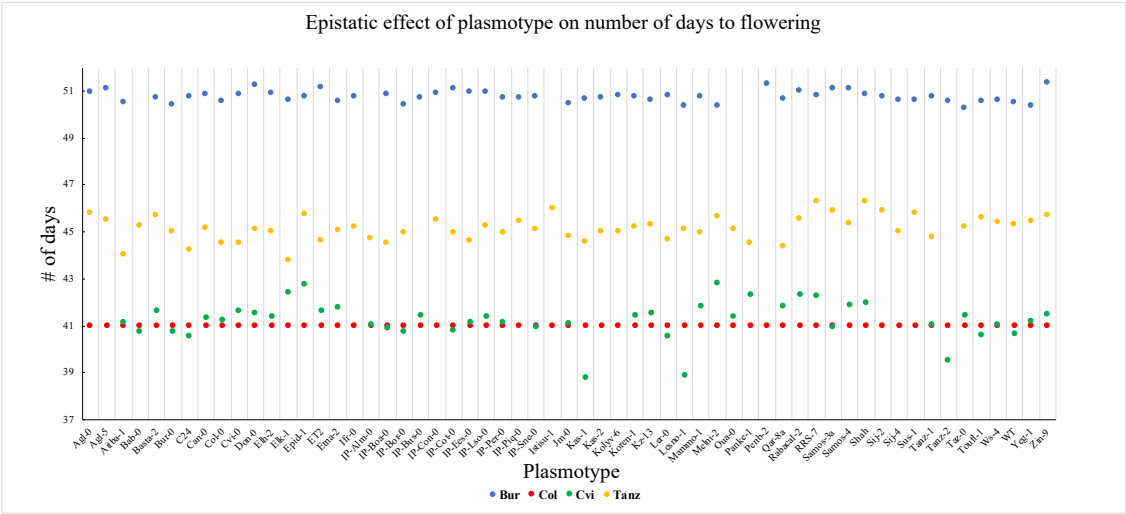

Extended data Fig. 8 Epistatic effects of plasmotype on number of days to flowering.

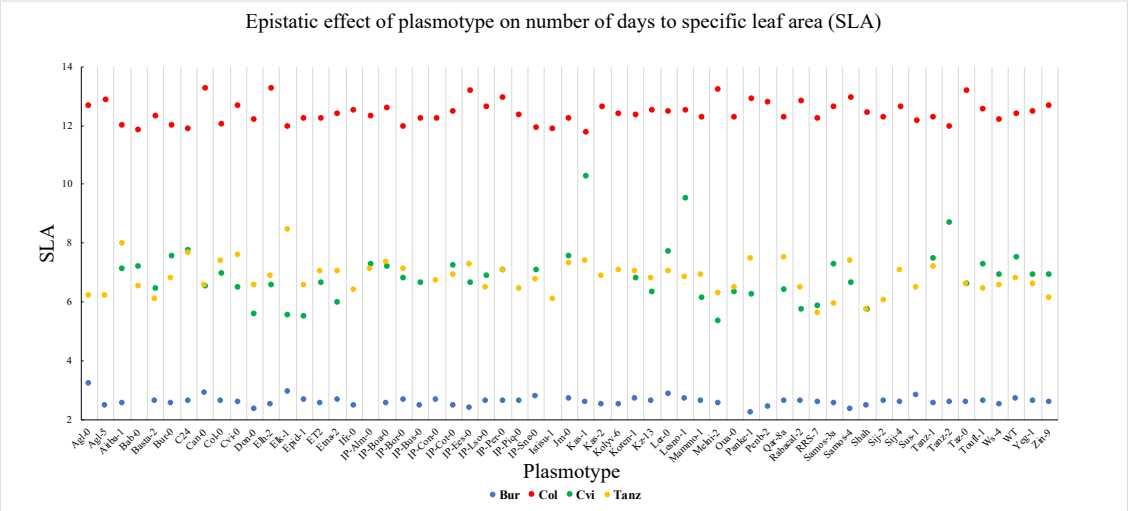

Extended data Fig. 8 Epistatic effects of plasmotype on SLA.

Supplementary List 1. DNA isolation protocol (Becker, unpublished).

1) Prepare 10 mL extraction buffer by adding 40 µL of 20 mg/mL RNAse A.
2) Grind the frozen sample tissue by securing the lids of the plates and using the mixer mill/lyser apparatus.
3) Spin the resulting dust down to the bottom of the wells.
4) Add 500 µL of extraction buffer to each sample.
5) Incubate at 37 °Celsius for one hour.
    a. Invert plates every 15 minutes.
6) Flash spin to pellet debris (3,000 rpm for 5 minutes).
7) Add 130 µL KAc plus Tween to each well of a new deep well plate.
8) Transfer 400 µL of the lysate to the KAc deep well plate.
9) Cover the wells with the lid and ensure a tight fit. Invert to mix for 1-2 minutes.
10) Incubate the plates on ice for a minimum of 10 minutes.
11) Centrifuge the plates at 3,000 rpm for 5 minutes.
12) Prepare new plates by combining SPRI beads and PEG buffer in a 1:1 ratio in each well.
13) Transfer 400 µL of the supernatant to the wells in the new plates containing SPRI beads and PEG buffer.
14) Place the plates on the shaking table for a minimum of 30 minutes.
15) Place the plate on the magnet and let the beads settle for a minimum of 5 minutes.
16) Remove the supernatant by inverting the plate gently over the sink.
17) Wash the beads three times by adding 500 µL of 80 percent EtOH and vortexing.
18) After the last wash, carefully remove all traces of EtOH and let the beads dry for approximately 10-15 minutes.
19) Resuspend the beads by adding 50 µL of 10mM Tris-HCl and let sit for 30-60 minutes.
20) Seal the plates tightly and mix by inversion of the plate.
21) Place the plate on a magnet for a minimum of five minutes.
22) Transfer eluate to fresh PCR plate by pipetting while being careful not to transfer any of the beads.

Supplementary List 2. Library preparation protocol for genomic sequencing (Theeuwen, unpublished).

1) Dilute BLT beads (Nextara) with nuclease free water to a 1:50 ratio for a minimum of ten µL needed per sample.
2) Add 25 µL of tagmentation buffer into each well of a fresh PCR plate under the fume hood.
3) Add 10 µL of 1:50 BLT beads, 5 µL DNA, and 5 µL miliQ water into each well containing the tagmentation buffer.
4) Perform tagmentation in a PCR machine for 15 minutes at 55 °Celsius followed by a holding period at 10 °Celsius.
5) Add 10 µL of 0.2 percent SDS solution to each well to stop the tagmentation.
6) Place the samples in a PCR machine for 10 minutes at 37 °Celsius followed by a holding period at 10 °Celsius.
7) Place the plate on a magnet and wait 3-4 minutes.
8) Remove the tagmentation/SDS solution by pipetting.
9) Wash the beads three times with 100 µL of PEG.
10) Add 17.5 µL miliQ water, 22.5 µL Takara Primestar Mastermix and 2.5 µL P5 oligo to each well in the plate. Add 2.5 µL of unique P7 oligo to each unique PCR plate well and record the coordinates.
11) Mix the solution in the PCR plates well. Spin down briefly.
12) Run the PCR machine at three minutes at 68 °Celsius, three minutes at 98°Celsius, 12 cycles of (45 seconds and 98 °Celsius, 30 seconds at 62 °Celsius, two minutes at 68 °Celsius), one minute at 68 °Celsius and lastly hold at 10 °Celsius.
13) Check the results on a 2 percent agarose gel.
    a. Use three µL of PCR product from each well and mix with 2 µL of 6× loading dye.
    b. Use one µL of 100 bp ladder.
    c. Run at 100 volts for 30 minutes.